

I

A PROCEDURE FOR THE ANALYSIS OF POLONIUM-210  
AND LEAD-212 IN ROCKS

II

A CHARACTERIZATION OF THE METEORITE FLUX  
AT THE EARTH'S ORBIT

Thesis by

Hugh Thompson Millard, Jr.

In Partial Fulfillment of the Requirements  
for the Degree of  
Doctor of Philosophy

California Institute of Technology  
Pasadena, California

1962

## ACKNOWLEDGEMENTS

I want to express my deepest appreciation to Professor Harrison Brown for providing the necessary guidance, encouragement, and council during the investigations described in this thesis. Other members of the Geochemistry Department, notably Dr. Leon T. Silver, Charles McKinney, and Walter Nichiporuk, have generously furnished timely advice and mineral samples, both of which were needed in large quantities.

I also wish to acknowledge the generous financial support furnished me by the Institute, the E. I. du Pont de Nemours Company, and the Alfred P. Sloan Foundation. The Graduate Teaching Assistantships awarded me were doubly rewarding in that they provided not only an income but also the opportunity to teach under the direction of Professors Norman Davidson and Jurg Waser.

Finally, I want to thank my wife, Carol, and my parents; the former for accepting the difficult role of a graduate student's wife including the work and sacrifice which that entails and the latter for instilling in me a desire for a higher education.

## ABSTRACT

### PART I

A method for the analysis of polonium-210 (138.4 day half-life) and lead-212 (10.6 hour half-life) in rocks has been studied. The procedure involves dissolution of the sample and addition of 10 mg. lead carrier. The polonium is separated by spontaneous electrodeposition on a silver-foil disk at room temperature from a 0.5F HCl medium containing 0.05F hydrazine and the alpha-activity from the polonium-210 measured with a scintillation counter. Sodium tartrate is added to the solution remaining from the polonium deposition, the pH raised to 4.7, and the lead-212 deposited with the lead carrier on a second silver-foil disk. The yield of lead is determined gravimetrically and the decaying alpha-activity supported by the lead-212 observed with the scintillation counter. The procedure has been calibrated by using minerals which had been analyzed for lead-210 and thorium-232 by other methods. The effects of temperature, volume, and inhibiting ions on the yield and rate of deposition of polonium were also studied. The procedure was tried on a synthetic uraninite-thorite mixture and on the zircon from the Pacoima Canyon pegmatite. The results indicate that extreme care must be taken to get all material into solution and to avoid high temperatures during fusion of the sample. The weight equivalent uranium found from the polonium-210 analysis on the zircon agreed with the mass spectrometric value for the uranium content to 3.3%.

## PART II

A study has been conducted in order to better characterize the meteorite flux at the earth's orbit with respect to type, mass, direction, and magnitude. A survey of the meteorite data was made by placing the information on punch cards and sorting these cards according to various categories. On the basis of the year of fall, it was noted that the achondrites were more abundant than the irons from 1850 to 1870 and that the reverse was true from 1890 and 1910. No enstatite chondrites fell prior to the 1860's and a large number of this type fell during 1930. A chi-squared test applied to the monthly patterns of fall indicates that the distributions for the veined-hypersthene chondrites, the veined-white hypersthene chondrites, the achondrites, and the howarditic achondrites were those least likely to be random, suggesting that these types may travel in definite orbits. As for the direction of the flux, the hourly patterns are heavily biased toward the daylight hours with no 6:00 maximum as in the case of sporadic meteors. The achondrites display an interesting bimodal distribution during the daylight hours. The magnitude of the flux shows significant variations with year among which the decrease since 1940 appears to be most important. The functional relationship between the rate of meteorite recovery and the rural population density has been investigated and an average value of 1.0 meteorite/10<sup>6</sup> sq. km.-year found for the total flux,  $R_0$ , arriving at the bottom of the atmosphere for the period 1810 to 1950.

## TABLE OF CONTENTS

<u>PART</u>	<u>TITLE</u>	<u>PAGE</u>
I.	A PROCEDURE FOR THE ANALYSIS OF POLONIUM-210 AND LEAD-212 IN ROCKS	
1.	INTRODUCTION . . . . .	1
	The Natural Radioactive Decay Chains . . . . .	1
	Spontaneous Electrodeposition of Polonium . . . . .	6
	Recent Methods for the Separation and Analysis of Radioactive Lead Isotopes . . . . .	13
2.	APPARATUS AND EXPERIMENTAL . . . . .	15
3.	DISCUSSION OF RESULTS . . . . .	33
	Procedure for Polonium-210 . . . . .	33
	Procedure for Lead-212 . . . . .	45
	Alpha-Counting Correction Factors and the Calibration of the Procedure . . . . .	59
	Combined Polonium-210 and Lead-212 Analyses . . . . .	63
	Precision of the Analyses . . . . .	72
4.	SUMMARY . . . . .	74
	REFERENCES . . . . .	77
II.	A CHARACTERIZATION OF THE METEORITE FLUX AT THE EARTH'S ORBIT . . . . .	80
1.	INTRODUCTION . . . . .	81
2.	PUNCH CARD CODING FORMAT AND SURVEYS . . . . .	83
3.	COMPOSITION AND DIRECTION OF THE FLUX AT THE EARTH'S ORBIT . . . . .	89
	Description of the Coordinate Systems . . . . .	89
	Type Composition of the Flux . . . . .	96

<u>PART</u>	<u>TITLE</u>	<u>PAGE</u>
	Mass Composition of the Flux . . . . .	128
	Direction of the Flux . . . . .	136
4.	MAGNITUDE OF THE FLUX . . . . .	151
5.	SUMMARY . . . . .	175
APPENDIX A	. . . . .	178
APPENDIX B	. . . . .	183
REFERENCES	. . . . .	220
PROPOSITIONS	. . . . .	223
REFERENCES FOR THE PROPOSITIONS	. . . . .	254

1. The end products of this decay  
are methods for the long-term dating of geological  
sites ( $2 \times 10^7$  to  $5 \times 10^8$  years) by the uranium-lead, thorium  
and lead-lead procedures (1).

**A PROCEDURE FOR THE ANALYSIS OF POLONIUM-210  
AND LEAD-212 IN ROCKS**

## 1. INTRODUCTION

### The Natural Radioactive Decay Chains

The science of geochemistry has benefited a great deal from the existence of the natural radioactive decay chains. A partial list of geochemical applications must include the following.

1. The end products of their decay, the lead isotopes, provide methods for the long-term dating of geological deposits ( $2 \times 10^7$  to  $5 \times 10^9$  years) by the uranium-lead, thorium-lead, and lead-lead procedures (1).

2. If certain time-related disequilibrium patterns exist among the members of the chains, then these can be used to date uranium deposits if their ages lie between 2,000 and 200,000 years (2).

3. The relative abundances of the chain members in rocks reveal facts concerning the geochemistry of uranium and thorium as well as that of their daughters (3,4).

4. A future use may arise from the fact that uranium and thorium are widely dispersed throughout all rocks. A study of the changes in the state of equilibrium across the weathering zone should yield information concerning weathering processes.

The members of the three chains are shown in Figure 1-1. Several characteristics which are of importance in geochemical applications should be noted.

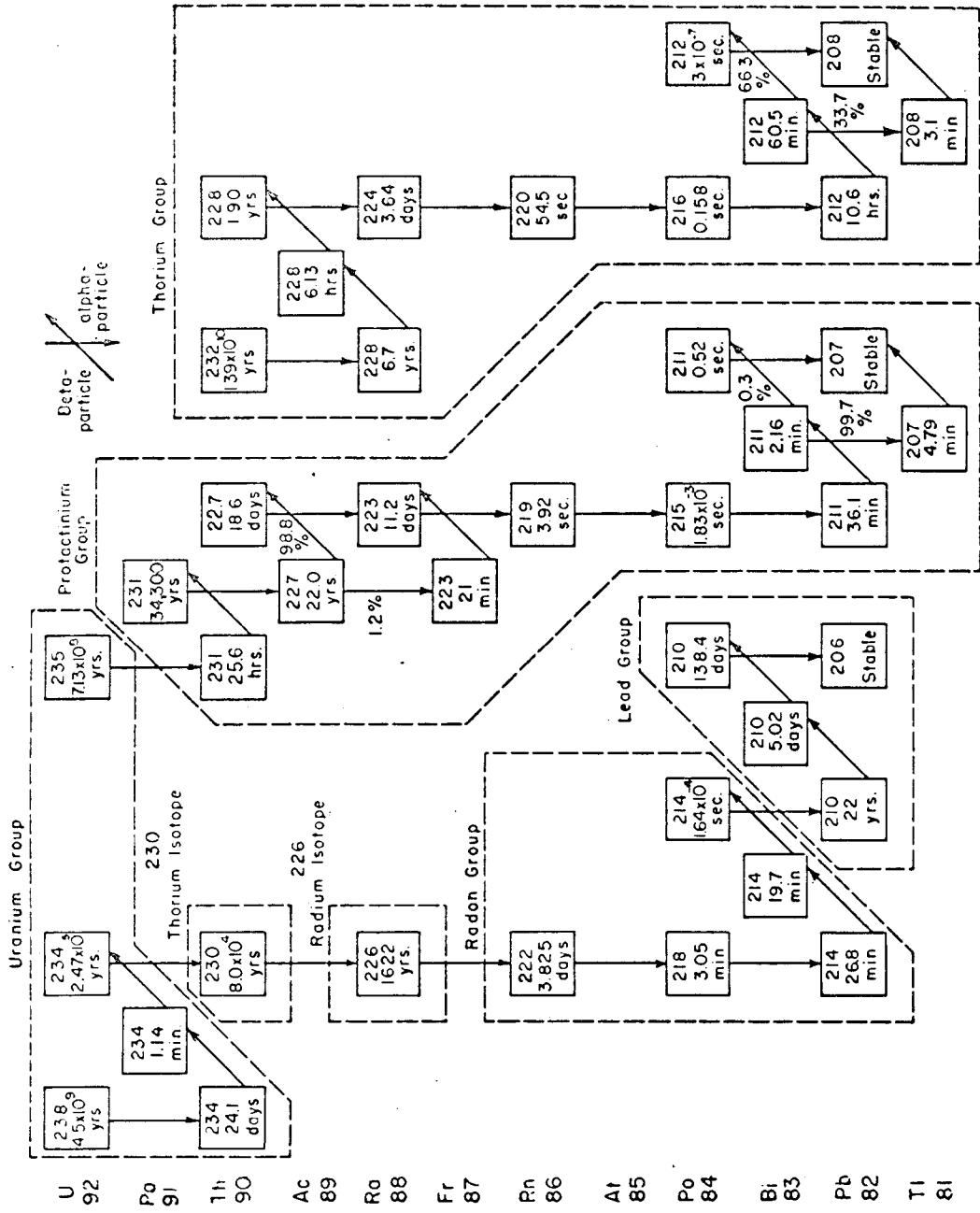


Figure 1-1. The natural radioactive decay chains (5).

(a) The parents of two of the chains are isotopes of the same element, uranium, and thus cannot be separated by geochemical reactions. Therefore, the ratio of uranium-238 to uranium-235 is a constant at any given time and the ratio of the radioactivity per chain member in equilibrium samples must also be a constant. No such relationship exists between the thorium series and either of the two uranium series because the ratio of uranium to thorium can assume any value.

(b) The half-lives of the chain members range from fractions of a second up to billions of years. Within this wide range only uranium-234, thorium-230, radium-226, and protactinium-231 (excluding the chain parents) have half-lives of the magnitude of the units used to measure geologic time. None of these are members of the thorium series. Now the maximum disturbance in the radioactive equilibrium of these chains occurs when all daughters are removed (with the exception of uranium-234 in the uranium-238 series and thorium-228 in the thorium-232 series). Following such a maximum disturbance, the time required for the chains to return to equilibrium is determined by the long-lived daughters in each series. The uranium-238 series requires a length of time on the order of 500,000 years; the uranium-235 series requires 200,000 years; and the thorium series requires 45 years. Thus the thorium series may ordinarily be assumed to be in equilibrium in geological samples.

(c) The only gaseous members of these chains are the isotopes of emanation. The rate of loss of these isotopes through diffusion processes depends upon the type of crystal, the degree of breakdown of the crystal, the temperature, and the initial location of thorium and uranium within the crystal (6). The loss of radon, in particular, is a potential source of disequilibrium in the uranium-238 series.

The disequilibria found in the decay chains in natural systems can be used to study certain geochemical problems. A leader in the study and classification of natural disequilibrium types has been J. N. Rosholt (2,5,7,8,9). His approach, as illustrated in Figure 1-1 is to break the chains down into groups having a parent whose half-life is much longer than those of its immediate daughters. Thus, the group daughters can be assumed to be in radioactive equilibrium with the group parent. A complete study of the disequilibrium present in any sample requires the determination of the quantity of each group present. These data then yield a profile of the disequilibrium in each series in the sample which can be used as a basis for the discussion of the geochemical reasons for this disequilibrium.

The radiochemical procedure employed by Rosholt (5,7) separates at least one member of each group on carrier precipitates. The alpha-activities of these precipitates are then observed as functions of time, any complex decay curves resolved, and the activity of a particular nuclide,

at the time of its chemical isolation from the decay chain, calculated. The lower limits for the determinations of the various groups by this procedure depend upon the uranium/thorium ratio in the sample. Thorium-232 can be determined down to 1 p.p.m. thorium in samples where this ratio is low (5). The reproducibility of the lead-210 analysis is about 8% for samples in which there is 1% uranium (7). In the published analyses of disequilibrium samples (2) the lowest lead-210 content analyzed was 20 p.p.m. equivalent uranium and the lowest radium-228 content was 50 p.p.m. equivalent thorium.

The present study was undertaken to find alternative procedures for the analyses of the lead and thorium groups. As was pointed out above, the thorium series may ordinarily be assumed to be in equilibrium in geological samples. Therefore, the analysis for any member of this group yields the thorium-232 content. In the uranium-238 series the loss of lead group members from a sample can only produce short term disequilibrium. However, because this group comes at the end of the series, an analysis for it is helpful in evaluating the state of equilibrium farther up the chain. This state of equilibrium is affected by the gain or loss of emanation-222 (radon), thorium-230 (ionium), or radium-226 and is of special importance in evaluating age data based on the lead-206 content.

Electroplating procedures naturally suggest themselves as alternatives to precipitation separations because they require a minimum amount of manipulation of the sample solution and yield the radionuclides in a form convenient for counting. In the lead group all of the nuclides may be electroplated but if alpha-counting is to be used, polonium-210 is the best choice. The lead and bismuth nuclides in the thorium group have combinations of half-life and decomposition potential which make them suitable for the determination of this group. The goal originally established for the analytical procedure was the determination of polonium-210 and lead-212 in the p.p.m. range in minerals to  $\pm 10\%$ .

#### Spontaneous Electrodeposition of Polonium

Electrode potentials for polonium and other half-reactions of interest are presented in Table 1-1. By applying the laws of thermodynamics we may conclude that at equilibrium:

1. polonium should deposit spontaneously on metals which form couples whose potentials are more negative than the Po ion/Po(s) couple, and
2. ions of couples having potentials more positive than that for polonium should react before polonium and therefore may interfere with its deposition.

According to the first of these rules, it should be possible to spontaneously electrodeposit polonium from a chloride

TABLE 1-1. Electrode Potentials for the Half-Reactions  
of Polonium and Other Species.

These are standard potentials except where noted.

Solution or Couple	Electrode Potential (V. vs. S.C.E.)	Reference
Po (about $10^{-5}$ F) in 1.0F HCl ( $\text{PoCl}_6^{--}$ , $\text{PoCl}_5^-$ , $\text{HPoCl}_7^-$ ?)	+ 0.23	(10)
Po in HCl + hydrazine	same as $\text{Po}^{\text{IV}}$	(10)
Po ( $10^{-10}$ F) on gold from 0.1F HCl	+ 0.37	(11)
Po (about $10^{-4}$ F) in 1.0F $\text{HNO}_3$ ( $\text{Po}(\text{NO}_3)_5^-$ , $\text{PoO}^{++}$ , $\text{Po}^{++++}$ , etc.)	+ 0.45	(10)
$\text{AuCl}_4^-/\text{Au}(\text{s})$	+ 0.76	(12)
$\text{NO}_3^-/\text{HNO}_2(\text{g})$	+ 0.70	(12)
$\text{PtCl}_4^{--}/\text{Pt}(\text{s})$	+ 0.49	(12)
$\text{FeCl}_4^-/\text{Fe}^{++}$ (1F HCl)	+ 0.46	(12)
$\text{HgCl}_4^-/\text{Hg}_2\text{Cl}_2(\text{s})$ ( $10^{-5}$ F Hg, 0.5F HCl)	+ 0.32	calc. from (12)
$\text{AgCl}(\text{s})/\text{Ag}(\text{s})$ (0.5F HCl)	+ 0.00	calc. from (12)
Au in 0.1F HCl + 0.9F thiourea	- 0.04	(13)
$\text{CuCl}_3^{--}/\text{Cu}(\text{s})$	- 0.06	(12)
$\text{BiCl}_4^-/\text{Bi}(\text{s})$	- 0.08	(12)
$\text{H}^+/\text{H}_2(\text{g})$ (Pt saturated with $\text{H}_2$ in dilute HCl)	- 0.30	(13)
$\text{Ni}^{++}/\text{Ni}(\text{s})$	- 0.48	(12)
$\text{N}_2(\text{g})/\text{N}_2\text{H}_5^+$ (1 atm. $\text{N}_2$ , 0.1F $\text{N}_2\text{H}_6 \cdot 2\text{HCl}$ , 0.5F HCl)	- 0.48	calc. from (12)

medium onto silver, copper, bismuth, nickel, and an H<sub>2</sub>-Pt electrode. Spontaneous deposition onto metals more noble than polonium will not occur in the absence of reducing agents such as hydrogen in the case of platinum, or complexing agents which can lower the electrode potential of the metal, such as thiourea in the case of gold. According to the second rule, the presence of nitrate ion, ferric ion, and the ions of gold, platinum, tellurium, or mercury should interfere with the deposition of polonium.

Bagnall (13) has reviewed the literature on the spontaneous deposition of polonium up to 1956. A more recent application is that of Ancarani and Riva (14) in which they determined polonium in minerals by spontaneous deposition on nickel. The most extensive recent study of the spontaneous electrodeposition of polonium on various metals was conducted to find methods for its determination in biological materials (15,16,17,18). Polonium has also been separated from irradiated bismuth and lead targets by spontaneous deposition on silver (19).

The factors which affect the recovery of polonium on silver from a chloride medium include the effect of stirring, the acidity, the concentration of polonium, the temperature, and the inhibiting effects of certain ions. Smith et al. (15) found that stirring was essential for high recoveries of polonium and that the recovery increased with the concentration of polonium as shown in Table 1-2. However, Black (16)

TABLE 1-2. Recovery of Polonium as a Function of Concentration (15). The polonium was plated from 100 ml. at 90°C. onto silver foil.

<u>Concentration</u> (c.p.m./100 ml.)	<u>Yield</u> (%)
15	89.65
114	90.60
1,061	93.01
10,457	92.44
21,163	93.82
199,713	96.01

found that at low concentrations of polonium (2 to 160 d.p.m./200 ml.) there was no correlation between the concentration and percent recovery of polonium at 94°C. on silver foils.

The recovery has been found to be independent of the HCl concentration as long as this was greater than about 0.1F (13,15). The consensus of opinion of many investigators has been that high temperatures produce smoother deposition and Krebs and Whipple (17) state flatly that high yields on silver can only be obtained at elevated temperatures. These conclusions appear to have been reached without undertaking a detailed study of the deposition as a function of time.

It has been observed that silver metal placed in a chloride solution containing ferric or nitrate ions or the ions of gold, platinum, tellurium or mercury develops a dark surface and that the yield of polonium by spontaneous deposition on the silver decreases (13). Whitaker et al. (20) noted the inhibiting effects of ferric iron and mercury and found that the yield of polonium rose from 38% to 98% when the solutions containing these ions were boiled after saturating with sulfur dioxide. Haissinsky (21) employed hydrazine in 20% HCl as a reducing agent to precipitate the interfering ions of gold, mercury, and platinum as the metal. Bagnall (13) lists methods for dealing with tellurium and

ferric ions. The latter may be reduced to the ferrous state by ascorbic acid, sulfur dioxide or it may be complexed with fluoride ion. Smith et al. (15) made a detailed study of the yield as a function of the ferric ion concentration and their results are presented in Table 1-3. The yield as a function of the concentration of nitric acid was investigated by Black (16) who concluded that a concentration of 0.16F nitric acid was the highest that could be tolerated.

Most investigators who have examined the recovery of polonium on silver and other metals have found it to be less than 100% (14,15,16,19). However, Feldman and Frisch (22) concluded from their experiments, with the successive plating of polonium from the same solution on three separate silver disks, that they were achieving an average of 99.8% recovery on the first plating. But since they used the sum of the activities of the three platings to calibrate their solutions and reported no independent calibration (e.g., evaporation and counting of aliquot portions of the solution) as did at least one other investigator (16), their conclusion must be questioned.

TABLE 1-3. Recovery of Polonium as a Function of the Ferric Ion Concentration (15).

<u>Concentration of Fe<sup>+++</sup></u> (moles/l.)	<u>Yield</u> (%)
0.5 x 10 <sup>-3</sup>	100.4
1 x 10 <sup>-3</sup>	88.9
2 x 10 <sup>-3</sup>	55.8
3 x 10 <sup>-3</sup>	22.0
4 x 10 <sup>-3</sup>	16.7
5 x 10 <sup>-3</sup>	10.4

Recent Methods for the Separation and Analysis of  
Radioactive Lead Isotopes

The half-lives of the radioactive lead isotopes may be found in Figure 1-1. If alpha-counting is performed on the lead separated from a sample containing all three decay chains, the alpha-activity resulting from lead-214 and lead-211 should decay to negligible levels by the time the alpha-activity from lead-212 has grown to complete equilibrium. The growth of alpha-activity supported by lead-210 should remain negligible until the determination of lead-212 is completed.

Rosholt does not directly determine any lead isotopes in his procedure. Recent methods for separating radioactive lead isotopes have employed precipitation, extraction, ion exchange, and electrochemical procedures. Godt and Sommermeyer (23) separated lead-210 from biological materials by precipitation of lead carrier with sulfide. Von Gunten and Ledent (24) and Alberti et al. (25) extracted lead isotopes as dithiozonates while Gorsuch (26) used sodium diethyldithiocarbamate for the extraction of lead-212. Chen and Wong (27), Dedek (28), and Gorsuch (29) have employed ion exchange in the separation of lead isotopes.

Harrison et al. (30) reported an electrochemical procedure for separating bismuth-212 and lead-212. The bismuth-212 plus bismuth carrier were deposited, using cathode potential control, from a 0.5F HCl solution heated to 80-90°C.

The lead-212 and lead carrier were then deposited on a new cathode with no control of the potential. Lingane (12) in his procedures for the controlled-potential cathodic deposition of lead employs a tartrate medium at a pH of 4.5 to 5.0 and room temperature. Ishibashi (31) also used a tartrate medium to successively separate bismuth-212 and lead-212.

## 2. APPARATUS AND EXPERIMENTAL

Spontaneous electrodeposition apparatus for polonium-210.--The apparatus shown in Figure 2-1 was used for the spontaneous electrodeposition of polonium-210. The silver surface to be plated was suspended in the solution by means of the 3.6-mm. diameter glass rod which passed through a hole in the 2.5-inch diameter watch glass. During the temperature studies the heating tape, regulated by a 110 V. Variac, was used to control the solution temperature. At other times the beaker was placed directly on the magnetic stirrer with asbestos between the two to minimize heat transfer from the stirring motor to the solution. The temperature of the solution could be monitored by immersing in it a thermistor which was wired to a voltage supply circuit. The current passed by the thermistor had been calibrated with respect to the temperature. A glass-encased magnetic flea, 1 inch in length, was rotated by the magnetic stirrer to provide stirring action. When the stirring motor Variac was set at 50 (half scale) the flea rotated in the solution at about 500 r.p.m.

Preparation of silver-antimony-glass plating surfaces.--The silver-antimony-glass disks were prepared by vacuum evaporation of antimony followed by silver onto glass disks. These disks were made from 0.05-inch thick soft glass and had diameters of 1.5 inches. A center hole, 0.13 inches in

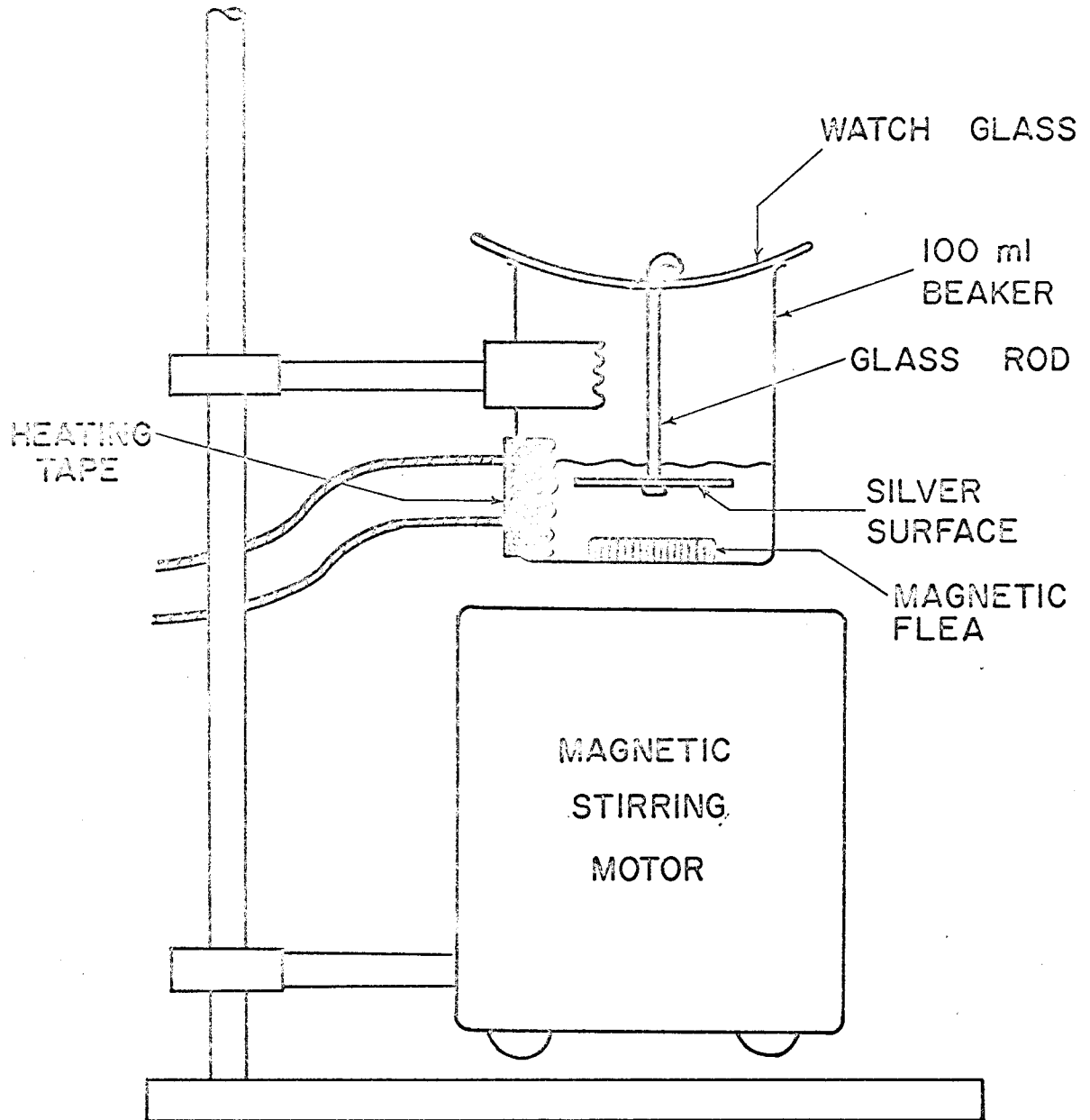


Figure 2-1. Apparatus for the spontaneous deposition of polonium.

diameter, was provided for the suspending glass rod when plating polonium or for the contact screw when plating lead. The glass disks were reused by dissolving the silver and antimony with hot concentrated nitric acid and cleaning with soap and water followed by a 30-minute treatment with 10% potassium hydroxide. These disks weighed about 3 grams.

Preparation of silver-foil disks.--The silver-foil disks were prepared by punching 1.25-inch diameter circles from Matheson, reagent grade silver foil (0.005 inches thick). A 0.13-inch diameter hole was punched in the center of each disk to accommodate the suspending glass rod or the contact screw. When used for plating polonium, the back and edges of each disk were painted with glyptal to prevent deposition on these surfaces. The area of one side of these disks was 7.8 sq. cm. When the disks were glyptalled for the deposition of polonium, this area was reduced to about 7.0 sq. cm. and when they were placed in the plating apparatus, the area exposed for lead plating was also about 7.0 sq. cm. These disks each weighed about 0.8 grams.

Preparation of polonium-210 solutions.--A stock polonium-210 solution was prepared by milking a radium-D-E-F solution. This was done by spontaneous electrodeposition of the polonium-210 from a 0.5F HCl solution onto a silver-plated platinum base at 95°C. The silver and polonium were then dissolved in 1.5 ml. concentrated nitric acid, the

solution diluted to 50 ml., the silver precipitated as silver chloride by adding 2 ml. 0.5F HCl, and this precipitate separated by filtration. The filtrate was evaporated to dryness and 10 ml. of 6F HCl added. The solution was again evaporated to dryness, 1 ml. concentrated HCl added, and the solution returned to 0.5F in HCl by dilution to 25 ml. These plating and precipitation steps were repeated once more to purify the polonium-210 and the final solution diluted to 250.00 ml. in a volumetric flask to give the stock polonium-210 solution (0.5F in HCl). When prepared, this solution had an alpha-activity of about 1700 c.p.m./5 ml. It was used over a period of 2.5 years to prepare working polonium-210 solutions which had alpha-activities of about 70 c.p.m./5 ml. This was done by transferring the required volume of the stock solution by pipet to a 250-ml. volumetric flask, adding an amount of concentrated HCl so that the final solution would be 0.5F in HCl, and diluting to 250.00 ml. with distilled water. The specific activity of the polonium-210 in these working solutions was determined from time to time by evaporating 1-ml. aliquot portions to dryness on the silver plating disks and counting the alpha-activity.

The rate of deposition of polonium as a function of the temperature.--The plating solutions were prepared by transferring 15.00 ml. of the polonium-210 stock solution to a 100-ml. beaker and diluting to 20 ml. with 0.5F HCl.

These solutions contained an alpha-activity of about 130 c.p.m. Each solution was raised to the desired temperature and a silver-foil disk hung in it for a period of time while the 1-inch magnetic flea was rotated at 500 r.p.m. To conclude each plating, the silver-foil disk was removed and the solution adhering to it washed back into the main solution with 1 ml. 0.5F HCl. The disk was rinsed with distilled water and alcohol, air dried, and counted. It was then returned to the solution for additional plating. This process was repeated five times. The final plating was at least 9 hours in length and served to remove all the remaining polonium-210 from solution. The activity on this last plate was assumed to be the "plateable" polonium-210 activity originally present in the solution and was used to calculate the fractions plated out in the previous platings.

The rate of deposition of polonium as a function of the volume.--Each plating solution was prepared by transferring 15.00 ml. of the polonium-210 stock solution to a 100-ml. beaker or, in the case of the 150 ml. solution, to a 200-ml. tallform beaker and diluting to the desired volume with 0.5F HCl. Each solution contained an alpha-activity of about 130 c.p.m. The plating procedure was performed in the same way as the temperature study but at room temperature.

Deposition of lead or bismuth under polonium-210 plating conditions.--Five separate solutions were used in this experiment. The first two of these solutions contained 5.00 ml. of

the thorium-232 solution, had total volumes of 20 ml. and were 0.5F in HCl. No lead carrier was added. A silver-antimony-glass disk was suspended in each stirred solution for 3 hours at room temperature. The disks were then removed, rinsed with 0.5F HCl, dried in a 110°C. oven, and counted.

The third plating solution (4-66-59) contained 10 mg. lead in addition to the thorium-232 solution. The disk used was plated and treated in the same way as the first two disks.

Finally, in order to standardize the thorium-232 solution, two disks (4-65-70, 4-65-77) were electroplated with lead from a 0.5F HCl solution using 10 mg. of the lead carrier and the yield determined gravimetrically.

The effect of hydrazine on the deposition of polonium.--  
The 20-ml. plating solution contained 5.00 ml. of the working polonium-210 solution and was 0.5F in HCl and 0.05F in hydrazine dihydrochloride. Deposition was performed on a silver-antimony-glass disk for 4 hours after which time the disk was removed, rinsed with 0.5F HCl, air dried, and counted.

The effect of mercury, tellurium, platinum, gold, and ferric iron on the deposition of polonium.--Each of the solutions used in this experiment contained 5.00 ml. of the working polonium-210 solution, 0.130 or 0.260 g. of hydrazine dihydrochloride (0.05 or 0.10F respectively) and milligram quantities of the interfering ions: mercury, tellurium,

platinum, gold, or ferric iron. These latter were taken from solutions of mercuric chloride, tellurium dioxide, platinum metal (dissolved in aqua regia, evaporated to dryness, and redissolved in dilute HCl), auric chloride and ferric oxide. A reduction step was used in which the solution was adjusted to 7F (20%) or 0.5F in HCl and heated near the boiling point for periods of time ranging from 10 to 60 minutes. The solution was then adjusted to 20 ml., made 0.5F in HCl and any precipitate which had formed was separated by filtration. Plating was then attempted by suspending silver-antimony-glass disks in the filtrate at room temperature while the solution was stirred at 500 r.p.m.

Controlled-potential electroplating apparatus.--The apparatus used for the controlled-potential electrodeposition of lead is shown in Figure 2-2. The parts were mounted on a Sargent Electroanalyzer which provided the stirring motor. The transistorized potentiostat was designed to control the potential of the working electrode to  $\pm 20$  mV. when the cell current was in the range 0-200 ma. The potential of the working electrode relative to the saturated calomel reference electrode was monitored with the aid of a Beckman Model-G pH Meter as a potentiometer and the cell current recorded using an Esterline-Angus Graphic Ammeter. The mercury pool contact was found necessary to provide low resistance contact between the cathode circuit and cathode assembly which was rotated at about 300 r.p.m. The saturated calomel

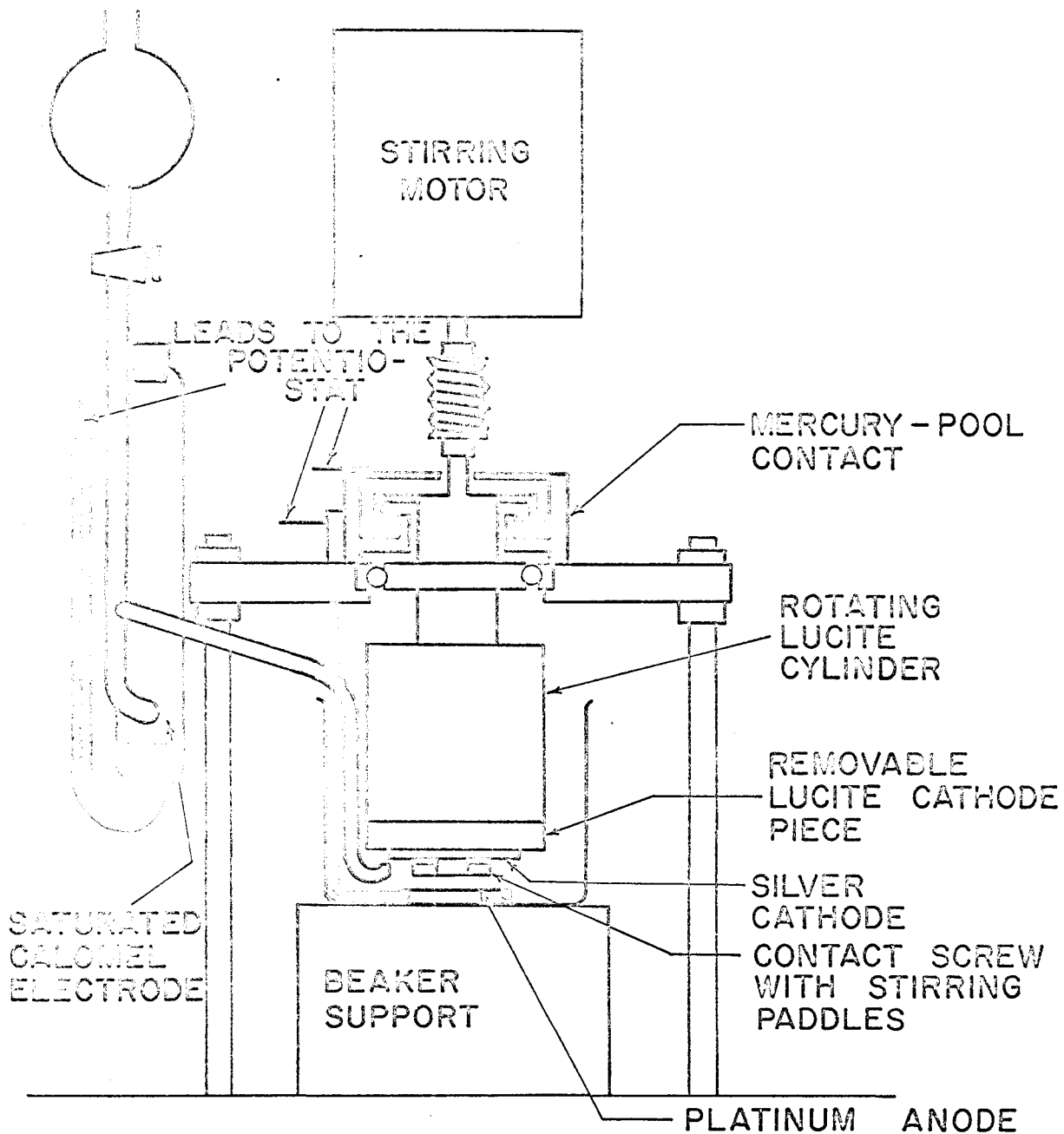


Figure 2-2. Apparatus for the controlled-potential deposition of lead.

electrode arm and the anode could be rotated to allow removal of the lucite cathode piece. The silver-foil disk and glass disk were held in place on the lucite cathode piece by a contact screw. The silver-foil disks were sealed to the glass disks, to prevent plating on the rear side, by a thin ring of stopcock grease around the outside edge.

The typical lead plating procedure began with the weighing of the silver-foil disk which was then placed in the apparatus, the saturated calomel electrode arm and the anode positioned, and the beaker containing the plating solution raised until the solution was above the level of the cathode. The stirring motor was started and plating commenced at the desired cathode potential (-0.70 V. vs. S.C.E.). After 30 minutes, the beaker was quickly lowered (while the stirring motor and the current remained on) and a beaker of distilled water raised into position to flush the cathode free of electrolyte. The lead-plated silver-foil disk was then removed from the assembly, the rear side wiped free of grease with a benzene soaked tissue, the disk rinsed in benzene and then alcohol, and weighed after air drying.

Decomposition potential for lead from a tartrate medium.--

An electroplating solution was prepared containing 5.00 ml. of lead carrier solution (10 mg. lead), 600 mg. sodium tartrate dihydrate, 260 mg. hydrazine dihydrochloride, and 20 ml.

0.5F HCl. The pH was adjusted to 4.8 with 2.4 ml. 5F NaOH. A silver-foil disk cathode was used and the current vs. cathode potential curve was taken by raising the total potential across the cell until the desired current flowed. The cathode potential relative to the saturated calomel electrode was then read on the Beckman Model-G pH Meter.

Preparation of the lead carrier solution.--0.6712 g. of lead chloride (Baker's reagent grade) were dissolved in about 200 ml. of hot distilled water and the pH adjusted to about 4 with very dilute HCl. This solution was then diluted to 250.00 ml. in a volumetric flask giving 10.00 mg. lead/5 ml. The lead concentration was checked by polarography and found to be  $10.0 \pm 0.1$  mg. lead/5 ml.

Preparation of the thorium-232 solution.--0.4020 g. of thorium nitrate (Baker's reagent grade,  $\text{Th}(\text{NO}_3)_4 \cdot 4\text{H}_2\text{O}$ ) were dissolved in 8.3 ml. concentrated HCl and this solution transferred to a 100-ml. volumetric flask where it was diluted to 100.00 ml. with distilled water. The calculated thorium-232 activity was  $2.07 \times 10^3$  d.p.m./5 ml. but due to the absence of radioactive equilibrium the daughter activities were less than this value. Calibration of the thorium nitrate by gamma-spectrometry indicated that the activity of the radium-228 group was  $62 \pm 5\%$  of the equilibrium value. This would mean  $1300 \pm 100$  d.p.m./chain member/5 ml. of solution.

Attenuation of polonium-210 alpha-radiation by electro-chemically deposited lead.---A silver-foil disk was placed in the lucite cathode piece and polonium-210 deposited from 20 ml. of the stock polonium-210 solution (about 170 c.p.m.). The disk was then removed, cleaned of grease, rinsed in alcohol, dried and weighed.

A lead plating solution was prepared from 20 ml. 0.5F HCl, 260 mg. hydrazine dihydrochloride, and 600 mg. sodium tartrate dihydrate. The pH was adjusted to 4.8 with about 2.2 ml. 5F NaOH. 2.00 or 5.00 ml. quantities of the lead carrier solution (4 and 10 mg. of lead respectively) were transferred to this solution by pipet before each plating of lead. The procedure for depositing the lead was begun by mounting the silver-foil disk (containing the polonium-210 and any previously deposited lead) in the lucite cathode piece. The lead was then deposited at a cathode potential of -0.70 V. vs. S.C.E. for at least 1 hour and the disk removed, cleaned of grease, rinsed in alcohol, dried, weighed and counted. This procedure was repeated five times.

Polarographic determination of lead plating yield.---Three plating solutions were prepared containing 20 ml. 0.5F HCl, 5 ml. distilled water, 600 mg. sodium tartrate dihydrate, 260 mg. hydrazine dihydrochloride and 5.00 ml. lead carrier solution (10 mg. lead). The pH of each solution was adjusted to 4.6 with 5F NaOH prior to plating. The lead was deposited at a cathode potential of -0.70 V.

vs. S.C.E. for 20 minutes, 30 minutes, and 40 minutes respectively and the lead yields determined gravimetrically. The volume of electrolyte remaining from each plating was reduced to less than 50 ml. and then adjusted to 50.00 ml. with distilled water in a volumetric flask. The amount of undeposited lead in these solutions was determined polarographically by comparing the wave height for each solution to that of a standard solution prepared by the same procedure as the original three solutions.

The lead plated silver-foil disks were stripped of lead with concentrated nitric acid. The resulting solutions were evaporated to dryness, the residue redissolved in 30 ml. 0.5F nitric acid, and any silver, which had dissolved during stripping, was deposited electrogravimetrically on platinum gauze at a cathode potential of +0.30 F. vs. S.C.E. The completeness of removal of silver was determined by withdrawing several drops of solution and adding HCl. The lead dioxide, which deposited on the anode during electrolysis, was removed with dilute HCl and combined with the nitrate electrolyte. A small silver chloride precipitate usually appeared at this point. The combined solutions were taken to dryness and the residue, except for the silver chloride, redissolved in 0.1F HCl. The volume was then adjusted to 50.00 ml. with additional 0.1F HCl. The lead in these solutions was determined polarographically using comparison standards.

Analysis of the Katanga pitchblende for polonium-210.--

0.0199 g. of the pitchblende were treated with 5 ml. aqua regia, warmed 30 minutes and evaporated to dryness. This treatment was repeated with a second 5 ml. portion of aqua regia and finally with 2 ml. concentrated HCl. 5 ml. 0.5F HCl were added and a crystalline white precipitate, which had been present since the aqua regia treatment, was separated by filtration. The alpha-activity of this precipitate on the filter paper was found to be about 13 alpha-c.p.m. or less than 1% of the activity per chain member for the total sample. The filtrate was diluted to 50.00 ml. with 0.5F HCl in a volumetric flask.

The polonium from 5.00-ml. aliquot portions of this solution was deposited for 11 to 14 hours on silver-foil disks and the alpha-activity determined.

Analysis of the Kivu thorite for lead-212.--5 to 10 mg.

samples of the thorite were weighed out, 5.00 ml. of the lead carrier solution added to each, and these solutions evaporated to dryness. Each residue was treated twice with 2 ml. aqua regia, warmed 30 minutes and evaporated to dryness. This treatment was repeated once more with 1 ml. concentrated HCl and the residue from this last evaporation dissolved in 20 ml. 0.5F HCl. In each solution a very small white precipitate remained but was ignored. 260 mg. hydrazine dihydrochloride and 600 mg. sodium tartrate dihydrate were added and the pH adjusted to 4.7 with 5F NaOH.

The lead was deposited at -0.70 V. vs. S.C.E. for 30 minutes from each sample and the alpha-activity determined.

Separation of polonium-210 and lead-212 from synthetic mixtures.--Several separate experiments were performed on synthetic mixtures of the polonium-210 and thorium-232 solutions. The various treatments given these solutions are listed below.

5-11-1: 5.00-ml. aliquot portions of a diluted polonium-210 working solution and of the thorium-232 solution were mixed, 5.00 ml. lead carrier solution added, and the volume adjusted to 20 ml. with 0.5F HCl. The polonium was deposited on 2 separate silver-antimony-glass disks. 600 mg. sodium tartrate dihydrate were added and the pH adjusted to 4 with 5F NaOH. The lead carrier was then deposited on a third silver-antimony-glass disk and the yield determined gravimetrically.

5-11-2: 5.00-ml. aliquot portions of a diluted polonium-210 working solution and of the thorium-232 solution were mixed and evaporated to dryness. 2 g. sodium peroxide were added to the residue, these combined solids dissolved in 10 ml. 20% HCl and taken once more to dryness. The residue was dissolved in 3 ml. 20% HCl, 260 mg. hydrazine dihydrochloride added and the solution carried through a reduction step in which it was heated 1 hour near the boiling

point and then evaporated to dryness. The residue was taken up with 15 ml. 0.5F HCl, 5.00 ml. lead carrier solution added, and the polonium and lead deposited as with solution 5-11-1.

5-11-3 and 4: These solutions were prepared and treated in the same way as 5-11-2 with the exception that no sodium peroxide was added. In addition, these solutions contained 2 mg. ferric iron plus 0.1 mg. each of mercury, tellurium, platinum, and gold. After the reduction step, the solutions were warmed until the yellow ferric ion had disappeared (about 15 minutes).

Preparation of the uranium-thorium solution.--0.0259 g. of the Happy Jack uraninite (GS/64/51) were treated with boiling aqua regia for 15 minutes yielding a solution plus five or six white particles which remained undissolved. The solution was carefully evaporated to dryness and the residue treated with 2 ml. concentrated HCl and 41 ml. distilled water giving a 0.5F HCl solution which was left for several days. After this period the solution was filtered through paper which was later found to have an alpha-activity of about 3 c.p.m. or about 0.1 c.p.m./5 ml. of final solution.

0.1223 g. of the Kivu thorite were treated with 20 ml. aqua regia for 1 hour giving a solution plus an amorphous white precipitate and some brown particles. The solution was carefully evaporated to dryness, 2 ml. concentrated HCl added, and the solution again taken to dryness. The residue

was taken up in 2 ml. concentrated HCl and 41 ml. distilled water giving a 0.5F HCl solution which was left for several days. The clear solution was removed from the now crystalline white precipitate by decantation and the precipitate treated again with 45 ml. 0.5F HCl. This solution was filtered and the filtrate combined with the main solution. Alpha-counting of the filter paper showed 40 c.p.m. or about 0.8 c.p.m./5 ml. of final solution.

The solutions of uraninite and thorite were combined and diluted to 250.00 ml. with 0.5F HCl in a volumetric flask. An analysis for the uranium in this combined solution was performed by Dr. Silver using the isotope dilution method. The analysis showed 0.000372 g. uranium/5 ml. of solution.

Preparation of the Pacoima zircon solution (5-38-1).--

1.8478 g. of the zircon were fused in four separate portions for 10 minutes in nickel crucibles. 2.5 g. of sodium peroxide were used for each portion. In each case the solidified melts were treated with 10 ml. 1.5F HCl and transferred to the same beaker where the solution was made acidic by slowly adding 25 ml. concentrated HCl and evaporated to dryness. The residue was taken up in 0.5F HCl leaving a crystalline precipitate and an amorphous silica precipitate. These were allowed to settle 9 days, then separated from the solution by centrifugation and transferred to a filter paper, which was then ashed leaving a 2.240 g. residue. Semi-quantitative

spectrographic analysis indicated that zirconium and silicon were the major constituents and alpha-counting showed negligible activity. The solution was transferred to a volumetric flask and diluted to 100.00 ml. with 0.5F HCl.

Preparation of the Pacoima zircon solution (7-63-1).--

0.6564 g. of the zircon were mixed with 1 g. of sodium hydroxide pellets and 4 g. sodium peroxide. This mixture was fused for 10 minutes in a nickel crucible. The solidified melt was treated with 10 ml. 1.2F HCl and transferred to a beaker. Roughly 10% of the zircon appeared to be unaffected and was treated a second time with a fusion mixture composed of 2 g. sodium peroxide and 1 g. sodium hydroxide. The solidified melt from this fusion was treated with an additional 14 ml. 1.2F HCl and combined with the first solution. The pH was adjusted to 1.0 with concentrated HCl. The silica precipitate was separated by centrifugation and transferred to a Teflon beaker where the silica was separated by distillation by adding 12 g. perchloric acid and 25 g. hydrofluoric acid and warming. The residue from this distillation was taken up in 0.5F HCl. A very slight residue, which appeared to be unattacked zircon, remained undissolved. This solution was combined with the main solution and diluted to 500.00 ml. with 0.5F HCl in a volumetric flask. The resulting solution was free of any appreciable colloidal material as evidenced by the absence of a Tyndall beam.

Dithizone extraction of lead carrier from solutions of the Pacoima zircon.--To the 170-ml. solutions remaining after the deposition of polonium, were added 25 ml. 25% ammonium citrate solution, 2 ml. 1% potassium cyanide--5% ammonium hydroxide solution and 12 ml. 20% ammonium hydroxide bringing the pH to about 9. The lead was then extracted with 70 ml. chloroform containing 15 mg. diphenylthiocarbazon (dithizone). 60 ml. 0.1F HCl were used to back extract the lead and the chloroform-dithizone phase was recycled seven times between these two aqueous solutions while the pH of each solution was maintained at its initial value. Finally, all the dithizone was removed from the 0.1F HCl solution (which now contained the lead) by extraction with fresh chloroform.

The volume of the 0.1F HCl solution was reduced to about 40 ml. by evaporation and 260 mg. hydrazine dihydrochloride and 600 mg. sodium tartrate dihydrate added. The pH was adjusted to 4.7 with 5F NaOH and the lead deposited by controlled-potential electrolysis.

### 3. DISCUSSION OF RESULTS

#### Procedure for Polonium-210

The plating apparatus used for the spontaneous electro-deposition of polonium-210 is shown in Figure 2-1. Several varieties of silver surface were used. These surfaces had to conform to the following polonium and lead plating and counting specifications.

1. They had to have sufficient mechanical strength to survive the cleaning, plating, and rinsing procedures.
2. They had to weigh less than 2 grams to allow determination of the weight of a 10 mg. lead deposit to 1% (assuming the weighing is good to one part in 20,000).
3. They had to possess cylindrical symmetry for alpha-counting.
4. They had to be free from irreproducible surface characteristics that could alter the decomposition potentials of polonium or lead.
5. They had to have as large an area as possible (limited, of course, by the dimensions of the plating apparatus and counting detector) in order to shorten the plating time.
6. They had to allow plating on only one surface in order to eliminate the need to count two surfaces.

Two types of silver surface came closest to fulfilling these requirements. The first was prepared by the vacuum evaporation of a thin layer of antimony followed by a thicker layer of silver onto soft glass disks (about 0.2 mg./sq. cm.). These were referred to as silver-antimony-glass disks. The antimony served to bond the silver to the glass and allowed the surface to survive the chemical and mechanical rigors of immersion in the stirred 0.5F HCl polonium plating solutions. The antimony must have been protected by the silver from chemical attack or the 0.5F HCl would have quickly removed it. This method of preparation provided reproducible plating surfaces and eliminated the need for preliminary cleaning. The disks each weighed about 3 grams and were very inexpensive because 30 or more could be prepared at one time from a small quantity of silver. However, after about 5 repeated uses of the same glass disks, the newly evaporated silver surfaces were no longer strong enough to withstand the 0.5F HCl and the use of this type of surface was discontinued.

The second type of silver surface consisted of disks punched from reagent grade silver foil. These naturally possessed the required mechanical strength but needed greasing or painting to prevent plating on the rear surfaces. Each disk weighed only 0.8 grams.

The experiments performed were designed to determine:

1. the rate of deposition of polonium as a function of the temperature of the solution;
2. the rate of deposition of polonium as a function of the volume of the solution;
3. whether any lead or bismuth codeposit with the polonium;
4. the effect of hydrazine on the deposition of polonium; and
5. methods for eliminating the inhibiting effects of mercury, tellurium, platinum, gold, and ferric iron.

If the rate of deposition of polonium is diffusion limited, it should be given by the first order equation

$$\frac{dC}{dt} = - \frac{DA}{Vd}C, \quad (3-1)$$

where D is the diffusion coefficient of the reacting species of polonium, A is the area of the deposit, V is the solution volume, d is the thickness of the diffusion layer, and C is the bulk concentration of the polonium (12). Bagnall (13) gives the expression

$$\frac{dx}{dt} = \frac{DA}{Vd}(x_0 - x) \quad (3-2)$$

for the rate of deposition of polonium from 0.7% nitric acid solution.  $x_0$  is the initial amount of polonium in solution

and  $x$  is the amount deposited. Dividing  $x$  and  $x_0$  by the volume produces equation 3-1. Haissinsky (32) presents the relationship

$$\frac{dx}{dt} = a(x_0 - x) - bx \quad (3-3)$$

where  $a$  and  $b$  are constants related to the probabilities for ionic discharge and for dissolution of the deposited atoms respectively. This equation is said to fit curves for the cathodic deposition of polonium at a concentration of  $10^{-9}F$  onto gold from  $0.5F$  nitric acid, the cathodic deposition of polonium from an alkaline medium, and the anodic deposition of polonium from an acidic medium. Integration of equation 3-1 between  $t = 0$  and  $t$  gives the expression relating the fraction of polonium remaining unplated,  $C_t/C_0$ , to the deposition time,  $t$ ,

$$\ln (C_t/C_0) = - \frac{DA}{Vd} t . \quad (3-4)$$

Two separate experiments were performed in order to determine: a) the time to plate one-half of the original polonium,  $t_{1/2}$ , and b) values for  $DA/Vd$  and  $D/d$  as functions of the temperature and volume. The results of these experiments are shown in Figure 3-1 and 3-2 and in Tables 3-1 and 3-2. The fraction remaining unplated at any time was calculated on the basis of the total amount finally plated, while the fractional yield was calculated from the amount of polonium

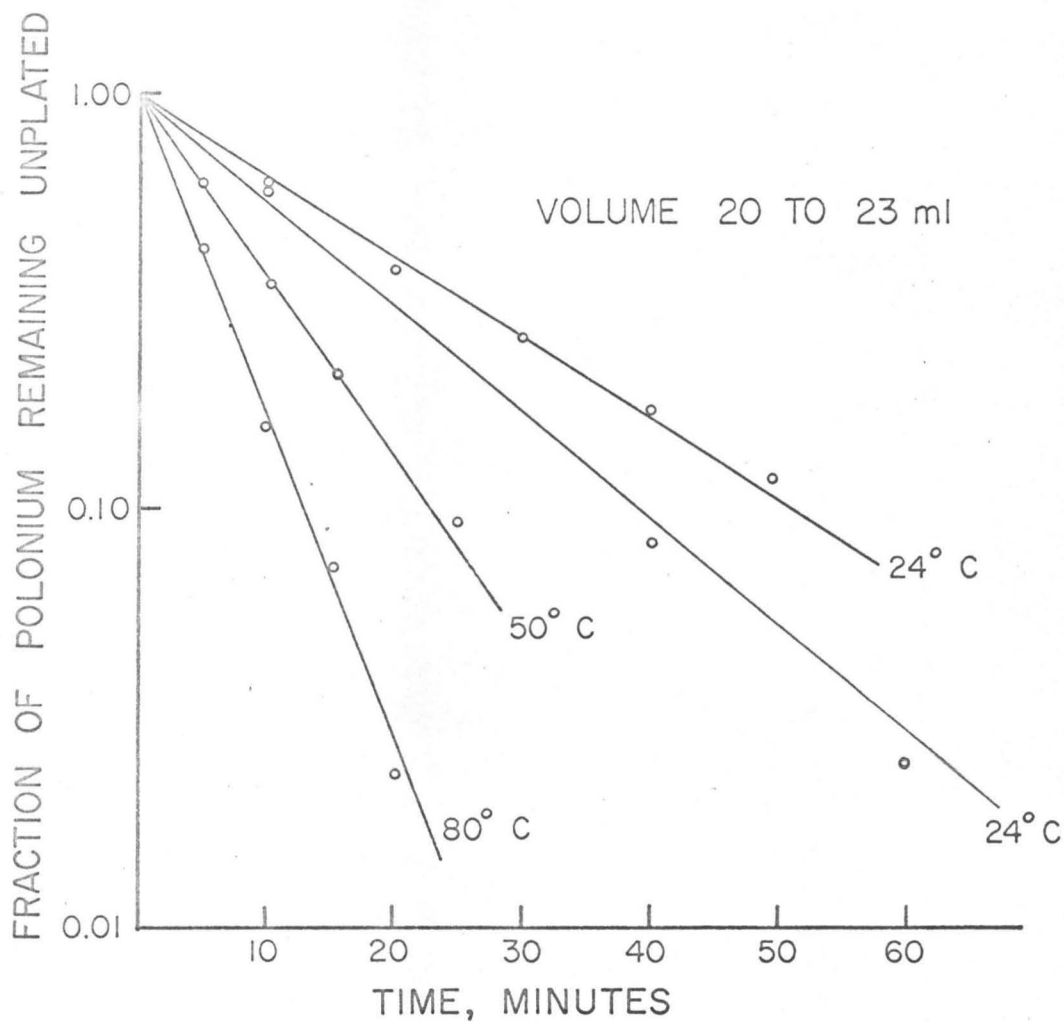


Figure 3-1. Rate of deposition of polonium as a function of the temperature.

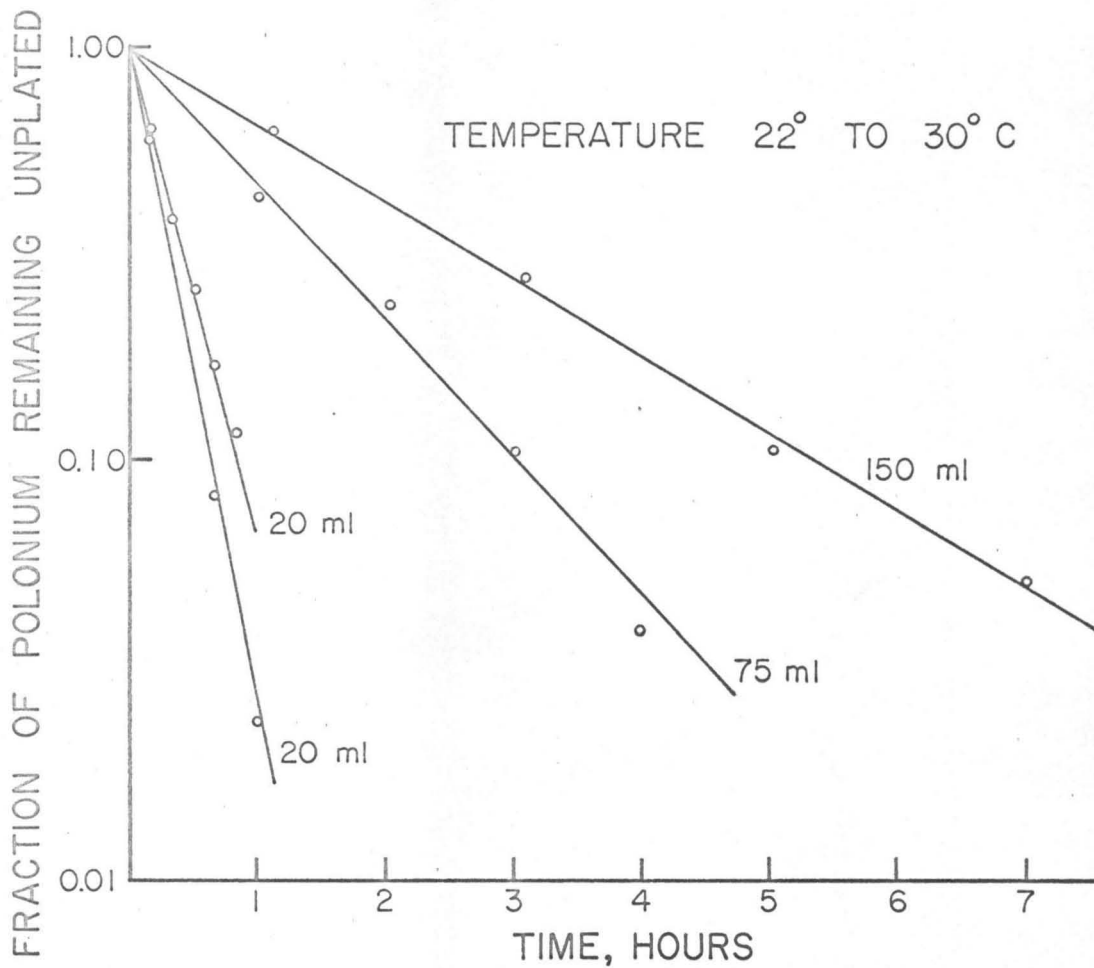


Figure 3-2. Rate of deposition of polonium as a function of the volume.

TABLE 3-1. Deposition of Polonium-210  
as a Function of the Temperature.

volume range = 20 to 23 ml.

<u>Disk No.</u>	<u>Temperature Range (°C.)</u>	<u>t<sub>1/2</sub> (hours)</u>	<u>DA/Vd (l/hour)</u>	<u>D/d (cm./hour)</u>	<u>Fractional Yield</u>
7-5-1 Po	23°-26°	0.20	3.5	10.5	0.94
7-8-3 Po	24°-26°	0.25	2.8	8.4	0.95
7-5-2 Po	49°-51°	0.12	6.0	18.0	0.93
7-5-3 Po	79°-81°	0.06	10.7	32.1	0.94

is caused by differing distances between the rot...

TABLE 3-2. Deposition of Polonium-210 as a Function of the Volume.

temperature range = 22° to 30°C.

The data under "Fractional Yield" indicate

<u>Disk No.</u>	<u>Volume Range (ml.)</u>	<u>t<sub>1/2</sub> (hours)</u>	<u>DA/Vd (1/hour)</u>	<u>D/d (cm./hour)</u>	<u>Fractional Yield</u>
7-8-1 Po	150-153	1.60	0.43	9.3	0.93
7-8-2 Po	75- 79	0.90	0.77	8.5	0.94
7-8-3 Po	20- 24	0.25	2.8	8.8	0.95
7-5-1 Po	20- 23	0.20	3.5	11.0	0.94

originally present as determined by evaporation of aliquot portions of the polonium solution.  $D/d$  in Table 3-2 is not constant with volume but this may be explained by variations in  $d$  caused by differing distances between the rotating magnetic flea and the silver surface. The values for  $t_{1/2}$  allow estimation of the time to quantitatively plate the polonium-210 which is available for plating (i.e., about six times  $t_{1/2}$ ). The data under "Fractional Yield" indicate that the yield of polonium in this concentration range is independent of the volume or the temperature of the solution. The location and state of the unplated polonium remains uncertain.

The results of experiments performed to determine the extent to which trace quantities of lead or bismuth deposit onto silver from 0.5F HCl are shown in Table 3-3. "Activity at  $t = 0$ " refers to the value of the lead-212 transient equilibrium curve when extrapolated to the time of removal from the solution. These results indicate that 0.5% or less of the available lead-212 or bismuth-212 plated out when no lead carrier was present and that only 0.2% plated out when 10 mg. of lead carrier were added. Thus codeposition of lead and bismuth with polonium-210 becomes a problem only when the ratio of the activity of the radium-228 group to that of the lead-210 group in the sample is very large. Even when these conditions prevail, the lead-212

TABLE 3-3. Deposition of Lead or Bismuth  
from 0.5F HCl onto Silver.

<u>Disk No.</u>	<u>10 mg. Pb Carrier</u>	<u>Plating Time (hours)</u>	<u>Activity at t = 0 (c.p.m.)</u>	<u>Fraction of Total Activity Plated</u>
4-66-68	no	3	1.0 ± 0.2	0.0028
4-66-41	no	3	1.7 ± 0.3	0.0046
4-66-59	yes	3	0.7 ± 0.1	0.0018
4-65-70 (standard)			362 ± 3.3	
4-65-77 (standard)			362 ± 3.2	

and bismuth-212 will have decayed to negligible levels within several days following deposition and the polonium-210 activity can then be determined.

The effect of hydrazine on the deposition of polonium-210 had to be determined because of its presence after certain reduction steps which will be discussed below. A recovery of 96% of the polonium-210 was achieved when hydrazine was present at a concentration of 0.05F as compared to 95% when it was absent. Thus the effect of the hydrazine is seen to be negligible.

As discussed in the Introduction, most of the methods devised to deal with substances which inhibit the deposition of polonium involve their reduction to a less troublesome oxidation state. A series of experiments was performed to devise a method for removing the inhibiting effects of mercury, tellurium, platinum, gold, and ferric iron by the use of hydrazine alone. The results of these experiments are summarized in Table 3-4. The absence of yellow color was accepted as an indication that the iron had been reduced to the ferrous state. Solutions 1, 2, 3, and 7 demonstrate that complete reduction of the ferric iron can take place only after dilution of the 7F HCl to 0.5F. If this procedure is followed, approximately 2 mg. of ferric iron per 30 ml. of solution ( $10^{-3}$ F) can be tolerated. Solutions 4, 5, 6, and 7 indicate that a mixture of 0.2 mg. (or more) each of mercury, tellurium, platinum, and gold definitely inhibits polonium deposition

TABLE 3-4. Interference by Mercury, Tellurium, Platinum, Gold, and Ferric Iron in the Deposition of Polonium-210.

Solution	Weights of Reagents (mg.)				HCl Concentration During Reduction	Heating Time During Reduction (min.)	Solution Color After Reduction	Total Po Deposition Time (hours)	Fractional Recovery of Po-210
	Hg	Te	Pt	Au Fe <sup>+++</sup> Hydrazine					
1				10	260	7F	60	3	0.21
2				10	130	0.5F	10	0.8	0.92*
3				2	130	0.5F	10	2.5	0.98*
4	2	2	2	3	130		no reduction step	3	0.18
5	2	2	2	2	260	0.5F	30	19	0.26
6	1	1	1	1	260	7F 0.5F	50 10	2	0.92
7	.2	.2	.2	.2	260	7F 0.5F	60 20	2.8	0.96

Solutions 2-6 : 5.00 ml. Po-210 working soln., 5.00 ml. Th-232 soln., 10 mg. Pb carrier.  
 Solutions 1,7,8: 5.00 ml. Po-210 working soln.

\*The platings were made on 2 separate silver-antimony-glass disks and the value for "Fractional Recovery" is the sum of the figures for these 2 disks.

even though the reduction procedure in 7F HCl is followed. The tolerable amount of any of these elements is much higher than that normally encountered in rock analyses and therefore these elements should cause no trouble. In all cases where low yields of polonium were obtained, the silver surface was blackened; thus the criterion used to establish whether the hydrazine reduction step was required was the presence of darkening of the silver surface. When the reduction step was required, the procedure followed was to heat the 7F HCl solution saturated with hydrazine dihydrochloride for 30 minutes near the boiling point, cool it slowly, and separate any precipitate by centrifugation or filtration. The solution was then diluted with distilled water until the HCl concentration was reduced to 0.5F, warmed until colorless, and the polonium deposited at room temperature for a length of time determined by the volume of the solution. It was most convenient to plate overnight and then perform the lead-212 analysis early the next day.

#### Procedure for Lead-212

The electroplating apparatus used to plate lead had to incorporate the following features:

1. some provision for stirring the solution;
2. dimensions which would keep the volume of the solution as low as possible (to shorten plating time);

3. an arrangement allowing removal of the electroplated disk for weighing and counting; and
4. a reference electrode to monitor the potential of the working electrode and a potentiostat which could control that potential to  $\pm 0.20$  volts.

These features were added to a Sargent Electroanalyzer as shown in Figure 2-2. Cathode potential control was required to prevent hydrogen evolution which not only produces rough lead deposits but, in this apparatus, can block the electrode completely if large bubbles form.

The plating procedure outlined by Lingane (12) was modified for use under the present conditions. After plating the polonium, the 0.5F HCl solution containing 0.05F hydrazine and 10 mg. lead carrier was made 0.1F in sodium tartrate and the pH adjusted to 4.5-5.0 with 5F NaOH. The current vs. cathode potential curve of such a solution taken with the present apparatus is shown in Figure 3-3. On the basis of this curve, a cathode potential of -0.70 V. vs. S.C.E. was chosen for plating the lead.

A lead carrier solution containing 10.0 mg. lead/5 ml. was prepared. In addition, a solution of thorium nitrate was prepared as a source of lead-212.

A series of experiments was performed in order to determine:

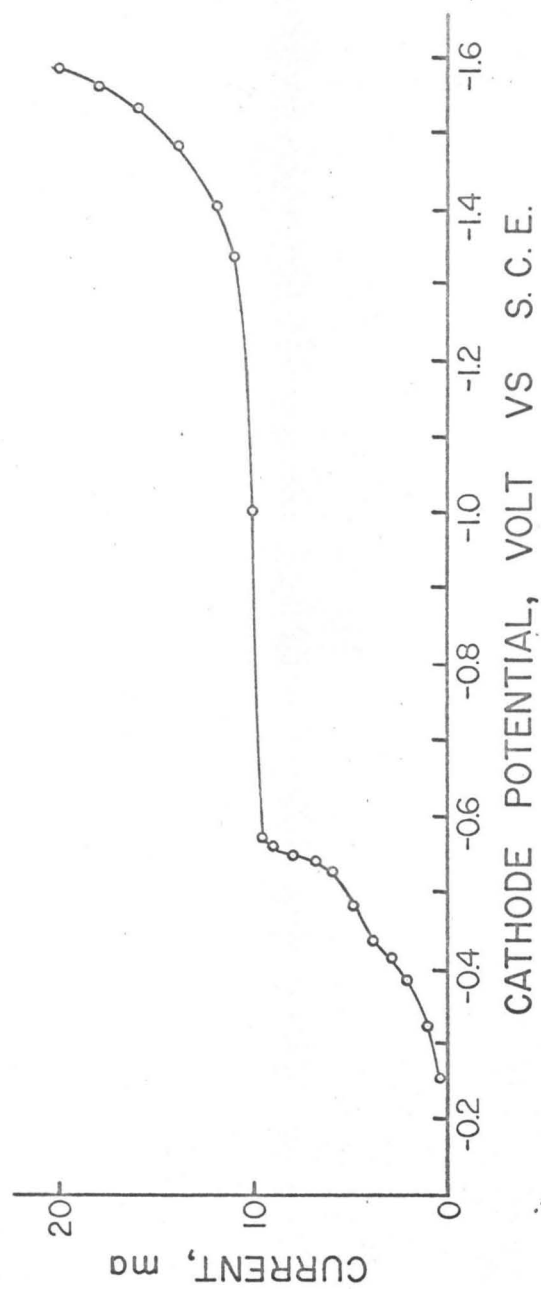


Figure 3-3. Current vs. cathode potential curve for lead from a tartarate medium. pH = 4.5 to 5.0.

1. the fractional attenuation by the lead carrier of the alpha-activity from bismuth-212 and polonium-212; and
2. the reliability of the gravimetric method for determining the yield of lead carrier.

As illustrated in Figure 3-4, the thickness of the lead layer through which alpha-particles must pass to reach a detector determines the average fractional solid angle,  $f_a$ , subtended by that detector. For alpha-particles of a particular energy emitted at a depth,  $x$ , in a layer of lead, there must exist a maximum path length,  $L$ . Alpha-particles travelling the distance  $L$  arrive at the detector with zero kinetic energy having expended their initial energy in penetrating the lead and air.

The equation relating  $L$  to the known parameters of the system is

$$\frac{1}{L} = \frac{\rho_{\text{air}}}{R_{\text{air}}} \frac{\epsilon'}{\epsilon} + \frac{1}{SR_{\text{air}}} \frac{mg \text{ Pb}}{A} \quad (3-5)$$

where  $R$  refers to the range,  $\rho$  is the density,  $\epsilon' = R'_{\text{Pb}}/R'_{\text{air}} = 3.15 - 0.64 \log (E'/4) - (0.41/R'_{\text{air}})$  (primed quantities denote residual values remaining after emergence from the lead into the air),  $\epsilon = 3.15 - 0.64 \log (E/4) - (0.41/R_{\text{air}})$ , and  $mg \text{ Pb}/A$  is the areal density of lead,  $x\rho_{\text{Pb}}$ . The curves for this function for the alpha-particle energies corresponding to polonium-210, bismuth-212, and polonium-212 are shown in Figure 3-5. They deviate very little from straight lines.

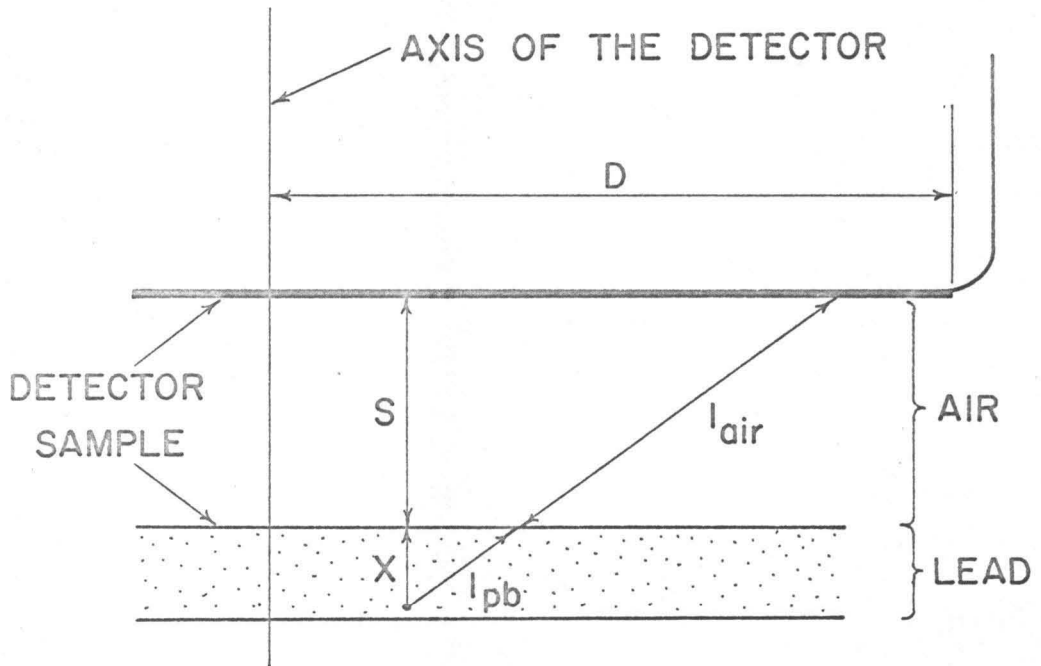


Figure 3-4. Counting geometry for alphas passing through lead. For the situation under discussion:

$$L = l_{Pb} + l_{air} \approx l_{air},$$

and  $s \gg x$ .

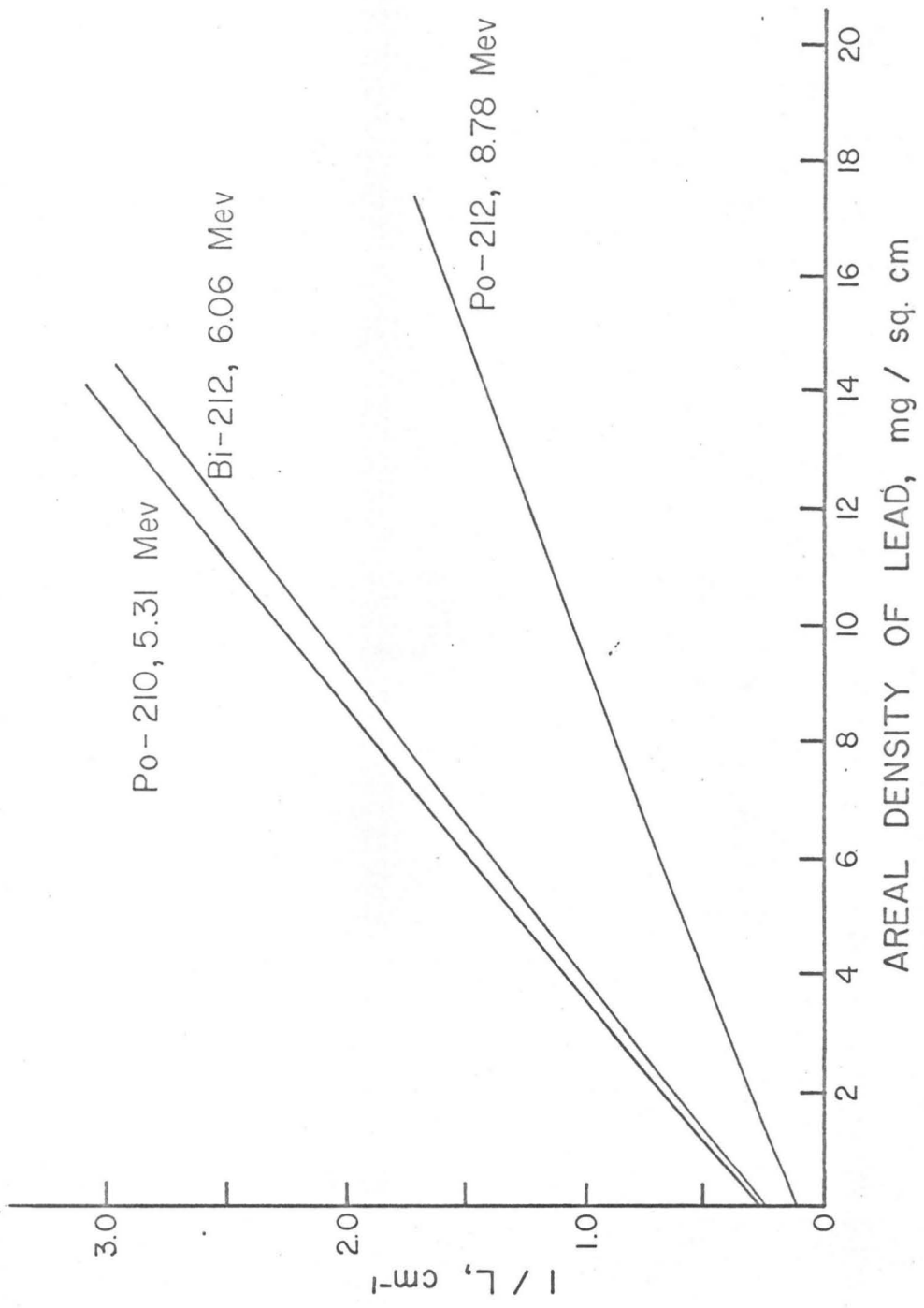


Figure 3-5. The reciprocal of L as a function of the areal density of lead.

over the region of areal density under consideration (i.e., less than 5 mg./sq. cm.).

Knowing  $1/L$  and measuring or assuming values for  $S$  and  $D$  allows the calculation of  $f_a$ . Curves for  $f_a$  vs.  $L$  and  $1/L$  are shown in Figures 3-6 and 3-7. The precise calculation of  $f_a$  is impossible because of the difficulty in measuring  $S$  and  $D$  accurately. The linear portion of the  $f_a$  vs.  $1/L$  curve can be described by the equation

$$f_a = (0.5 S)(1/L) + b \quad (3-6)$$

for which the slope is  $0.5S$ . The data from Figures 3-5, 3-6 and 3-7 were combined to yield the curves, shown in Figure 3-8, of  $f_a$  vs. mg. lead for polonium-210 on several areas. It should be noted that for each area, there is a characteristic slope for the linear portion of the curve. This slope is independent of  $S$  because if equation 3-5 is substituted into equation 3-6,

$$\begin{aligned} \text{slope} &= (0.5 S) (1/SR_{\text{air}}^{\epsilon A}) \\ &= (0.5)/R_{\text{air}}^{\epsilon A}. \end{aligned}$$

A plating experiment was performed in which the activity due to an initial deposit of polonium-210 was measured as a function of the weight of lead plated over it. Now

$$(\text{measured activity, c.p.m.}) = f_a \times f_d \times (\text{true activity, d.p.m.})$$

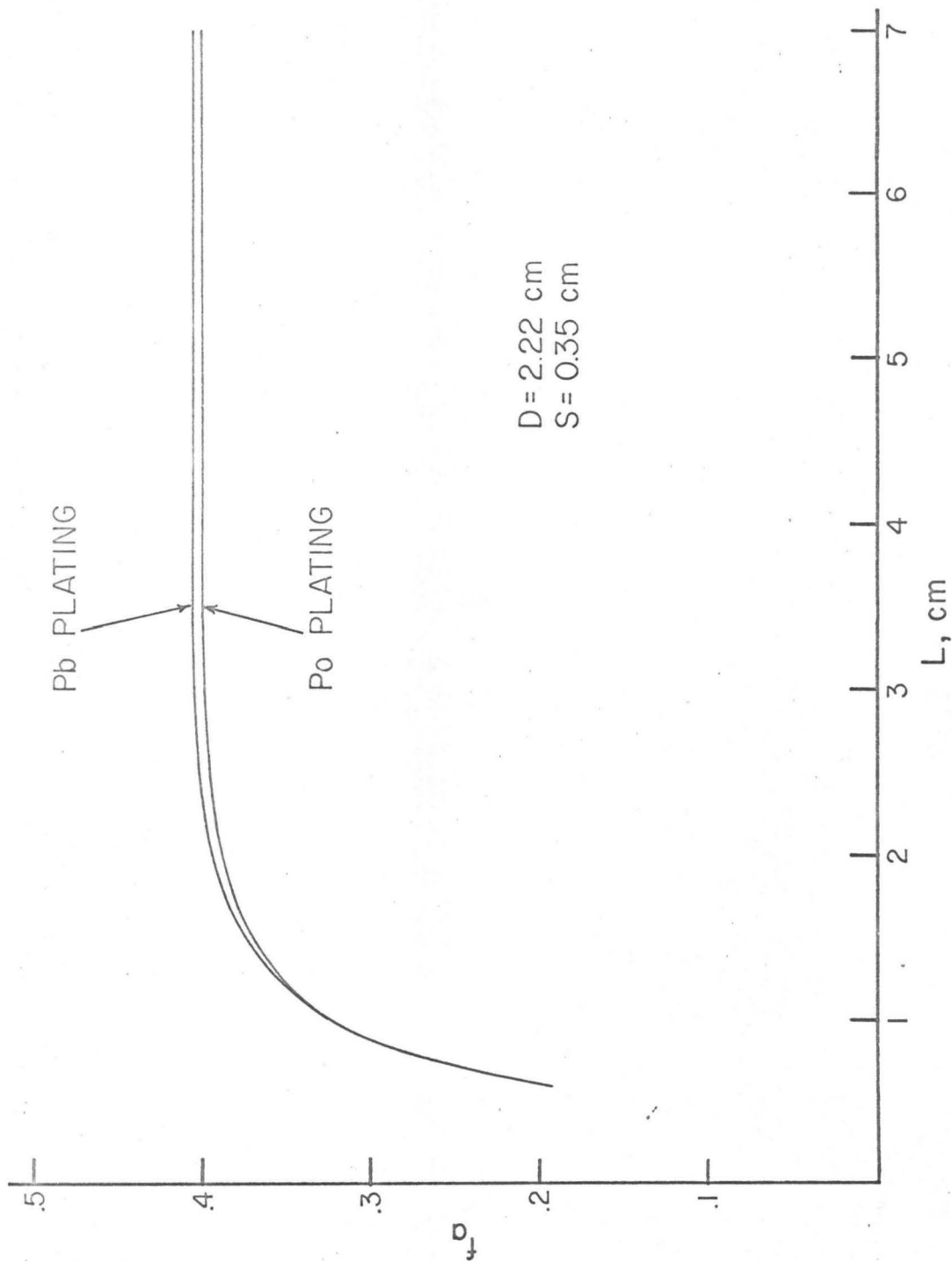


Figure 3-6.  $f_a$  as a function of  $L$  for the measured values of  $D$  and  $S$ .

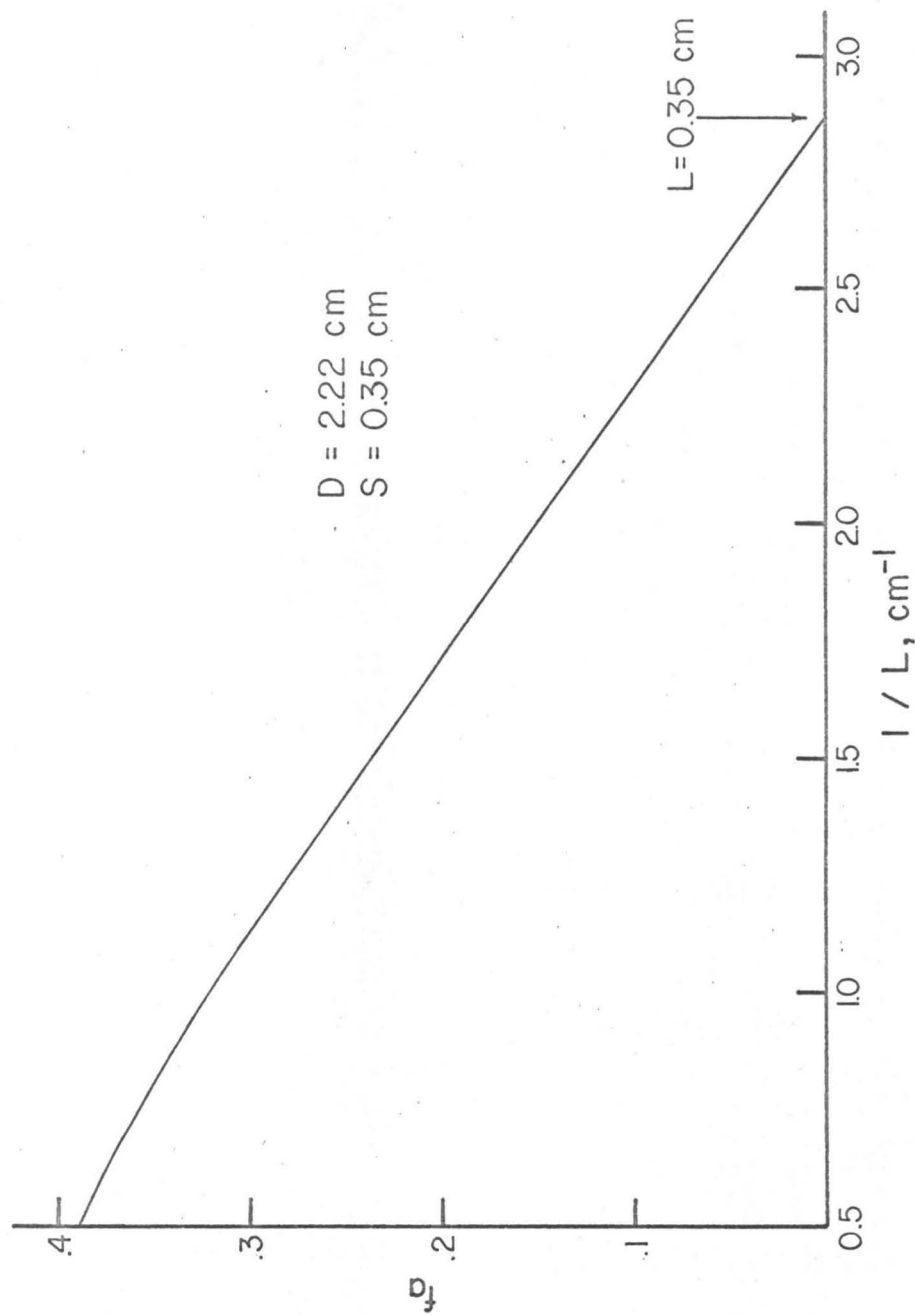


Figure 3-7.  $f_a$  as a function of  $1/L$  for the measured values of  $D$  and  $S$ .

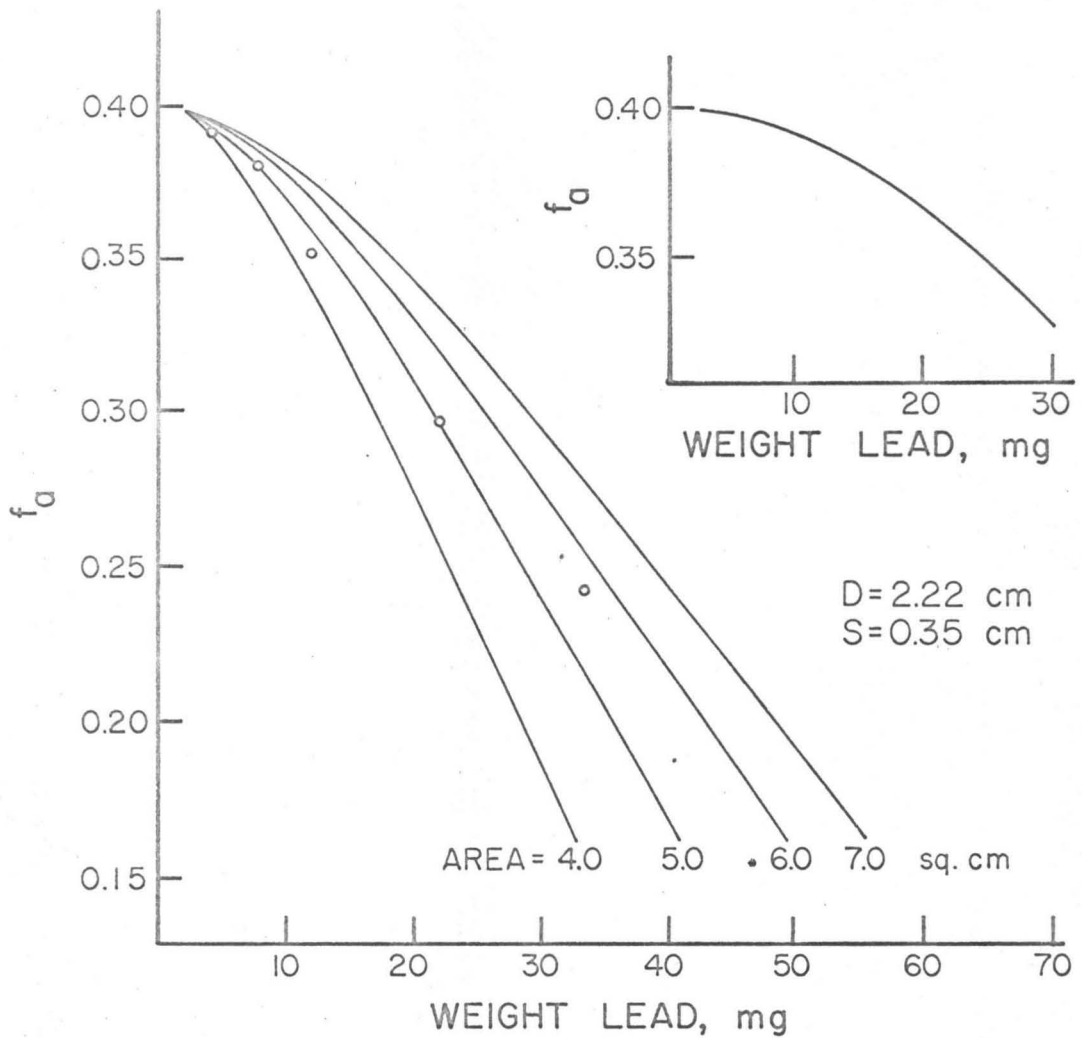


Figure 3-8.  $f_a$  as a function of the weight of lead for various deposit areas. The open circles are experimental points from the plating experiment.

where  $f_d$  is the detection coefficient. Thus dividing the measured activity by the theoretical  $f_a$  should yield a constant value for all weights of lead. As may be seen in Table 3-5, this was not found to be the case for the assumed values of 0.35 cm. for S, 2.22 cm. for D, and 7.0 sq. cm. for the deposit area. In addition, as was noted above, the slope of the experimental curve in the linear region should match that of the theoretical curve for the same area and this was not true. Now it was established above that this slope is not a function of S and  $f_a$  is not a drastic function of D. Thus it must be assumed that the "effective" area of the deposit is not 7.0 sq. cm. Table 3-5 indicates that an effective area of 5.0 sq. cm. gives the most constant value for measured activity/ $f_a$ . This conclusion seems reasonable since graininess would be difficult to avoid in electroplating lead and just such a phenomenon would yield the observed results. The experimental points from the plating experiment are shown plotted as open circles in Figure 3-8 for an area of 5.0 sq. cm. The insert in Figure 3-8 shows the calculated curve for  $f_a$  vs./mg. lead for bismuth-212 and polonium-212 alpha-particles from deposits having an area of 5.0 sq. cm. The branching ratio for the decay of bismuth-212 is taken into account. It is apparent that for even the maximum quantity of lead carrier (10 mg.) used in the plating of lead-212, a correction of only 1% in the measured activity is required.

TABLE 3-5. Attenuation of Polonium-210

Alpha-Activity by Lead.

<u>Weight Pb</u> (mg.)	<u>Measured Activity</u> (c.p.m.)	Area (sq. cm.) =	<u>Measured Activity/f<sub>a</sub></u>			
			<u>4.0</u>	<u>5.0</u>	<u>6.0</u>	<u>7.0</u>
4.3	137.9		355	352	351	350
7.6	133.5		360	351	348	345
12.0	123.5		363	345	335	330
22.0	104.0		403	354	328	312
33.3	85.2		<u>546</u>	<u>394</u>	<u>331</u>	<u>304</u>
		Average (of first 4) =	370	350	340	334
		Average deviation =	16	3	9	13

The reliability of the gravimetric method for determining the yield of lead carrier was determined by polarographic methods. Platings of lead were made from a tartrate medium originally containing 10.0 mg. of lead and the weight of undeposited lead found polarographically in this same tartrate medium. The yield of lead on the disk was found by the conventional gravimetric method and the lead was then stripped with nitric acid and redetermined polarographically in a chloride medium. The results are shown in Table 3-6. The polarographic data, which are good to a few percent, confirm the gravimetric data well enough to provide confidence in the latter method for determining yield.

Experience showed that there are several sources of difficulty in the stripping of the lead deposit and in the polarographic determination of lead from a tartrate medium. When stripping the lead, a portion of the silver surface must also be removed in order to free lead which has presumably migrated into the silver. A similar effect is observed with platinum where the surface must be protected by a layer of copper to prevent alloying with lead (12). The polarographic determination of lead in a tartrate medium is complicated by the fact that the wave height decreases with time. This is probably due to tartrate precipitation of the lead since a white precipitate is observed to form after a period of time. For this reason, the polarograms were taken as soon as possible after the addition of tartrate.

TABLE 3-6. Polarographic Determination  
of Lead Plating Yields.

	<u>Solution</u> <u>1</u>	<u>Solution</u> <u>2</u>	<u>Solution</u> <u>3</u>
weight Pb deposited (by polarography)	2.7 mg.	3.8 mg.	7.2 mg.
weight Pb deposited (by gravimetry)	3.0 mg.	3.8 mg.	7.3 mg.
weight Pb undeposited (by polarography)	<u>6.5</u> mg.	<u>6.6</u> mg.	<u>2.6</u> mg.
original weight Pb (check)	9.5 mg.	10.4 mg.	9.9 mg.

Alpha-Counting Correction Factors and the  
Calibration of the Procedure

The detector used to count the alpha-radiation consisted of a zinc sulfide screen applied with rubber cement to the face of an RCA 5819 photomultiplier tube. The sample and detector were both placed inside a light-tight box during periods of counting. The photomultiplier was coupled to a conventional electronic scaler and high-voltage power supply. The inflection point in the voltage vs. counting rate curve was determined from time to time and the counter operated at this voltage.

In order to correlate counting data before and after changes in the high-voltage setting, a counting standard was prepared by plating a relatively large amount of polonium-210 (about 500 c.p.m.) on a silver-foil disk. The intention was to count the standard before and after counting samples and to correct for the decay of polonium-210 since some convenient base date. However, it was discovered that this procedure did not yield a constant value for the activity on the base date but rather a uniform decrease in the activity as the elapsed time from the base date increased (2 to 7% per month). This was interpreted as a decrease in the detection efficiency,  $f_d$ , of the counter and had to be applied as a "counter correction" to all counting data.

The other corrections applied to the counting data were:

1. background (5 to 20 c.p.h.),
2. decay since removal from radioactive equilibrium (i.e., since plating),
3. plating yield (in the case of lead), and
4. self absorption in the sample (in the case of lead).

Now,

$$\frac{(\text{corrected counting rate, c.p.m.})}{\text{true activity, d.p.m.}} = (\text{chemical yield}) \times f_a \times f_d$$

where, as stated previously,  $f_a$  equals the ratio of the average solid angle subtended by the detector to  $4\pi$  and  $f_d$  is the detection coefficient. The right side of the equation will be referred to as the "conversion factor."  $f_a$  cannot be accurately determined because the face of the photomultiplier bulges out in the center making the measurement of the source to detector distance very difficult. The product,  $f_a \times f_d$ , was not determined because a standard having the same dimensions as the samples to be counted could not be obtained. For these reasons, I acquired analyzed samples which could be used to determine the conversion factors for the lead-212 and polonium-210 analyses.

The sample used to calibrate the polonium-210 procedure was the Katanga pitchblende (MS-OR). This sample was obtained directly from J. N. Rosholt who assured me that this sample was as close to equilibrium as any he had analyzed. The analytical data for this material is reported in the

literature (5). His results are expressed in the unit, "percent equivalent," which is defined as

$$\text{percent equivalent} = 100 \times \frac{\text{weight equivalent U}}{\text{weight of sample}}$$

where "weight equivalent U" is that weight of uranium which would support the daughter activity present in the sample in equilibrium. Using this terminology, the published analysis for this sample is:

	<u>percent</u> <u>U</u>	<u>percent equivalent</u> <u>Rn-222</u>	<u>Pb-210</u>
Katanga pitchblende (MS-OR)	44.96	42.9	42.5

Thus there are 315 d.p.m./chain member/mg. pitchblende at the lead-210 group.

The lead-212 procedure was calibrated using a sample of the Kivu thorite obtained from L. T. Silver. The analytical data for this same sample also appears in the literature where Poulaert (33) reports:

$$\begin{aligned} \text{thorium} &= (56.3 \pm 1.1)\% \\ \text{uranium} &= (0.1 \pm 0.05)\% , \end{aligned}$$

which means 138.5 d.p.m./chain member/mg. thorite. As Poulaert points out, the extremely low U/Th ratio for this material makes it ideal for calibration purposes.

The results of analyses of these two samples are presented in Table 3-7. Average values for the conversion

TABLE 3-7. Analyses of the Katanga Pitchblende and the Kivu Thorite.

<u>Run No.</u>	<u>Weight Sample</u> (mg.)	<u>Weight eU</u> (mg.)	<u>Corrected Activity</u> (c.p.m.)	<u>Specific Activity</u> (c.p.m./mg.eU)	<u>Conversion Factor</u> (on 8/15/60)
Katanga pitchblende (MS-OR, 42.5%eU at Pb-210, there are 738.1 d.p.m./mg.eU):					
7-43-1	1.99	0.846	249.4	294.7	0.399
7-43-2	"	"	242.0	286.0	0.388
7-43-3	"	"	242.0	286.0	0.388
7-43-4	"	"	238.9	282.4	0.383
7-43-5	"	"	256.2	302.6	0.410
7-43-6	"	"	255.7	302.1	<u>0.409</u>

Average = 0.396 ± 0.012

	<u>Weight eTh</u> (mg.)	<u>Specific Activity</u> (c.p.m./mg.eTh)
Kivu thorite (56.3% Th, there are 245.7 d.p.m./mg.eTh):		
7-46-1	5.6	3.15
7-46-2	5.6	3.15
7-46-3	9.3	5.24

\* Average = 0.367 ± 0.006

factor were calculated from these analytical data and are also shown in this table. These values, which agree very well with each other, were used in subsequent analyses to calculate the weight-equivalent of uranium or thorium from the corrected counting rate.

#### Combined Polonium-210 and Lead-212 Analyses

The first attempts at separating polonium-210 and lead-212 from the same solution were made on synthetic mixtures of the polonium-210 working solution and the thorium-232 solution. These experiments were designed to test the reproducibility (precision) of the yields for the chemical and plating procedures:

- (a) over a ten-fold variation in the polonium-210 concentration,
- (b) for solutions containing high concentrations of sodium ion or boric acid (as would be the case if sodium peroxide or borax were employed as a flux to decompose the sample), and
- (c) for solutions in which the reduction step is employed owing to the presence of ferric iron or the ions of mercury, tellurium, platinum, or gold.

The results of these experiments are tabulated in Table 3-8. The standard deviations of these determinations are used as an index to the reproducibility and appear to be

TABLE 3-8. Combined Polonium-210 and Lead-212 Analyses.

Solution	Plating Time (hours)	Reproducibility of the Po-210 Yield		Fractional Yield	Reproducibility of the Pb-212 Activity Plated	
		Taken (c.p.m.)	Found (c.p.m.)		Fractional Carrier Yield	Found (c.p.m.)
5-11-1 (1)	4	3.5	3.4	0.97	0.80	377
5-11-2 (1)	4	3.5	3.5	1.00		
5-11-3 (1)	6	3.5	3.5	1.00	1.01	397
5-11-4 (1)	5	3.5	3.1	0.89	0.83	398
5-28-1 (2)	5.5	41.5	39.8	0.96	1.02	376
5-28-3 (2)	3	41.5	39.5	0.95	1.02	378
7-56-1 (3)	15		75.5			
7-56-2 (3)	15		73.8			
				Average = 0.95 ± 0.05	Average = 385 ± 10.3	

(1) 5.00 ml. diluted Po-210 working soln., 5.00 ml. Th-232 soln., 5.00 ml. lead carrier soln. 5-11-2 was evaporated to dryness and 2 g. sodium peroxide added. It was then carried through the reduction step before depositing the polonium. Conc. of Na<sup>+</sup> = 2.5F. 5-11-3 and 5-11-4 were evaporated to dryness and carried through the reduction step with no addition of sodium peroxide.

(2) 5.00 ml. Po-210 working soln., 5.00 ml. Th-232 solution, 5.00 ml. lead carrier soln., 2 mg. Fe<sup>+++</sup>, and 0.1 mg. each of Hg, Te, Pt, and Au. These solutions were evaporated to dryness and carried through the reduction step.

(3) 5.00 ml. U-Th soln., 5.00 ml. lead carrier soln., 260 mg. hydrazine dihydrochloride. To 7-56-1 were added 15 ml. 0.5F HCl giving a pH of 0.3. To 7-56-2 were added 15 ml. distilled water and 2.0 g. sodium tetraborate and the pH adjusted to 0.3. The soln. was 0.5F in Na<sup>+</sup> and 1.1F in H<sub>3</sub>BO<sub>3</sub>.

acceptable (within  $\pm 5\%$ ) considering the variety of treatments given these solutions. The excessive scatter in the polonium-210 determinations is probably due to the low activity present in the first four solutions. The last two solutions, in which the activity was greater by a factor of ten, reproduce each other (and the average) quite well. Thus the dilution of the polonium-210 by a factor of ten in this concentration region does not affect the yield.

Haissinsky (32) states that high concentrations of alkali salts adversely affect the yield of polonium. These would enter the present analytical procedure through the fusion step during the preparation of the sample solution and thus their effect had to be determined. Solution 5-11-2 indicates that the concentration of sodium ion resulting from a fusion involving 2 g. of sodium peroxide does not lower the yield. Solution 7-56-1 and 7-56-2 were identical except that 7-56-2 had concentrations of sodium ion and boric acid which would result from a fusion involving 2 g. of borax. There is approximately a 2% reduction in the amount of polonium plated but this is within the expected scatter and therefore may not be significant.

Finally, the hydrazine reduction procedure used for solutions 5-28-1 and 5-28-2 was sufficient to eliminate any interference from 2 mg. ferric iron or 0.1 mg. each of mercury, tellurium, platinum, and gold.

Up to this point in the study, the polonium-210 and lead-212 had been taken from sources which were already in solution or were relatively easy to dissolve. There still remained the task of analyzing for these two nuclides in materials which were more difficult to bring into solution. Polonium, in particular, offered difficulty if any material remained undissolved because it required a relatively long time to return to equilibrium with lead-210.

A synthetic sample solution providing high activities of polonium-210 and lead-212 was prepared from portions of the Happy Jack uraninite and the Kivu thorite, both supplied by L. T. Silver. Analytical data for the uraninite was furnished by Rosholt (34):

	<u>percent U</u>	<u>percent equivalent U</u>				
		<u>Pa-231</u>	<u>Th-230</u>	<u>Ra-226</u>	<u>Rn-222</u>	<u>Pb-210</u>
GS-64/51	72.8	76.5	74.6	73.0	68.5	69.1

where the "percent U" value is an average of the values obtained in the Washington, D.C. and Denver laboratories of the U.S. Geological Survey. During dissolution of these samples precipitates formed. These were separated by filtration through filter paper and counted on the paper. The alpha-activity was less than 1% of the alpha-activity per chain member for either chain. A separate analysis for uranium in this solution was performed by Dr. Silver using the isotope dilution method (35). He found 0.372 mg. uranium/5 ml. of solution which is in agreement with values calculated from

the analysis furnished by Rosholt. This value for uranium also confirms the very low content of uranium in the Kivu thorite reported by Poulaert. As shown in Table 3-9, the results of analyses performed on aliquot portions of this solution over a period of 475 days indicate that the polonium-210 was out of equilibrium at the time the solution was prepared and still had not returned completely to equilibrium after the 475 days. The lead-210 values indicate that this nuclide also was out of equilibrium and required the 475 days to grow back.

The best illustration of the care which is required in preparing sample solutions is provided by the analyses of the R200 mesh zircon from the Pacoima Canyon pegmatite. This sample was provided by L. T. Silver and analytical data covering its uranium content and thorium content will soon be published (35). The values are:

uranium =  $208.2 \pm 1.0$  p.p.m. (average of 12 analyses)

thorium =  $63.0 \pm 1.0$  p.p.m. (analysis performed by

Dr. G. R. Tilton, Geophysical Laboratory).

Zircon is an extremely refractory material and thus presents problems during fusion. In addition, its high silica content results in a large silica precipitate upon acidification following fusion. Finally, zirconium hydroxide precipitates as the pH is raised prior to plating the lead

TABLE 3-9. Results of Analyses of Synthetic Mixture  
of the Happy Jack Uraninite and the Kivu Thorite.

<u>Disk No.</u>	<u>Time Since Solution Prepared (days)</u>	<u>Corrected Activity (c.p.m.)</u>	<u>Weight eU</u>		<u>Ratio</u>
			<u>Found (mg.)</u>	<u>Taken (mg.)</u>	
Po-210: 5-59-1 Po	6	83.7	0.286	0.372	0.770
5-59-2 Po	6	81.1	0.277	"	0.745
5-59-3 Po	12	86.9	0.297	"	0.799
5-59-4 Po	12	87.2	0.298	"	0.801
5-64-1 Po	29	85.1	0.291	"	0.784
7-32-1 Po	300	87.8	0.300	"	0.806
7-32-2 Po	300	89.4	0.305	"	0.821
7-32-3 Po	300	89.5	0.306	"	0.822
7-50-1 Po	400	99.9	0.341	"	0.917
7-50-2 Po	400	99.3	0.339	"	0.913
7-50-3 Po	475	95.9	0.328	"	0.882

			<u>Weight eTh</u>		<u>Ratio</u>
			<u>Found (mg.)</u>	<u>Taken (mg.)</u>	
Pb-212: 5-59-1 Pb	6	82.5	0.915	1.377	0.66
5-59-2 Pb	6	94.3	1.046	"	0.76
5-59-3 Pb	12	70.3	0.780	"	0.57
5-59-4 Pb	12	89.3	0.991	"	0.72
5-64-1 Pb	29	73.1	0.811	"	0.59
7-32-1 Pb	300	117.7	1.306	"	0.95
7-32-2 Pb	300	115.7	1.283	"	0.93
7-32-3 Pb	300	105.2	1.167	"	0.85
7-50-1 Pb	400	117.3	1.301	"	0.94
7-50-3 Pb	475	126.9	1.407	"	1.02

5.00 ml. of the uranium-thorium solution were used in each run.

carrier. Four separate solutions of this zircon were prepared and analyses made on aliquot portions of these. The results are shown in Table 3-10.

The first two solutions were prepared using sodium peroxide as the fusion flux. The silica residue which resulted upon acidification was simply separated by filtration and no attempt made to recover adsorbed decay chain members. The recovery of both polonium-210 and lead-212 was quite low and remained constant over a period of 150 days indicating that longer-lived parents of these nuclides were lost on the silica.

The third solution (7-58-1) was prepared with the aid of a borax flux. In addition, a recovery of material adsorbed on the silica was attempted by evaporating silicon as the tetrafluoride. The recovery of polonium from an aliquot portion of this solution was extremely low. Two sources of loss of the polonium were considered: 1) the borax fusion is conducted at about  $1100^{\circ}\text{C}$ . for several hours and polonium loss by evaporation would be very likely; 2) if polonium formed a stable hexafluoride then loss could occur during the evaporation of silicon tetrafluoride. The second of these possibilities was eliminated, at least under the conditions used, because polonium fluorides are extremely difficult to stabilize (36). In order to test the first hypothesis, a fourth solution (7-63-1) of the zircon was prepared using sodium peroxide as the flux but still employ-

TABLE 3-10. Results of Analyses of the Zircon  
from the Paccima Canyon Pegmatite.

Solution	Disk No.	Time Since Solution Prepared (days)	Corrected Activity (c.p.m.)	Weight eU		Ratio
				Found (mg.)	Taken (mg.)	
Po-210:						
(1)	5-37-1 Po	~ 20	4.03	0.0138	0.0199	0.694
5-38-1 (2)	5-40-2 Po		7.83	0.0268	0.0384	0.697
	5-40-3 Po		7.95	0.0271	"	0.706
	5-41-4 Po	> 5	3.88	0.0133	0.0192	0.694
	5-41-5 Po	> 5	3.87	0.0132	"	0.689
	5-64-2 Po	80	11.37	0.0389	0.0576	0.675
	5-64-3 Po	150	11.62	0.0397	"	0.689
	5-64-4 Po	150	10.82	0.0370	"	0.642
(3)	7-59-1 Po	2	1.18	0.0041	0.0345	0.118
7-63-1 (4)	7-63-1 Po	1	11.57	0.0396	0.0410	0.966
	7-63-2 Po	2	11.55	0.0395	"	0.964
	7-63-3 Po	12	11.64	0.0398	"	0.971
						Average =
						+ 0.004
Pb-212:						
(1)	5-38-1 Pb	~ 20	0.30	0.0034	0.0060	0.57
5-38-1 (2)	5-40-3 Pb		0.64	0.0071	0.0116	0.61
	5-41-4 Pb	> 5	0.50	0.0056	0.0058	0.97
	5-41-5 Pb	> 5	0.36	0.0040	"	0.69
	5-64-2 Pb	80	1.07	0.0119	0.0175	0.68
	5-64-4 Pb	150	1.11	0.0124	"	0.71
7-63-1 (4)	7-63-1 Pb	1	1.98	0.0220	0.0124	1.77
	7-63-2 Pb	2	1.10	0.0122	"	0.98
<p>(1) 0.0958 g. of zircon were fused with sodium peroxide and the entire sample analyzed.</p> <p>(2) 100 ml. of solution prepared by peroxide fusion of 1.8478 g. of zircon and 5.00, 10.00, or 15.00-ml. aliquot portions used for each run.</p> <p>(3) 500 ml. of solution prepared by borax fusion of 0.608 g. of zircon, the silica distilled as the tetrafluoride, and a 150.00-ml. aliquot portion used for the run.</p> <p>(4) 500 ml. of solution prepared by peroxide fusion of 0.6564 g. of zircon, the silica distilled as the tetrafluoride, and 150.00-ml. aliquot portions used for each run.</p>						

ing the evaporation of silicon tetrafluoride for the recovery of adsorbed ions. The results of the analyses for polonium in aliquot portions of this solution indicate that the lead group in this zircon is in radioactive equilibrium with the uranium.

The low thorium content made analysis for lead-212 extremely difficult. This difficulty was compounded by the fact that the recovery yields of lead carrier were quite low (about 50%) presumably because of adsorption of lead on the zirconium hydroxide precipitate which formed when the pH was raised to 4.7. An attempt was made to circumvent this difficulty in the case of solution 7-63-1 by extracting the lead as the dithizonate with chloroform prior to the pH adjustment. The results were disappointing in that the yield of lead carrier was increased by only about 10%. However, the extraction procedure used was adapted from that employed to extract quantities of lead in the p.p.m. range and could probably be improved for the present application by further modification. The lead-212 analysis could also be improved by lowering the background counting rate of the alpha-counter. The rate was between 7 and 15 c.p.h. during these analyses.

Precision of the Analyses

In order to provide a guide to the reproducibility of the polonium-210 and lead-212 analyses, Table 3-11 was prepared. This table lists the standard deviations for the analyses shown in previous tables. In samples having high concentrations of uranium and thorium (on the order of 50%) the chemical procedure, rather than counting errors, should be the principle cause for reduced precision. The maximum standard deviation in these samples is 3% and this value will be considered to be the standard deviation due to the chemical procedure. As the concentrations of uranium and thorium are reduced, the maximum amount of radioactivity which can be plated is limited by the amount of material available for analysis and solubility considerations. Thus counting errors become more and more important for the precision, especially in the case of lead-212 which is disappearing with a 10.6 hour half-life. The high standard deviation for the analysis of lead-212 in the Pacoima Canyon zircon illustrates this point but would no doubt be improved considerably if more runs were made. The very favorable standard deviation for the polonium-210 in this zircon is somewhat surprising in the light of what has been said.

TABLE 3-11. Standard Deviations of the Analyses.

	Po-210 Analyses			Pb-212 Analyses			
	<u>U</u> Content	<u>No. of</u> <u>Runs</u>	<u>Activity</u> <u>per Run</u> (c.p.m.)	<u>Th</u> Content	<u>No. of</u> <u>Runs</u>	<u>Activity</u> <u>per Run</u> (c.p.m.)	<u>Standard</u> <u>Deviation</u> (%)
Thorium nitrate				42%	5	385	3
Katanga pitchblende	42.5%	6	250				
Kivu thorite				56.3%	3	280-480	2
Polonium solution		6	3.5-41.5				
Pacoima Canyon zircon 208 p.p.m.		3	11.6	63 p.p.m.	2	1-2	56

#### 4. SUMMARY

The detailed study of radioactive disequilibrium patterns in rocks is relatively new. Rosholt has reported a radiochemical procedure for finding the amounts of the various groups in the decay chains. The present study was undertaken to find alternative procedures for the analyses of the lead and thorium groups and a method for the successive determination of polonium-210 and lead-212 was found. The analysis for the lead group provides an indication of the state of radioactive equilibrium farther up the chain while the analysis for any member of the thorium group almost always gives the thorium content. According to the procedure, the sample is decomposed by fusion with sodium peroxide and taken up in HCl. This solution is made 0.05F in hydrazine, 10 mg. lead carrier added, and the HCl concentration adjusted to 0.5F. The polonium-210 is deposited on a silver-foil disk and the alpha-activity from the polonium-210 on the disk is measured with a scintillation counter. 0.60 grams of sodium tartrate dihydrate are added to the solution remaining from the polonium deposition, the pH is adjusted to about 4.7 with NaOH, and the lead electro-deposited at a cathode potential of -0.70 V. vs. S.C.E. on a second silver-foil disk. The yield of lead carrier on this disk is determined gravimetrically and the decay of the 10.6 hour lead-212 supported alpha-activity observed

as a function of time. The procedure was calibrated by finding the conversion factors to calculate the disintegration rates from the measured counting rates. The conversion factor for polonium-210 was determined by analyzing a sample of the Katanga pitchblende. Analysis of the Kivu thorite gave the conversion factor for lead-212. These two factors differed by 7%.

The rate of deposition of polonium was studied as a function of the volume and temperature of the plating solution and the results allow an estimation of the minimum plating time which can be used. The maximum yield of polonium in the activity range of 3 to 40 c.p.m. remained almost constant under conditions of varying temperature (23 to 81°C.) and volume (20 to 150 ml.) and averaged 95%. The codeposition of lead-212 and bismuth-212 with polonium-210 was found to be less than 0.5% thus eliminating any chance of interference from these nuclides. The darkening of the silver surface during the polonium deposition is indicative of the presence of interfering ions which can reduce the yield of polonium. A reduction procedure employing hydrazine in 7F HCl was found effective in eliminating the interference from 0.2 mg. each of mercury, tellurium, platinum, and gold. Lowering the HCl concentration to 0.5F and warming eliminates the interference from up to 2 mg. of ferric iron. The gravimetric determination of lead carrier yield was verified by polarographic methods and the attenuation of the alpha-radiation by the maximum amount of lead carrier was found

to be only 1%. It was found extremely important that all of the sample be dissolved in order to avoid disturbing the state of radioactive equilibrium.

The standard deviation due to the chemical procedures is estimated to be about 3%. The procedure for polonium-210 was tested on the Pacoima Canyon zircon and the value found for weight equivalent uranium agreed with the mass spectrometric value for the uranium content to 3.3%. Thus the lead group is in equilibrium with the parent uranium and the polonium-210 procedure is suitable for this very refractory mineral. The standard deviation for the lead-212 analysis increases as the thorium content decreases and reached 56% for the two runs on the Pacoima Canyon zircon which contains 63 p.p.m. thorium. The principle advantages offered by this procedure are: 1) freedom from manipulation of precipitates and 2) the obtaining of the radioactive deposits in a form most convenient for counting.

REFERENCES

1. Faul, H., Nuclear Geology, John Wiley and Sons, Inc. (New York, 1954), pp. 282-300.
2. Rosholt, J. N., Jr., Geol. Survey Bull. 1084-A (1959), 30 pp.
3. U. S. Geol. Survey, Prof. Papers 320 (1959), 236 pp.
4. Walton, H. F., Chem. and Eng. News 38, No. 25, 118-122 (June 20, 1960).
5. Rosholt, J. N., Jr., Anal. Chem. 29, 1398-1408 (1957).
6. Cherdyntsev, V. V., Abundance of Chemical Elements, The University of Chicago Press (Chicago, London, 1961), pp. 99-102.
7. Rosholt, J. N., Jr., Anal. Chem. 26, 1307-11 (1954).
8. Rosholt, J. N., Jr., Advances in Nuclear Engineering, Vol. II, part 2, Dunning, J. R. and Prentice, B. R. (editors), Pergamon Press (New York, 1957), pp. 300-4.
9. Rosholt, J. N., Jr., Proceedings of the Second United Nations International Conference on the Peaceful Uses of Atomic Energy, Vol. 2, United Nations (Geneva, 1958), p. 230.
10. Bagnall, K. W. and Freeman, J. H., J. Chem. Soc., 2770-4 (1956).
11. Ziv, D. M. and Sinitsyna, G. S., Trudy Radievogo Inst. im. V. G. Khlopina 8, 127-37 (1958); Nucl. Sci. Abstr. 15, 9559 (1961).
12. Lingane, J. J., Electroanalytical Chemistry, 2nd Edition, Interscience Publishers, Inc. (New York, 1958).
13. Bagnall, K. W., Chemistry of the Rare Radioelements, Academic Press, Inc. (New York, 1957).
14. Ancarani, L. and Riva, L., Comit nazl. ricerche nucleaire CNG-31 (1959); Chem. Abstr. 54, 10666 f.
15. Smith, F. A., Della Rosa, R. J., and Casarett, L. J., AEP Report UR-305 (1955).

16. Black, S. C., U. S. Atomic Energy Comm. UR-463 (1956).
17. Krebs, C. A. and Whipple, G. H., U. S. Atomic Energy Comm., Rep. UR-501 (1957).
18. U. K. A. E. A. Report IGO-AM/W-167 (1958); Anal. Abstr. 5, 3434 (1958).
19. Templeton, D. H., Howland, J. J., and Perlman, I., Phys. Rev. 72, 758-65 (1947).
20. Whitaker, M. D., Bjorksted, W., and Mitchell, A. C. G., Phys. Rev. 46, 629-30 (1934).
21. Haissinsky, M., J. Chim. Phys. 33, 97-8 (1936).
22. Feldman, I. and Frisch, M., Anal. Chem. 28, 2024-5 (1956).
23. Godt, K. J. and Sommermeyer, K., Atomkernenergie 5, 282-5; Chem. Abstr. 55, 138 i (1961).
24. von Gunten, H. R. and Ledent, D., Chimia (Switz.) 12, 146-7 (1958).
25. Alberti, G., Bettinali, C., and Salvetti, F., Ann. Chim., Roma 49, 193-8 (1959); Anal. Abstr. 6, 3798 (1959).
26. Gorsuch, T. T., Analyst 84, 170-2 (1959).
27. Chen, Y. and Wong, C., J. Chinese Chem. Soc. Ser. II 6, 55-67 (1959); Anal. Abstr. 7, 2156 (1960).
28. Dedek, W., Z. anal. Chem. 173, 399-411 (1960); Anal. Abstr. 7, 4678 (1960).
29. Gorsuch, T. T., Analyst 85, 225-6 (1960).
30. Harrison, A. D. R., Lindsey, A. J., and Phillips, R., Anal. Chim. Acta 13, 459-64 (1955).
31. Ishibashi, M., Fujinaga, T., and Kusaka, Y., J. Chem. Soc. Japan 75, 13-14 (1954); Anal. Abstr. 2, 561 (1955).
32. Haissinsky, M., La Chimie Nucleaire et Ses Applications, Masson et Cie (Paris, 1957).

33. Poulaert, G., Chimia 12, 116-7 (1958).
34. Rosholt, J. N. (personal communication).
35. Silver, L. T., McKinney, C. R., Deutsch, S., and Bolinger, J., J. of Geology (Nov. 1962, in press).
36. Weinstock, B. and Chernick, C. L., J. Am. Chem. Soc. 82, 4116-17 (1960).

W. G. J. BOGERTON

174

175

of fall within the group of meteorite.

It is hoped that these observations would shed some light

on the flux of meteorites at the Earth's orbit.

AT THE EARTH'S ORBIT

the amount of which travel in similar orbits

similar objects of composition and mineralogy

## II

### A CHARACTERIZATION OF THE METEORITE FLUX

## 1. INTRODUCTION

This study was undertaken in order to characterize the meteoritic flux at the orbit of the earth during recent times with respect to its type composition and mass distribution, its direction, and its magnitude. A further objective of the study was the search for correlations in the patterns of fall within and among the various types of meteorites with the hope that these correlations would shed some light on the origin and history of these objects. Such correlations in fall pattern, if found, would indicate families of meteorites the members of which travel in similar orbits and might have similar chemical composition and mineralogical structure.

Unfortunately, we must start with the flux of meteorites arriving at the surface of the earth because no methods exist at the present time to observe these bodies beyond the earth's atmosphere. This limitation immediately exposes us to extrinsic biasing factors (the time of day, the season, the population density and its scientific cultural level) which affect the frequency and quality of observations, and to intrinsic biasing factors (variations in the effects of atmospheric ablation, variations in the effect produced by striking the surface of the earth, resistance to weathering, variations in the degree of dissimilarity to terrestrial rocks, and mass) which affect the probability of recovering a meteorite. The quality of the available data varies widely. Because of the random arrival of these bodies,

most observations have been made by persons untrained in the scientific method. In addition, the statistics are poor because the number of meteorites brought to the attention of scientists and collectors is small (about 700 falls and 800 finds) and many of these have not been fully classified.

With these limitations in mind, I proceeded with the survey because: 1) significant correlations might still be found and 2) even negative results would provide valuable information. The data were placed on punch cards to allow machine sorting of the cards according to various classifications.

## 2. PUNCH CARD CODING FORMAT AND SURVEYS

The most complete and concise source of meteorite information is the Catalogue of Meteorites by Prior and Hey (1). Quoting from the introduction to this catalog,

the data supplied for each meteorite include: the name by which it is generally known; the locality, with the latitude and longitude of the actual place of fall, where possible; the date of fall or find; the chief synonyms; the classificatory descriptive name; details and original weight of the fall or find; references to the literature; the present repository . . . of the main masses; and a list of the specimens (with their weights in grams). . . .

In addition, the results of reliable chemical analyses are presented,

by stating approximately, (1) the percentage (f) of nickeliferous iron; (2) the ratio (n) of the percentage of iron to that of nickel in the nickeliferous iron; and (3) the ratio (m) of the molecules of MgO to those of FeO in the magnesian silicates.

This catalog lists about 1500 meteorite falls and finds (excluding "doubtful" meteorites) and includes meteorites known up to December, 1952. Meteorites which came to the attention of collectors after 1952 are described in The Meteoritical Bulletin (2) and the information concerning these meteorites is taken from this source. The classification system for meteorites used by Prior, and shown in Table 2-1, was retained in this survey.

The format used for the layout of data on the punch cards is shown below. One card was used for each meteorite.

TABLE 2-1. Rose-Tschermak-Brezina System for the  
Classification of Meteorites as  
Modified by Prior (1).

- I. Irons--consist mainly of nickeliferous iron.
  - a. Nickel-poor Ataxites--nickel less than 6%.
  - b. Hexahedrites--nickel about 7%.
  - c. Octahedrites (Coarsest, Coarse, Medium, Fine, and Finest)--nickel from 7 to 14%.
  - d. Ataxites, Metabolites--nickel 7 to 14%.
  - e. Nickel-rich Ataxites--nickel greater than 14%.
- II. Stony-irons--iron and stony matter both in large amounts.
  - a. Pallasites--olivine stony-irons.
  - b. Siderophyres--bronzite-azmanite stony-irons.
  - c. Lodranites--bronzite-olivine stony-irons.
  - d. Mesosiderites--hypersthene-achondritic stony irons.
- III. Stones--consist mainly of stony matter, with nickeliferous iron and troilite, when present, scattered through as small grains.
  1. Chondrites--contain chondrules, classified according to increasing percentage of nickel in the nickeliferous iron and correspondingly increased amount of iron oxide in the magnesian silicates.

TABLE 2-1 (continued)

- a. Enstatites
- b. Bronzites
- c. Hypersthene

further qualified by color (white, intermediate, grey, black), structure (crystalline, spherical, brecciated, veined), and composition (carbonaceous, etc.).

2. Achondrites--chondrules absent.

a. Calcium-poor achondrites

- 1) Aubrites--enstatitic achondrites.
- 2) Ureilites--clinobronzite-olivinic achondrites.
- 3) Amphoterites, Rhodites--hypersthene-olivinic achondrites.
- 4) Diogenites--hypersthene achondrites.
- 5) Chassignites--olivinic achondrites.

b. Calcium-rich achondrites

- 1) Angrite--augitic achondrites.
- 2) Nakhilites--diopside-olivinic achondrites.
- 3) Eucrites, Shergottites--clinohypersthene-anorthitic achondrites.
- 4) Howardites--hypersthene-clinohypersthene-anorthitic achondrites.

<u>Columns</u>	<u>Information</u>
1,2,3,4	Reference number--meteorites taken in alphabetic order and only every fifth number used to allow for the insertion of new meteorites.
5,6,7	Year of fall or find--(1)001 A.D. to (1)960 A.D.
8,9	Month of fall--01 to 12.
10,11	Day of fall--01 to 31.
12,13,14	Hour of fall--00.0 to 23.9.
15,16	Type of meteorite--iron, stoney-iron, chondrite, or achondrite plus the subclassification (e.g., hexahedrite, bronzite, eucrite, etc.) and the physical classification (e.g., crystalline, spherical-black, etc.).
17,18,19	Latitude--North or South and 00° to 90°.
20,21,22	Longitude--000° to 360°.
23,24,25	Mass--two significant figures and the power of 10.
26	Mass--interval in base 2 logarithm system.
27	Number of pieces--corresponds to the mass given above.
28,29,30	"f," % nickeliferous iron--00.0 to 99.9%.
31,32	"n," Fe/Ni--00 to 98; 99 = any ratio greater than 98.
33,34	"m," MgO/FeO--0.0 to 9.8; 9.9 = any ratio greater than 9.8.

- 35,36 "t," % troilite--0.0 to 9.8%; 9.9 = any  
percentage greater than 9.8.
- 37,38,39 % Ni--00.0 to 99.9%.

This format uses only 39 of the 81 available columns on an IBM punch card and thus additional information, such as more complete chemical analytical data or the political subdivision in which the fall or find occurred, can be punched on the same card.

When the data for the 1500 meteorite falls and finds had been placed on punch cards it became a relatively simple task to conduct the surveys listed below in outline form. The required separations or orderings were made by a sorting machine and then the cards (including all of the information on each card) were printed out as lists. Thus the results of each survey were presented in a convenient and permanent form.

Geographical surveys:

- 1) northern and southern hemisphere falls ordered by latitude.
- 2) northern and southern hemisphere falls ordered by longitude.
- 3) northern and southern hemisphere finds ordered by latitude.
- 4) northern and southern hemisphere finds ordered by longitude.

- 5) transformed coordinates of fall (using a computer for the necessary calculations).

Chronological surveys:

- 1) falls ordered by year.
- 2) falls ordered by month and day.
- 3) falls ordered by local hour.
- 4) northern and southern hemisphere falls ordered by latitude and by month.
- 5) northern and southern hemisphere falls ordered by latitude and by hour.

Classificational surveys:

- 1) iron falls ordered by type.
- 2) stoney-iron falls ordered by type.
- 3) chondrite falls ordered by type.
- 4) achondrite falls ordered by type.
- 5) iron finds ordered by type.
- 6) stoney-iron finds ordered by type.
- 7) chondrite finds ordered by type.

Mass and compositional surveys:

- 1) iron falls ordered by mass.
- 2) chondrite falls ordered by mass.
- 3) achondrite falls ordered by mass.
- 4) stoney finds ordered by mass.
- 5) falls ordered by metal-phase content.
- 6) finds ordered by metal-phase content.
- 7) iron meteorites ordered by nickel content.

3. COMPOSITION AND DIRECTION OF THE FLUX  
AT THE EARTH'S ORBIT

Description of the Coordinate Systems

The polar equation of an elliptical orbit in the heliocentric coordinate system with the origin at the sun is

$$r = p/(1 + e \cos \theta) , \quad (3-1)$$

where  $r$  is the distance from the sun,  $\theta$  is the angle in the plane of the orbit measured from perihelion (position of closest approach to the sun) with the positive direction the same as the direction of motion of the earth in its orbit,  $e$  is the eccentricity of the ellipse, and  $p$  is the semilatus rectum. The semi-major axis,  $a$ , is given by

$$a = p/(1 - e^2) . \quad (3-2)$$

Another element of the orbit is the inclination,  $i$ , which is the dihedral angle between the plane of the orbit and the ecliptic plane. Whenever possible,  $i$  is assumed to be  $0^\circ$ . The coordinates  $r_e, \theta_e$  and  $r_a, \theta_a$  are of special interest since they represent the values of  $r$  and  $\theta$  at the earth's orbit and at the asteroid belt respectively. The radius of the earth's orbit,  $r_e$ , is the unit used to measure solar system distances and is designated 1 astronomical unit (a.u.). Some of these quantities are indicated

in Figure 3-1 which shows a hypothetical meteorite orbit lying in the plane of the ecliptic.

The components of the heliocentric velocity,  $v$ , at any point in the orbit will be designated by  $v_r$  and  $v_\theta$ . The velocity of the earth in its orbit (assumed to be circular) is  $V_e$  (29.8 km./sec.). For a body receding from the sun, the angle between  $v_r$  and  $-v$  will be called  $\phi_{out}$  while for a body approaching the sun, the angle between  $-v_r$  and  $-v$  will be called  $\phi_{in}$ . These angles are necessary to give the direction of the flux at the earth's orbit. Now since the earth is moving in its orbit at a speed comparable to that at which meteorites are moving, the velocity of the flux,  $v$ , must be combined vectorially with that of the earth,  $V_e$ , to yield the direction of the flux in the geocentric coordinate system. This coordinate system is also that of the center of mass because the mass of the meteorite is negligible compared to that of the earth. The new angles between the transformed flux direction and midnight will be designated  $\phi'_{in}$  and  $\phi'_{out}$  as shown in Figure 3-2. The two angles will be symmetric with respect to the  $90^\circ$ - $270^\circ$  axis for meteorites travelling in the same orbit.

Figure 3-3 shows the quantities necessary for the transformation of  $\phi_{out}$  to  $\phi'_{out}$ . In order to develop the transformation equations, we may begin by assuming a value for the semi-major axis,  $a$ , and the eccentricity,  $e$ , of the meteorite orbit.  $p$  may then be calculated by using

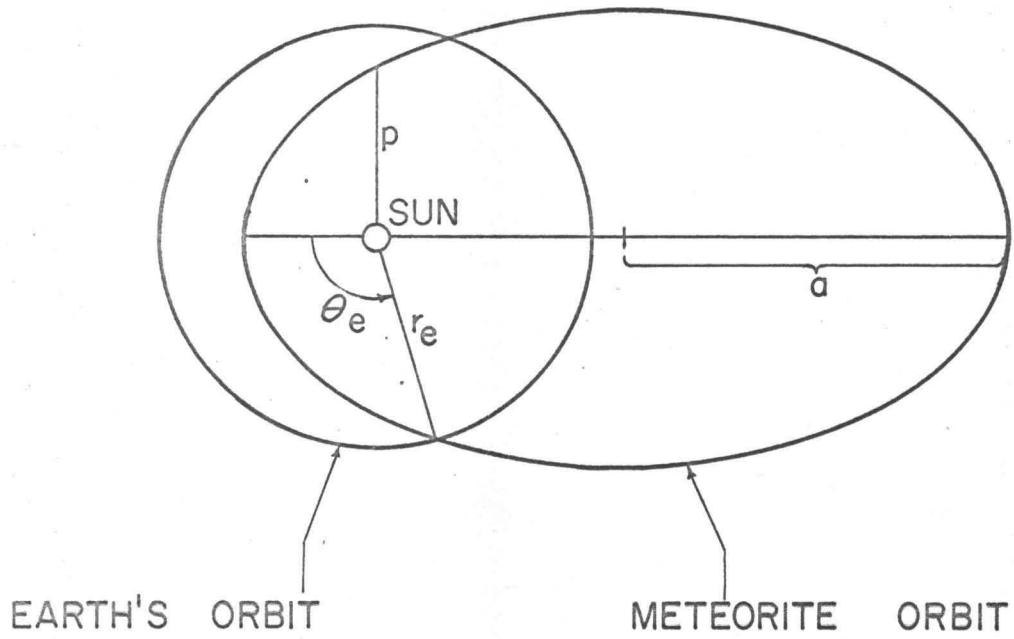


Figure 3-1. Intersection between the orbit of the earth and a meteorite orbit lying in the plane of the ecliptic.

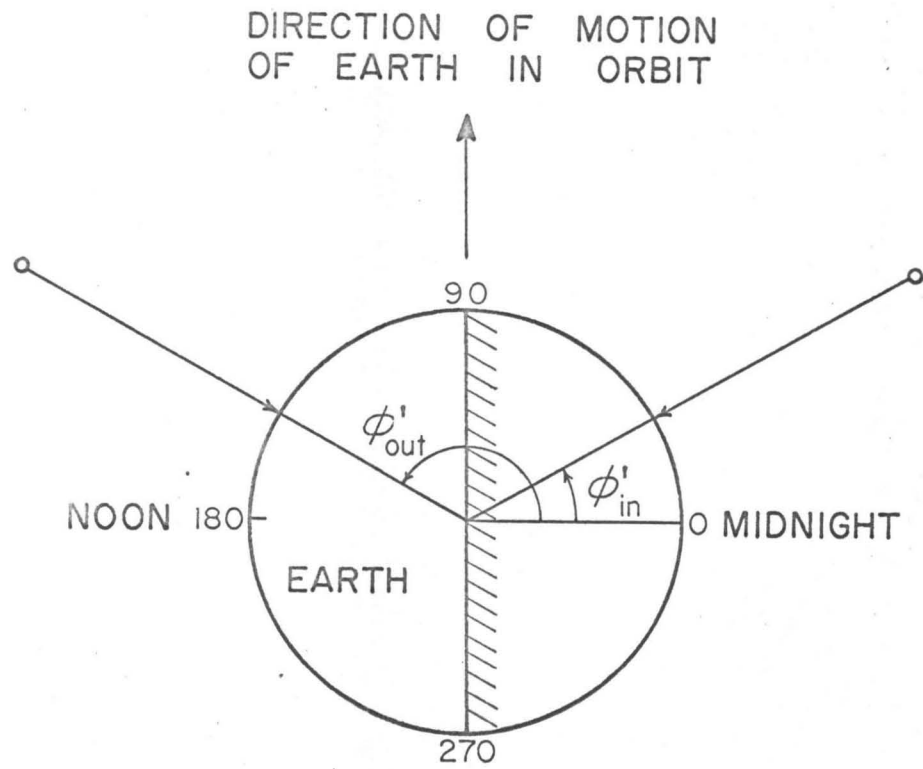


Figure 3-2. Projection of flux directions onto the plane of the ecliptic.

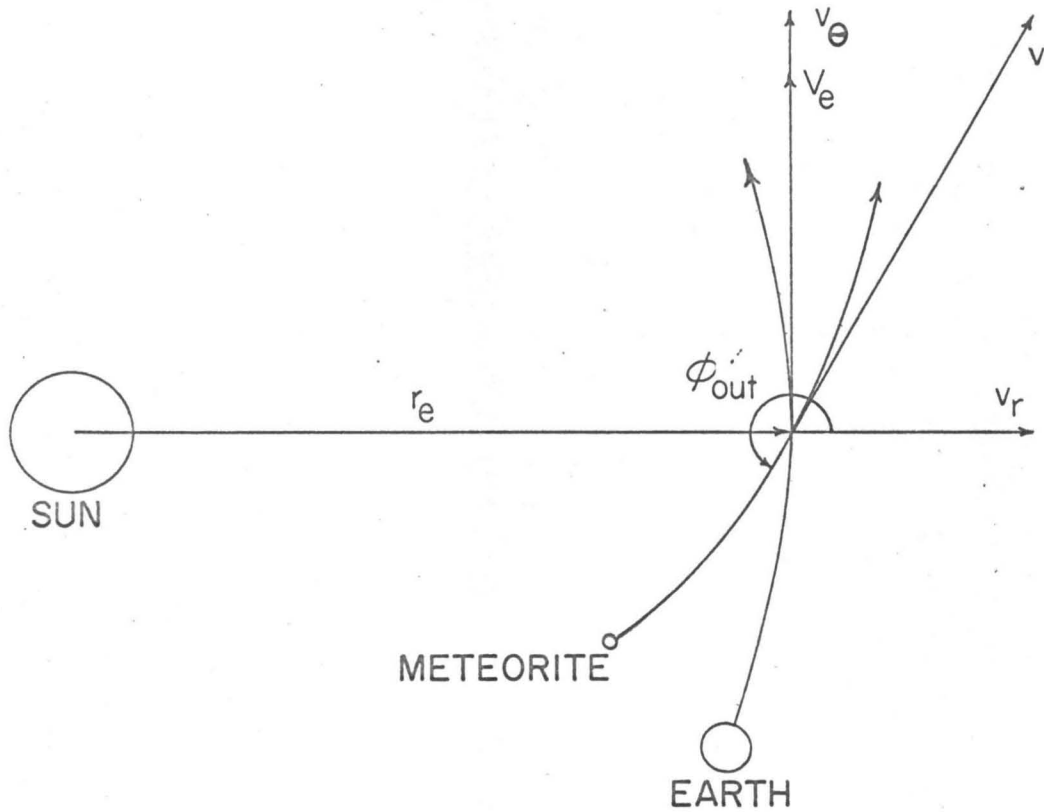


Figure 3-3. Quantities used for the vectorial transformation to the geocentric coordinate system.

equation 3-2 and  $\theta_e$  found from equation 3-1. The angle of intersection between the two orbits,  $\phi_{out}$ , is given by

$$\phi_{out} = \cot^{-1} (e \sin \theta_e / (1 + e \cos \theta_e)) , \quad (3-3)$$

and the components of the velocity are

$$v_{\theta} = Kp^{\frac{1}{2}}/r_e , \text{ and} \quad (3-4)$$

$$v_r = v_{\theta} \cot \phi_{out} \quad (3-5)$$

where  $k = 29.6 \text{ km.-a.u.}^{\frac{1}{2}}/\text{sec.}$  The vectorial transformation to the geocentric coordinate system is made by the equations

$$v'_r = v_r , \quad (3-6)$$

$$v'_{\theta} = v_{\theta} - V_e , \text{ and} \quad (3-7)$$

$$\phi'_{out} = \tan^{-1} (v'_{\theta}/v'_r) . \quad (3-8)$$

Substitution of equations 3-1 through 3-7 into equation 3-8 gives  $\phi'_{out}$  in terms of  $p$  and  $e$  and the constants  $K$  and  $V_e$  (in astronomical units):

$$\phi'_{out} = \tan^{-1} (p - V_e p^{\frac{1}{2}}/K) / (e^2 - (p-1)^2)^{\frac{1}{2}} . \quad (3-9)$$

The curves for  $\phi'_{out}$  vs.  $e$  for various values of  $a$  are shown in Figure 3-4.

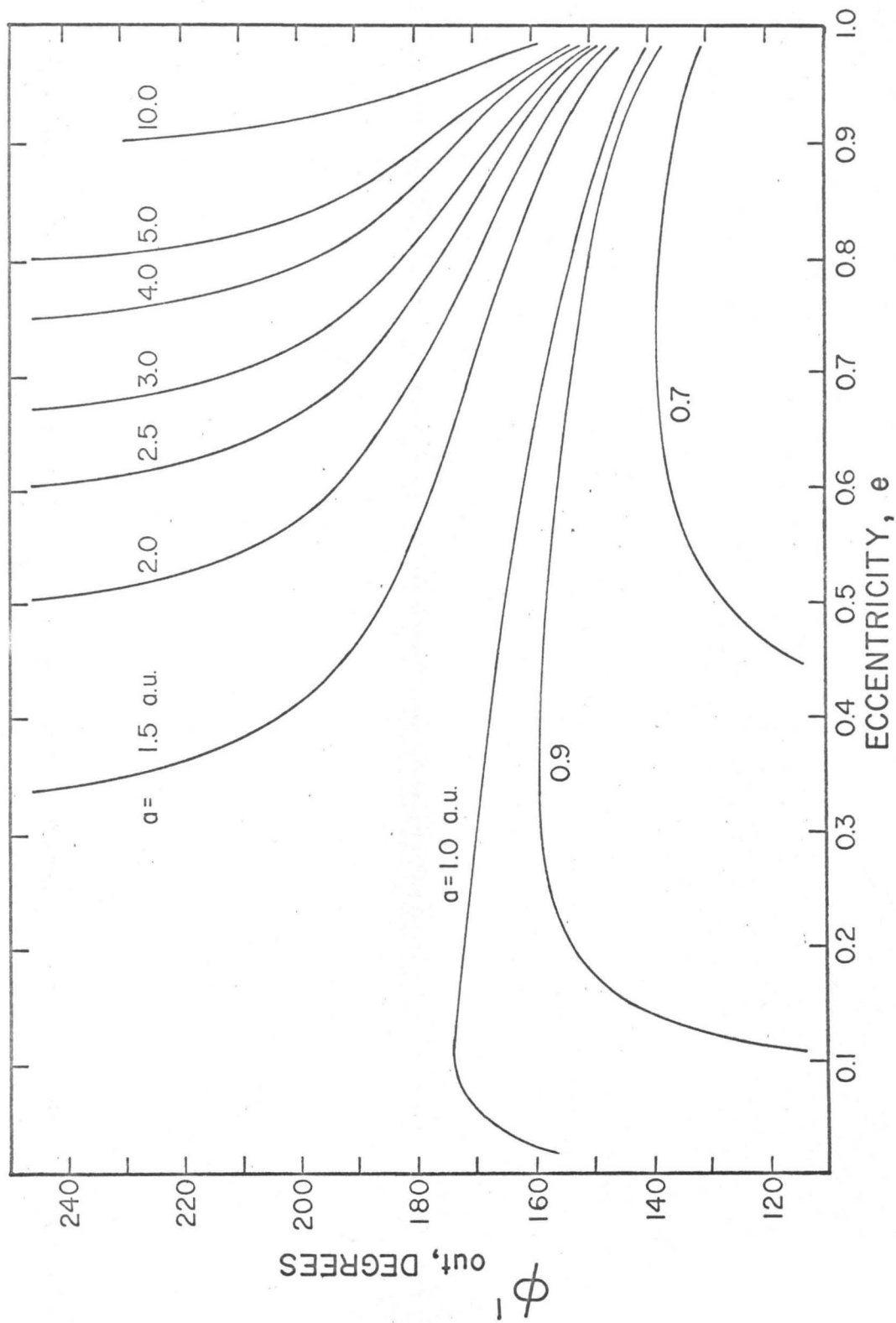


Figure 3-4.  $\phi'_{out}$  vs.  $e$  for various values of  $a$ .

### TYPE COMPOSITION OF THE FLUX

Much evidence has been compiled concerning the origins of meteorites, and among the firm conclusions reached so far are the facts that they were once part of one or more larger bodies and that their history has been quite complex. Newton in 1888 (3), after examining the radiants of fall for 116 meteorites, concluded that the bodies had travelled in solar system orbits with aphelia in the asteroid belt. Whipple and Hughes (4) concurred and, in addition, found the meteorites to be part of the sequence: radio-meteors, visual meteors, photographic meteors, fainter fireballs, great fireballs, detonating bolides, and meteorites. The contribution from cometary particles decreases within this sequence as also do the eccentricity and inclination of the orbits in which the bodies travel. These authors also determined the root-mean square atmospheric velocity of meteorites to be 17 km./sec.

In order to be able to interpret the observed yearly, monthly, and hourly patterns of fall, I began by considering a model for the injection of meteorites into orbits which intersect the earth's orbit in order to see what patterns resulted. Before discussing this model let us consider the possible number of intersections between the orbit of a meteorite and the orbit of the earth. If the orbit lies in the plane of the ecliptic ( $i=0$ ), then there are:

- no points of intersection ( $p/1+e$  greater than 1 a.u.),
- 1 point of intersection ( $p/1+e = 1$  a.u.), or
- 2 points of intersection ( $p/1+e$  less than 1 a.u.).

If the orbit of the meteorite is inclined to the plane of the ecliptic ( $i \neq 0$ ), there are:

- no points of intersection ( $p/1+e$  greater than 1 a.u. or  $p/1+e$  less than 1 a.u. and a node does not occur at 1 a.u.),
- 1 point of intersection ( $p/1+e$  less than 1 a.u. and a node occurs at 1 a.u.), or
- 2 points of intersection ( $p/1+e$  less than 1 a.u. and  $p = 1$  a.u., i.e., the line joining the points of intersection is the latus rectum; this is a rather special orbit).

To get some idea of the relative proportions of single and double intersections, we may examine the distribution for comets and meteor streams (5). 3 out of 25 known cometary or meteor stream orbits intersect the earth's orbit twice while 22 do so only once. Since Whipple and Hughes (4) found that the orbits of meteorites have lower inclination than meteor or cometary orbits, a reasonable guess at the proportion for these bodies would be:

- 1 intersection - 80%
- 2 intersections - 20% .

To return to the model, assume that the asteroid belt is the source of meteorites and that collisions between

asteroids alter their orbits so that they can intersect the earth's orbit. Piotrowski (6), who performed calculations on collision frequencies in the asteroid belt, concluded that:

- a) the mean value of the relative collision velocity is about 5 km./sec.;
- b) one catastrophic collision occurs on the order of  $10^7$  to  $10^8$  years;
- c) an asteroid is reduced to  $\frac{1}{2}$  of its initial mass by non-catastrophic collisions over a period of time on the order of  $\frac{1}{3}$  of the time for one catastrophic collision; and
- d) several times  $10^9$  tons of material are pulverized annually.

Most of the observed asteroid orbits have relatively low eccentricities (average  $e = 0.15$ , average  $a = 2.89$  a.u., and average  $p = 2.8$  a.u.) and low inclination to the ecliptic plane (average  $i = 10^\circ$ ). In order for a body travelling in such an orbit to change to another orbit which will intersect that of the earth, at least 5 km./sec. would have to be added vectorially to the initial velocity of 17.7 km./sec. If the asteroid is travelling in a less probable, more eccentric orbit having  $e = 0.5$ ,  $a = 3.3$  a.u., and  $p = 2.5$  a.u. then at  $r_a = 2.8$  a.u. (approaching the sun) about 3.5 km./sec. or more are still required to accomplish the transition. Thus collision processes yielding velocities on the order of

1 to 10 km./sec. (in the center of mass coordinate system for the asteroids involved) are required to inject these bodies into earth colliding orbits.

With the knowledge presently available, it is difficult to describe the phenomena attending collisions between bodies of asteroidal size moving at 5 km./sec. relative to each other. The only comparable event, for which the results are available for examination, is that of the collision between a large meteorite and the earth or moon. Our understanding of these events has been increased in recent years by studies of the meteorite impact craters here on earth (7,8). Baldwin (7) concluded that in such a collision the meteorite, which is travelling at speeds greater than sound in the medium, buries itself using up its kinetic energy in the formation of a tremendously compressed plug of matter. After the meteorite is brought to rest the stored energy produces a tremendous explosion which results in the crater. Krinov (9) cites the theoretical work of Staniukovich and Fedynskii on the conditions of fall of gigantic meteorites. According to their work, the transition from a shattering, splashing type of collision to an explosive event takes place at velocities of 3-4 km./sec. and at 5 km./sec. the explosive action of the meteorite is equivalent to that of an equal mass of conventional explosive material. Immediately following impact, the solid body of the meteorite possesses the characteristics of a strongly compressed gas

because the energy in the shock wave is much larger than that due to the intermolecular cohesive forces. Shoemaker (8) advances a description of the events attending these collisions for which he draws upon data compiled from sub-surface nuclear explosions. The high-velocity meteorite penetrating the ground is shattered and fused by the resulting shock wave and its kinetic energy is used to compress and fuse the rock ahead of it which expands outward producing a cavity. A shock wave propagates away from this expanding cavity and is reflected from the surface of the ground as a rarefaction wave. During reflection, momentum is trapped in the material above the cavity producing an upward and outward movement which yields the crater.

There is some risk involved in any attempt to extrapolate these hypotheses to collisions in the asteroid belt. Asteroidal bodies are of comparable size and some of the energy of collision must be wasted in a partial transfer of momentum which would mean less energy is available for the explosion. Since the average velocity of collision given above (5 km./sec.) is near the threshold velocity for an explosion, this wasted energy might lower the effective velocity below the threshold value. However, the 5 km./sec. collision is an average and many collisions must exceed this value. Since collisions between two bodies of different size are more probable than between bodies of the same size, it will be assumed that the smaller asteroid buries itself

in the larger, perhaps altering the orbit of the latter to some degree. A rupturing explosion then takes place injecting the fragments of the larger body into their new orbits.

The question as to whether an explosive process can produce fragment velocities of the order of 1 to 10 km./sec. must still be answered. The events attending small explosions, used for blasting rock, were investigated by Noren (10). He found that the rock was broken up by the primary and reflected shock waves and then the burden moved out by the expanding gases. He also cited experiments performed in water which indicate that only a small fraction of the energy from the explosion is found in the shock wave. If the same picture is true for the explosions we are considering (this seems to contradict the description given by Shoemaker), then the maximum velocity which the fragments can attain is that of the gas molecules driving them. In Table 3-1 are listed the calculated root-mean square speeds of iron and silicon atoms at various temperatures. This crude calculation shows the minimum temperatures required to yield velocities of the order in which we are interested. No attempt will be made to show whether these temperatures can actually be achieved although it is certainly evident that the energy is available because at 5 km./sec., there are  $3 \times 10^4$  calories per gram of asteroid. As for explosions

TABLE 3-1. Calculated Root-mean Square Speed of Iron and Silicon Atoms as a Function of Temperature. The expression  $\bar{c} = (3RT/M)^{\frac{1}{2}}$  was used for the calculation. The boiling point for iron is 3300°K. and for silicon is 2900°K.

<u>T (°K)</u>	<u><math>\bar{c}</math> (km./sec.)</u>	
	<u>Fe</u>	<u>Si</u>
5,000	1.49	2.11
10,000	2.11	2.98
15,000	2.58	3.64
20,000	2.98	4.20

which are more familiar and amenable to experimental observation, the light-weight fragments from an exploding shell casing attain velocities of 3.1 km./sec. (11).

An explosion was applied to one asteroid for each of two situations. In each case the fragments resulting from the explosion were considered to be distributed isotropically with respect to the frame of reference of the stationary asteroid and at velocities,  $v'_0$ , of 5, 8, and 10 km./sec. in the same reference frame. The simplified 2-dimensional case where the fragments remain in the plane of the ecliptic was the only one considered. (The limits calculated for the monthly distributions should remain the same for the 3-dimensional case.) The two situations were:

- 1) asteroid initially travelling in a circular orbit with  $r_a = 2.8$  a.u.; and
- 2) asteroid initially travelling in an orbit with  $e = 0.5$ ,  $a = 3.3$  a.u., and  $p = 2.5$  a.u. and the explosion occurring while the body is moving toward the sun at  $r_a = 2.8$  a.u.

Some obvious departures from reality for such calculations are:

- a) the fragments are probably not distributed isotropically,
- b) all the fragments don't leave the explosion with the same velocity,

- c) the 2-dimensional approximation,
- d) the differences in the amount of time spent by bodies in different orbits crossing the earth's orbit have been ignored (i.e., differences in probability for collisions with the earth), and
- e) the perturbations over long periods of time produced by the major planets and the Poynting-Robertson effect.

Using the above model, the monthly patterns of fall to be expected were calculated and are shown in Figure 3-5 and 3-6. The months in these graphs are measured from the negative side of the radius vector from the sun which passes through the point of the explosion. It should be noted that all of the patterns are qualitatively similar with maxima located near the outer limits of each distribution. The initially circular asteroid orbit yields a symmetrical pattern while the initially non-circular orbit gives an asymmetric pattern. The month-range of the patterns decreases with decreasing  $v_0'$  and although narrow, well-defined streams (as in the case of meteors) do not result, the broad maxima do approximate streams. In the asymmetric situation, the periods for orbits corresponding to different months of fall may vary quite widely (over factors of about 40).

The fact that different types of meteorites exist and that even within one type chemical groupings appear (12) raises the question: was the asteroid, which gave rise

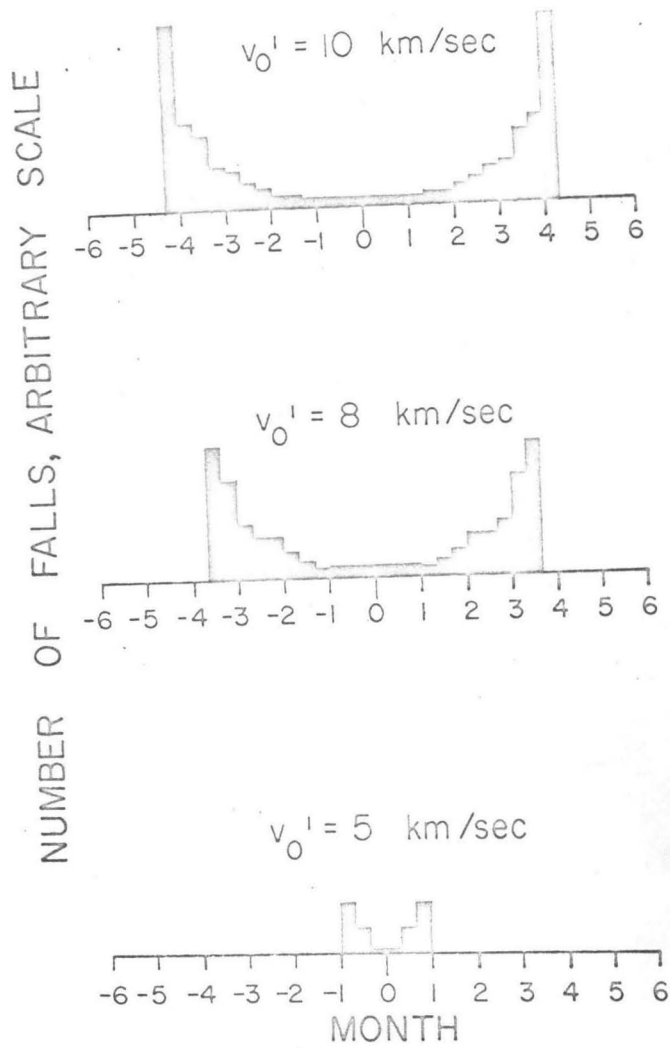


Figure 3-5. Monthly pattern of fall at the earth's orbit following isotropic breakup of asteroid. Initial orbit of asteroid: circular with  $r_a = 2.8$  a.u.

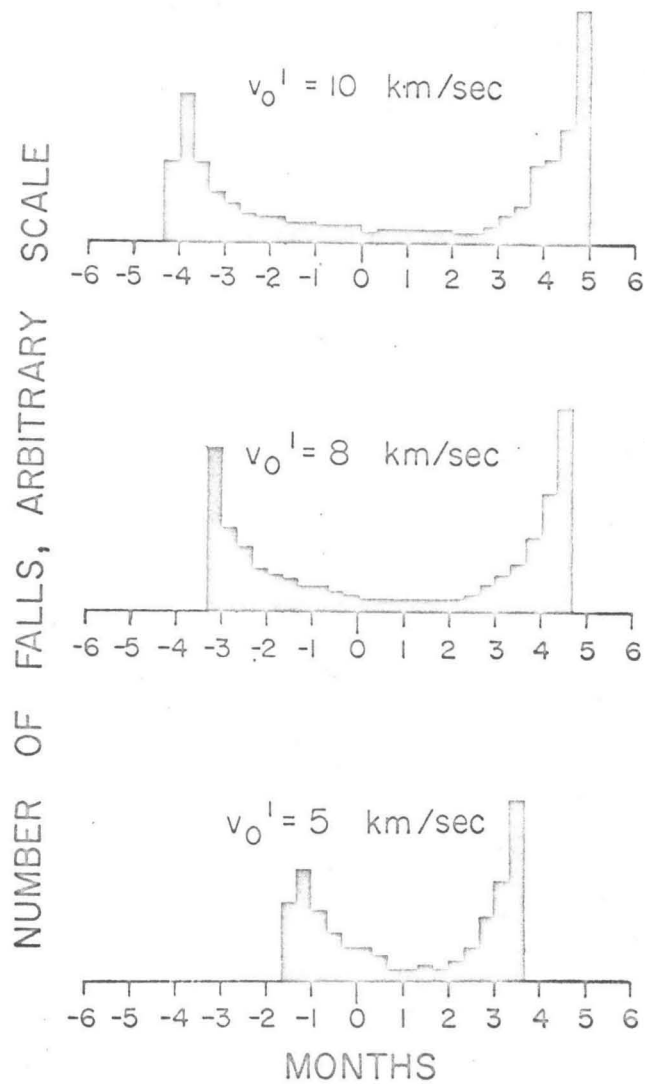


Figure 3-6. Monthly pattern of fall at the earth's orbit following isotropic breakup of asteroid. Initial orbit of asteroid:  $e = 0.5$ ,  $a = 3.3$  a.u.,  $p = 2.4$  a.u., with breakup occurring at  $\theta = 2560$ ,  $r_a = 2.8$  a.u.

to the meteorite, composed only of the type of meteoritic material found in the meteorite or was it composed of a mixture of different types of meteoritic material? If the first idea is correct, then the differentiation producing the various types and groupings of meteorites occurred in a larger body or system of bodies. If the second idea prevails, then the possibility exists that the differentiation occurred within the asteroidal body itself. If an asteroid of nearly uniform composition (first hypothesis) is broken up according to the model described above and the fragments are injected into earth colliding orbits, then the patterns of fall for a single type of meteorite might reflect this history. It is obvious that the resolution inherent in such an approach depends upon the frequency of occurrence of explosive collisions in the asteroid belt. An examination on the basis of chemical similarities or groupings of meteorites would be more valuable than one conducted only on the basis of mineralogical classification but such a study must wait until more extensive analytical data are obtained for a much larger number of meteorites.

The observed monthly pattern should be affected by the changing seasons; the yearly pattern should be affected by the increasing world population density; and the hourly pattern should be influenced by the changing amount of daylight. The effect of these observational factors was reduced by plotting the data on a fractional basis. Figures 3-7 and 3-8 show the log of the fraction of classified falls

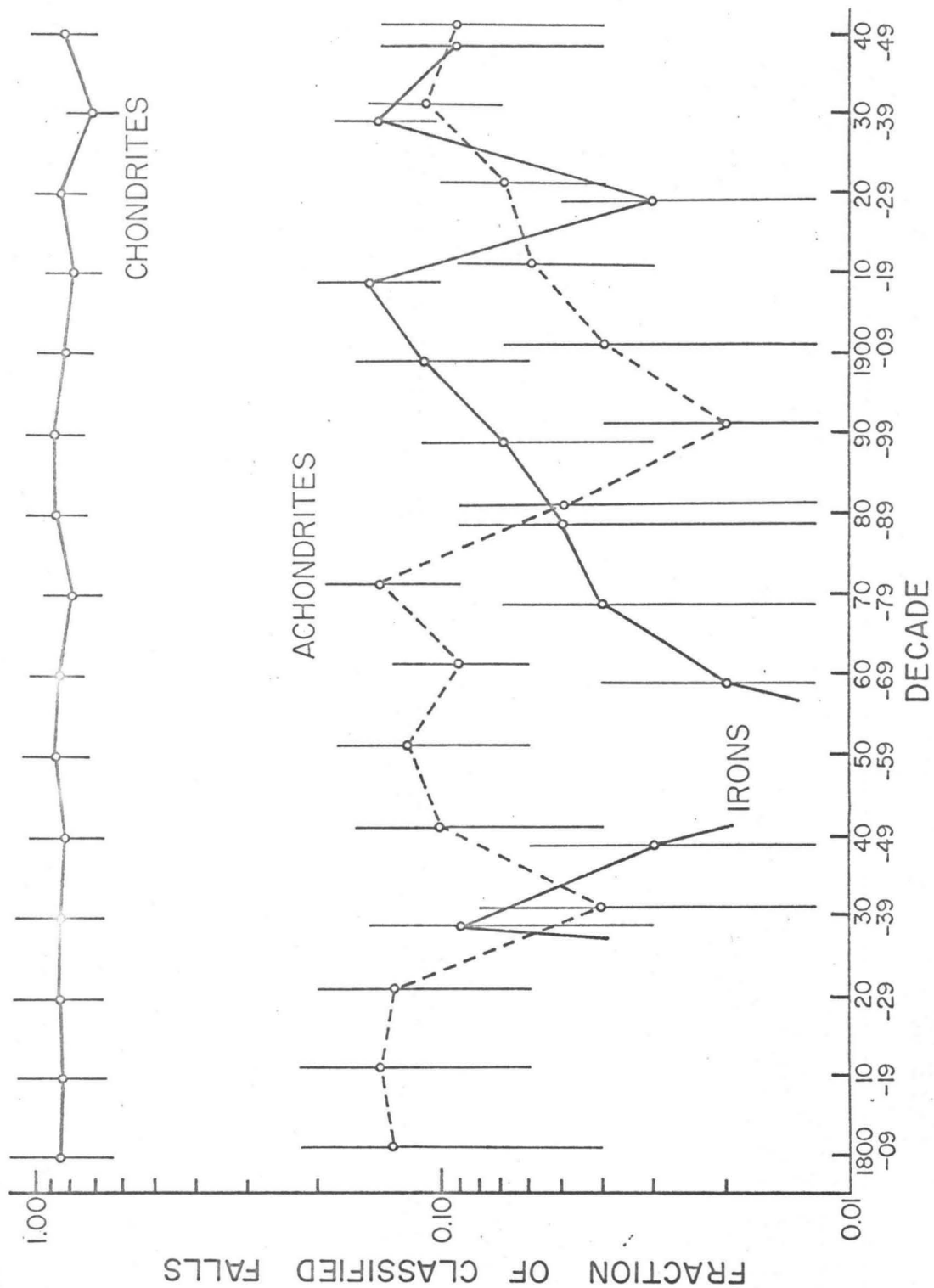


Figure 3-7. Composition of the total flux as a function of the decade.

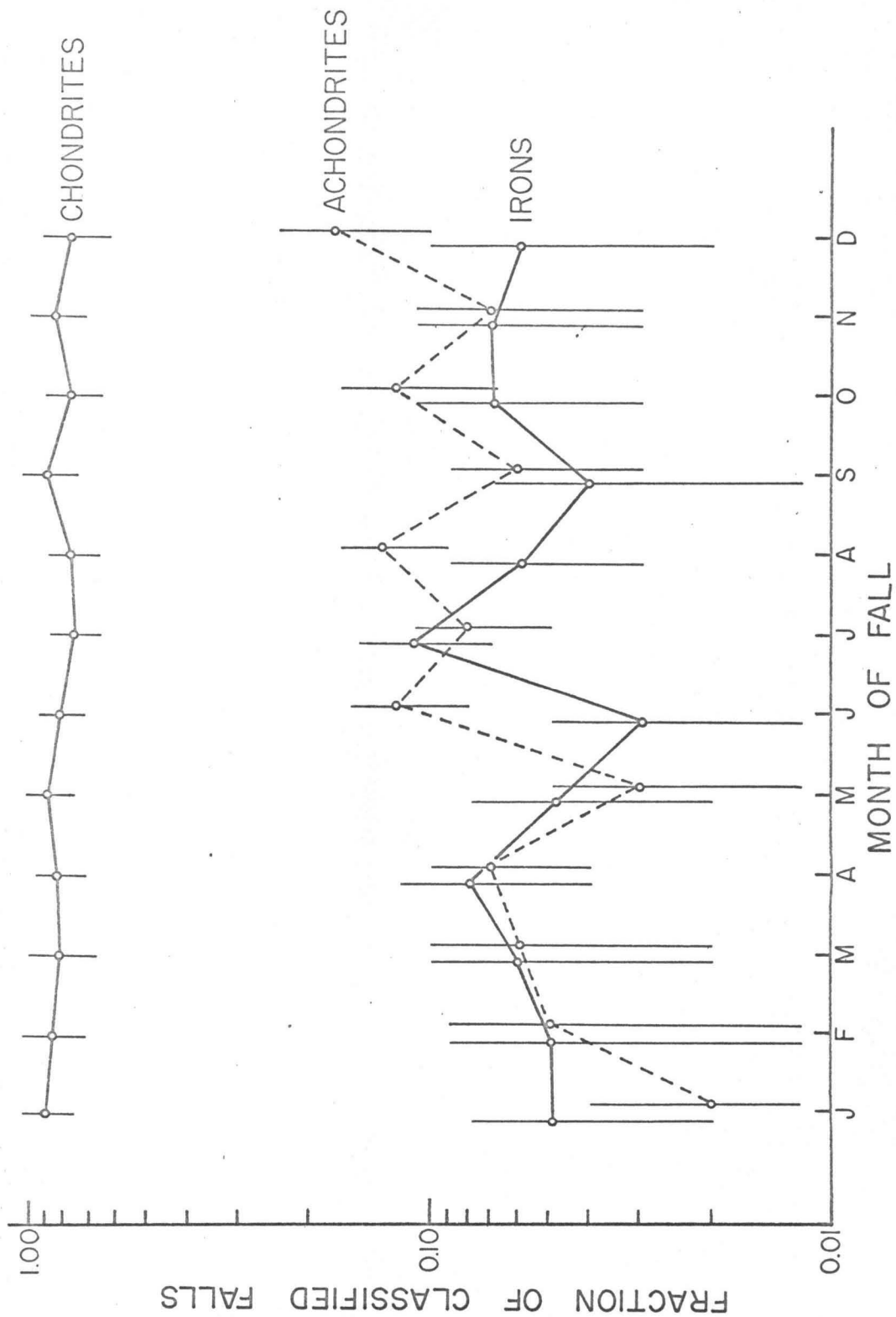


Figure 3-8. Composition of the total flux as a function of the month.

as a function of decade and of month respectively. Since the chondritic falls predominate at all times, only the curves for the irons and achondrites show wide fluctuations and poor statistics play a part in these. The standard deviation (square-root of the number of meteorites) is shown as a vertical line through each point. Some fluctuations appear to be larger than those due to statistics. These include the high achondritic-low iron flux between 1850 and 1870 and the low achondritic-high iron flux from 1890 to 1910. The monthly patterns for irons and achondrites parallel each other except for June where the achondrites are more abundant than the irons by a factor of 5.

In order to bring out more detail in the chondritic flux, it is shown broken down according to type in Figures 3-9 and 3-10. The bronzite flux fluctuates more widely than that for hypersthene chondrites with both decade and month and shows a pronounced maximum in May. The statistics for the carbonaceous chondrites and eucrites are very poor although the carbonaceous chondrites do show a maximum in April. No meteoritic type shows a clear-cut preference for any particular month. Although these graphs are necessary to characterize the flux, they do not contribute much to the search for correlations in fall patterns between the different types.

Further resolution is achieved by plotting the month vs. year for falls according to type. These graphs are

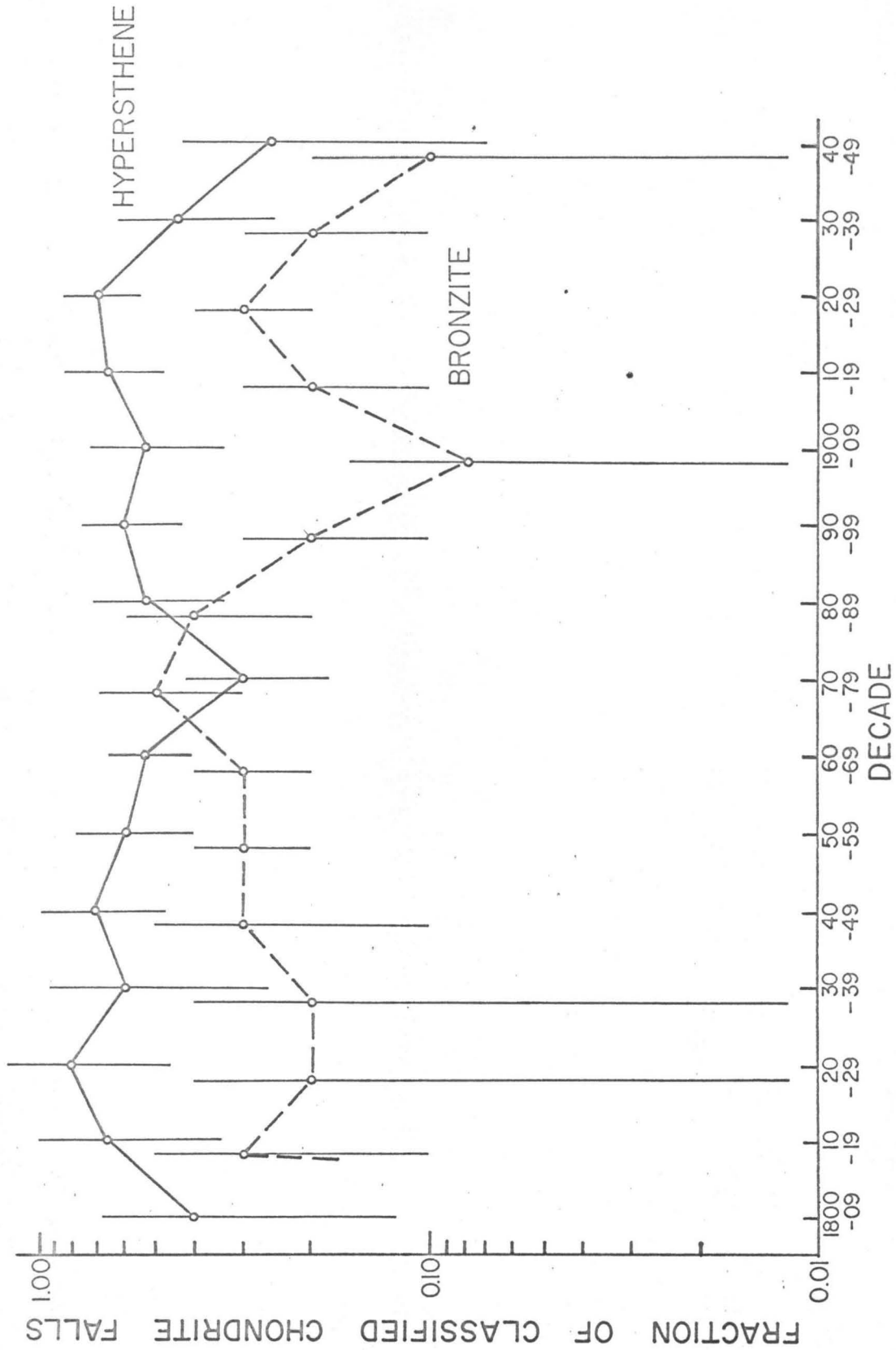


Figure 3-9. Composition of the chondritic flux as a function of the decade.

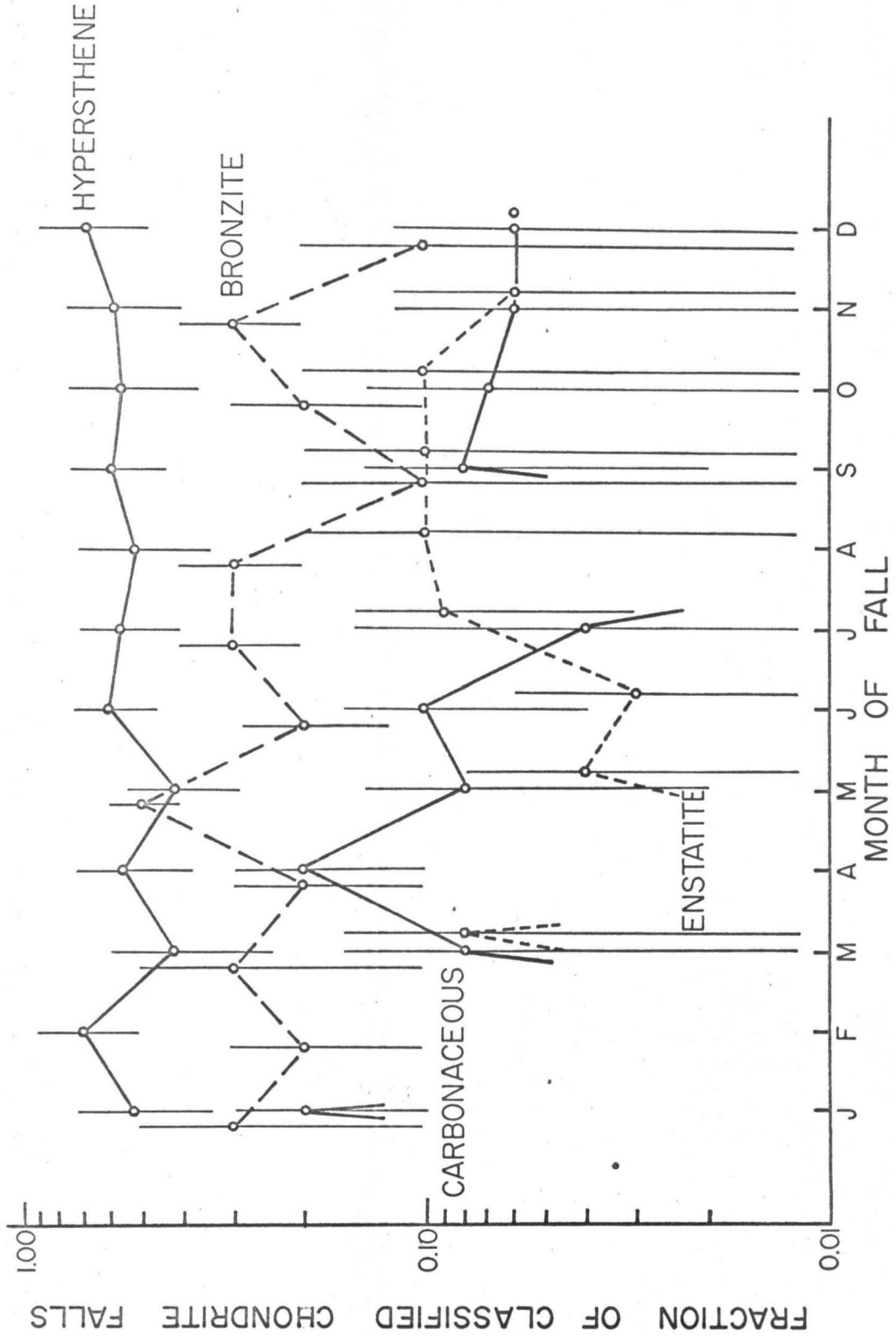


Figure 3-10. Composition of the chondritic flux as a function of the month.

shown in Figures 3-11 through 3-20 along with histograms of the monthly patterns (by 10-day intervals) and yearly patterns. The open circles in these graphs represent daytime falls, the solid circles represent nighttime falls, and falls for which the hour is unknown are shown as crosses. The statistics for the 10-day interval histograms are poor and since these were evaluated for randomness, synthetic distributions were generated for comparison by using a random digit table (13). These are shown plotted in Figure 3-21. The features displayed by the graphs for the observed patterns will be presented in outline form.

Irons:

- a) evenly distributed with month except for higher rates during Mar. 20-Apr. 20 and July 1-Aug. 10;
- b) rate of recovery increased after 1900;
  - 1850-1900 - 8 falls
  - 1900-1950 - 23 falls ;
- c) prominent group of falls around July, 1935.

Octahedrite Irons:

- a) more highly concentrated during Mar. 20-Apr. 20 and July 10-Aug. 10 than other irons;
- b) July, 1935 group still present;
- c) no fall since 1935.

Stoney-Irons:

- a) appear to be randomly distributed with month;

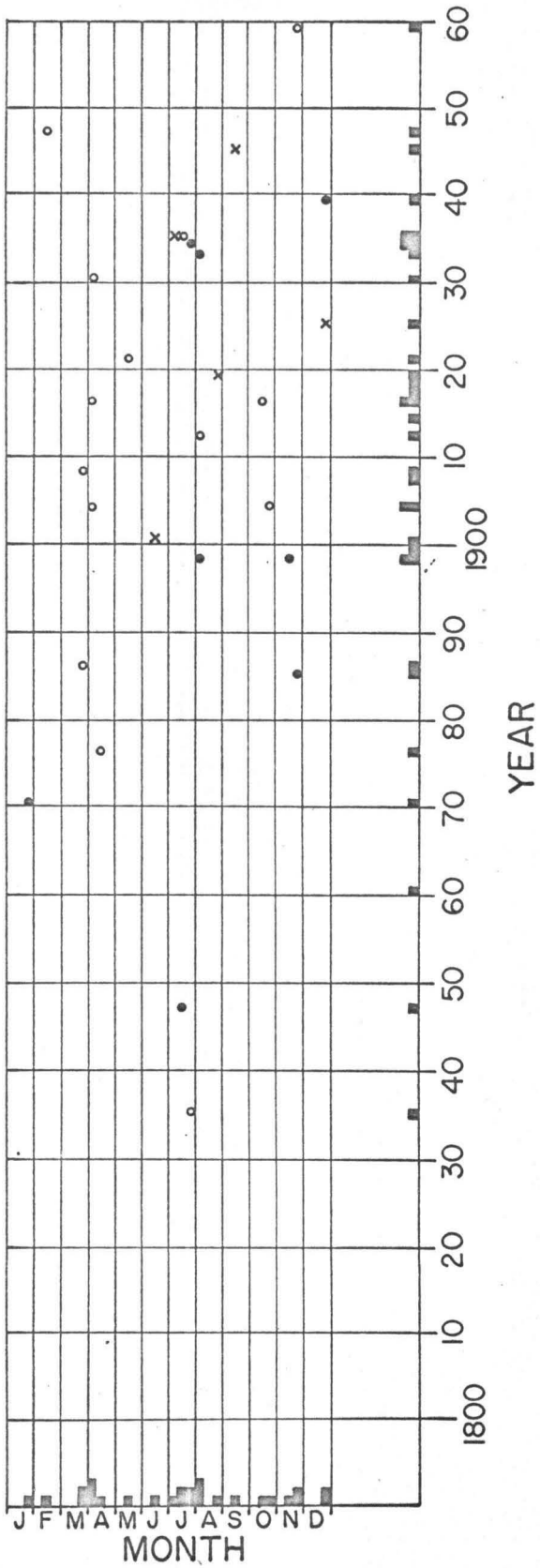


Figure 3-11. Month of fall vs. year for irons.

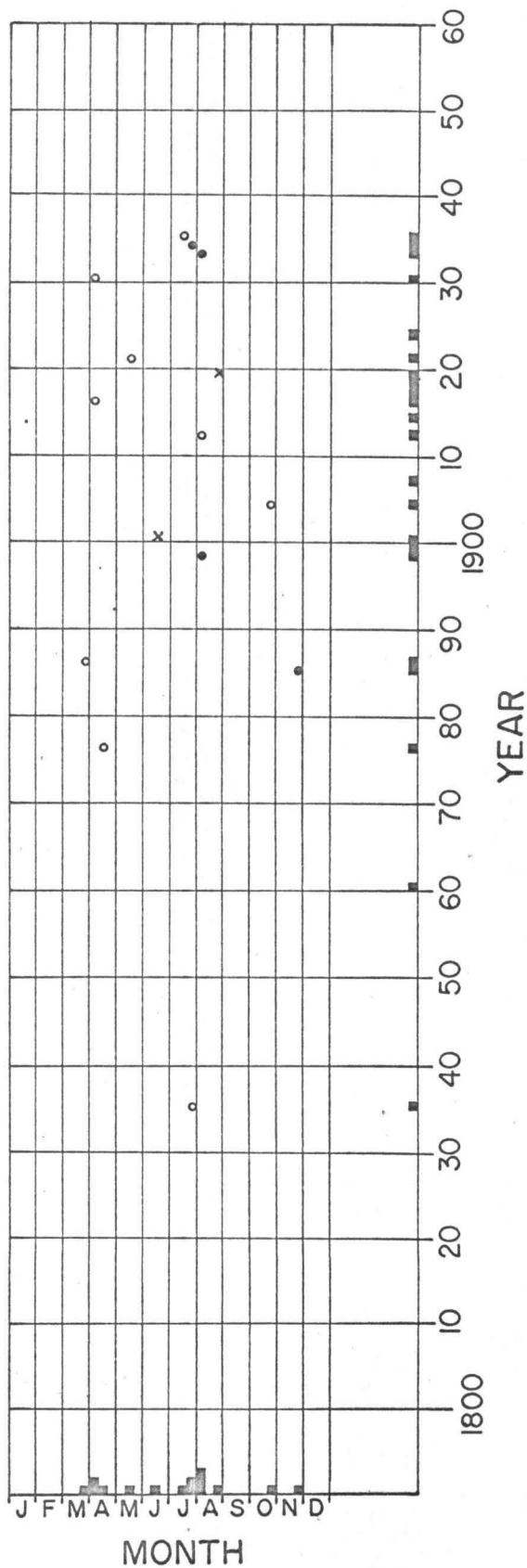
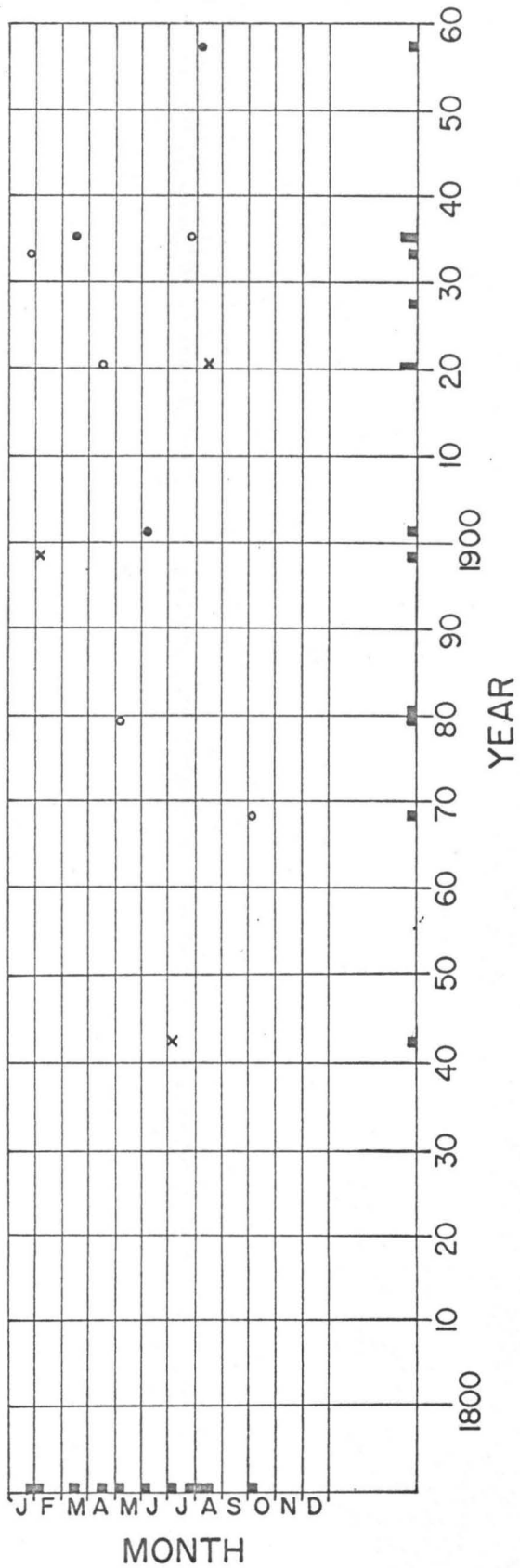


Figure 3-12. Month of fall vs. year for octahedrite irons.



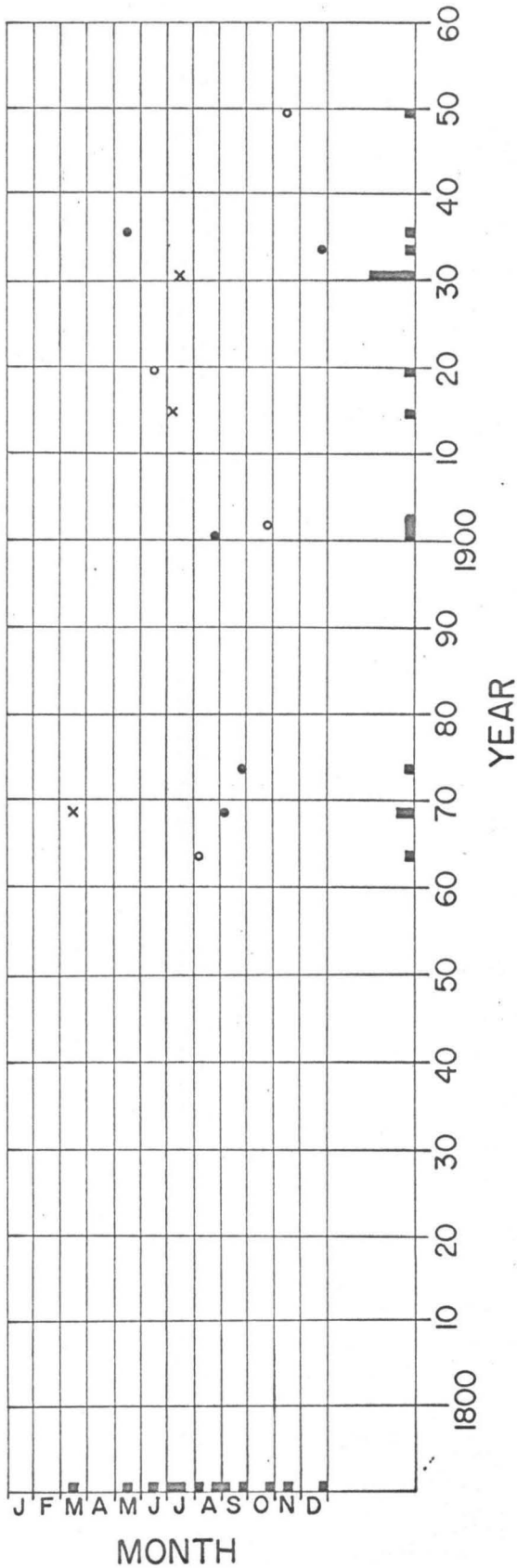


Figure 3-14. Month of fall vs. year for enstatite chondrites.

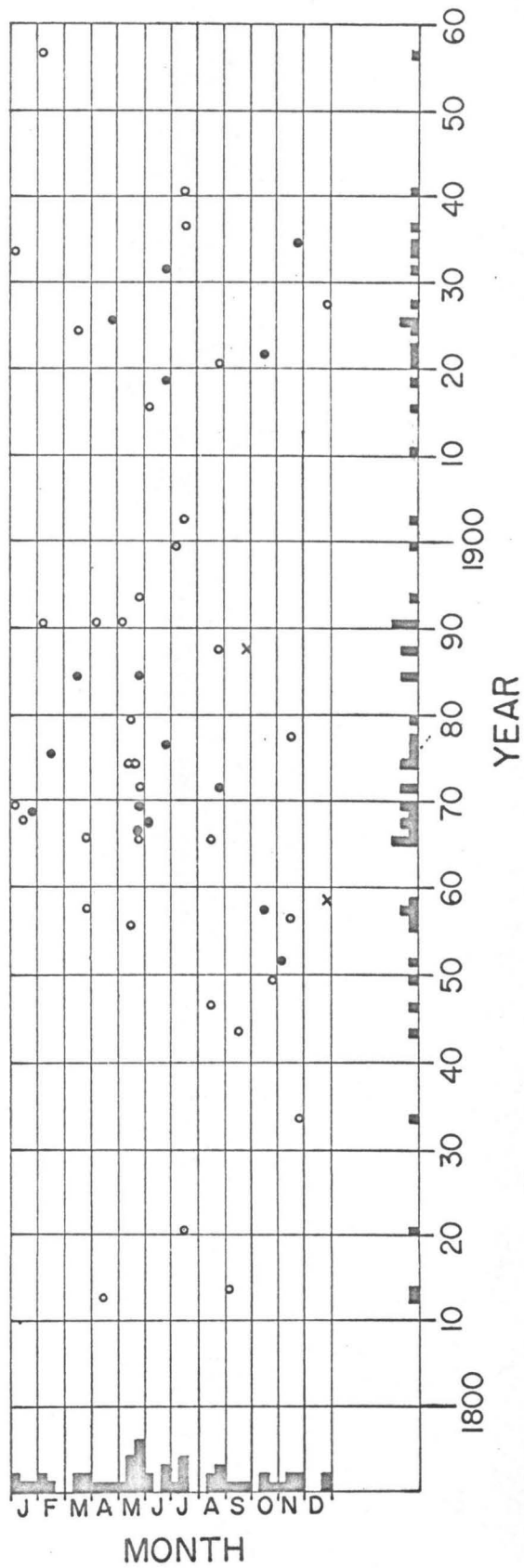


Figure 3-15. Month of fall vs. year for bronzite chondrites.

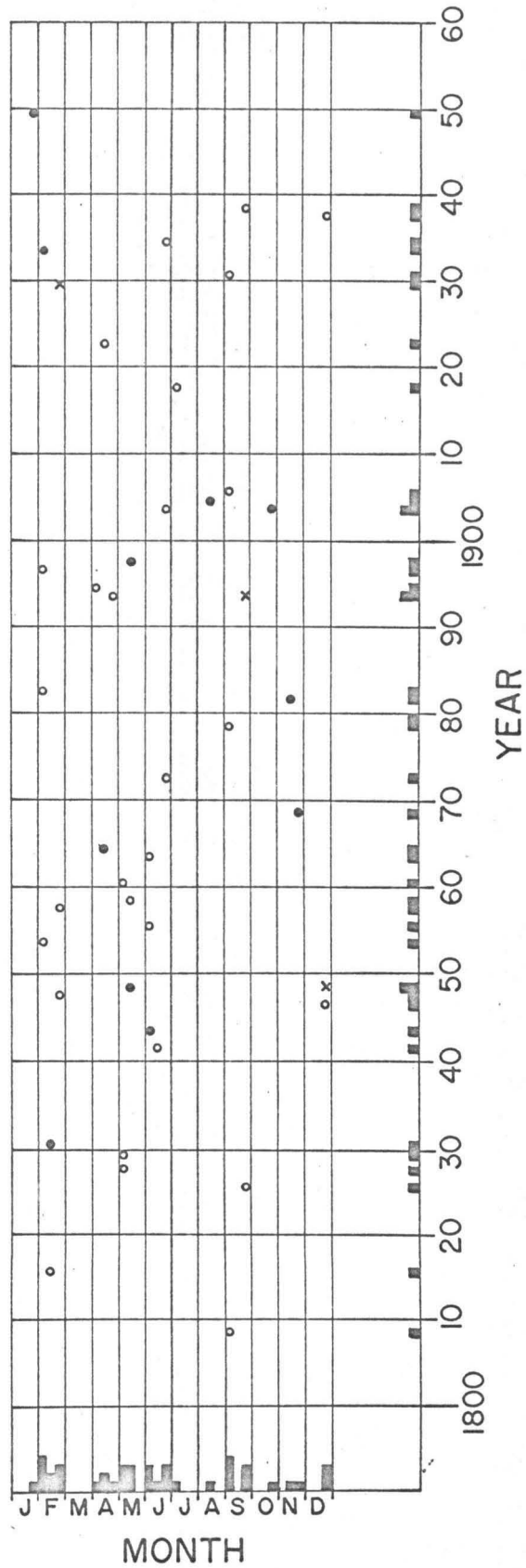


Figure 3-16. Month of fall vs. year for veined hypersthene chondrites.

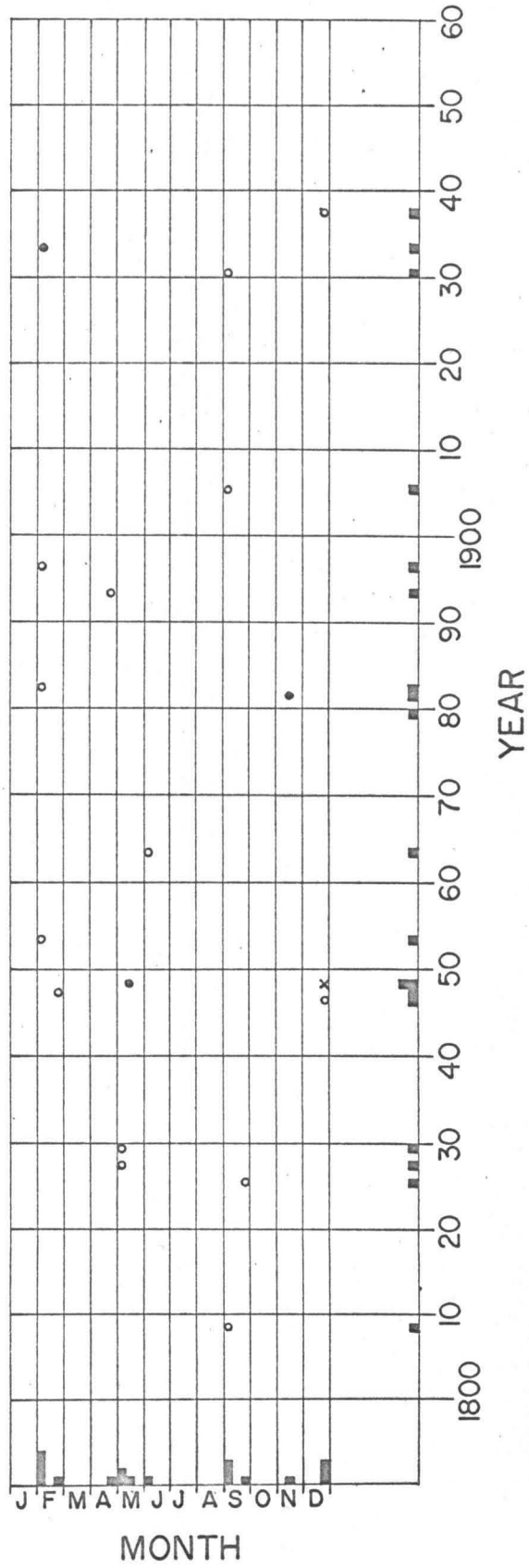


Figure 3-17. Month of fall vs. year for veined-white hypersthene chondrites.



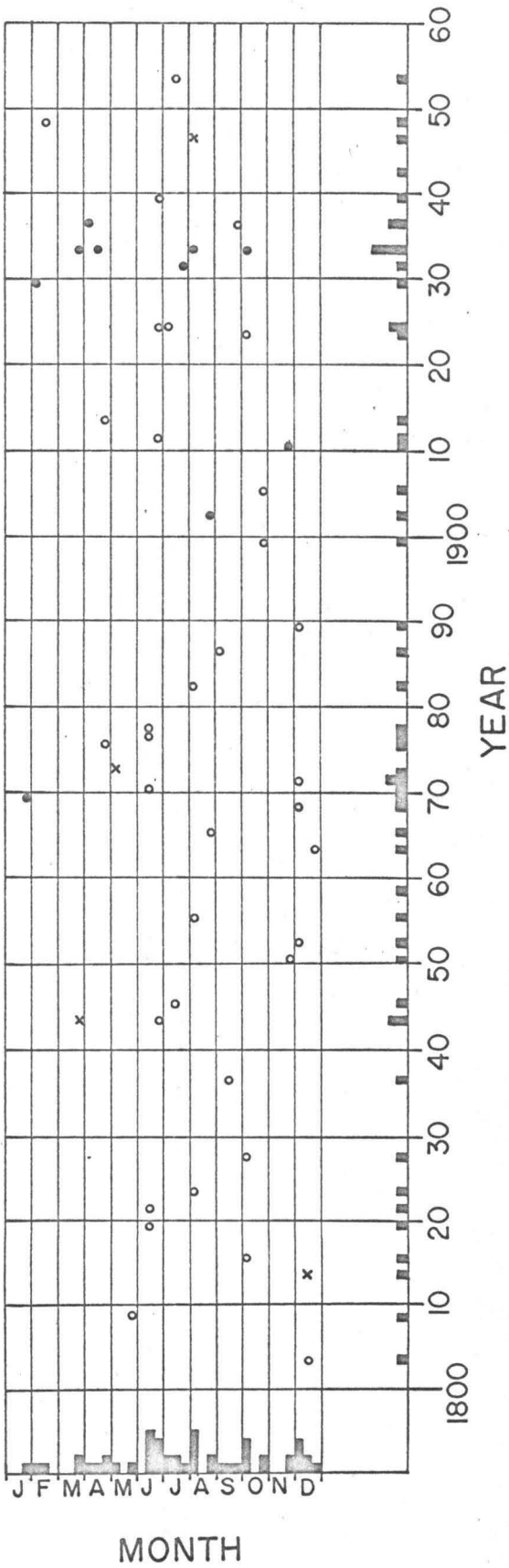


Figure 3-19. Month of fall vs. year for achondrites.



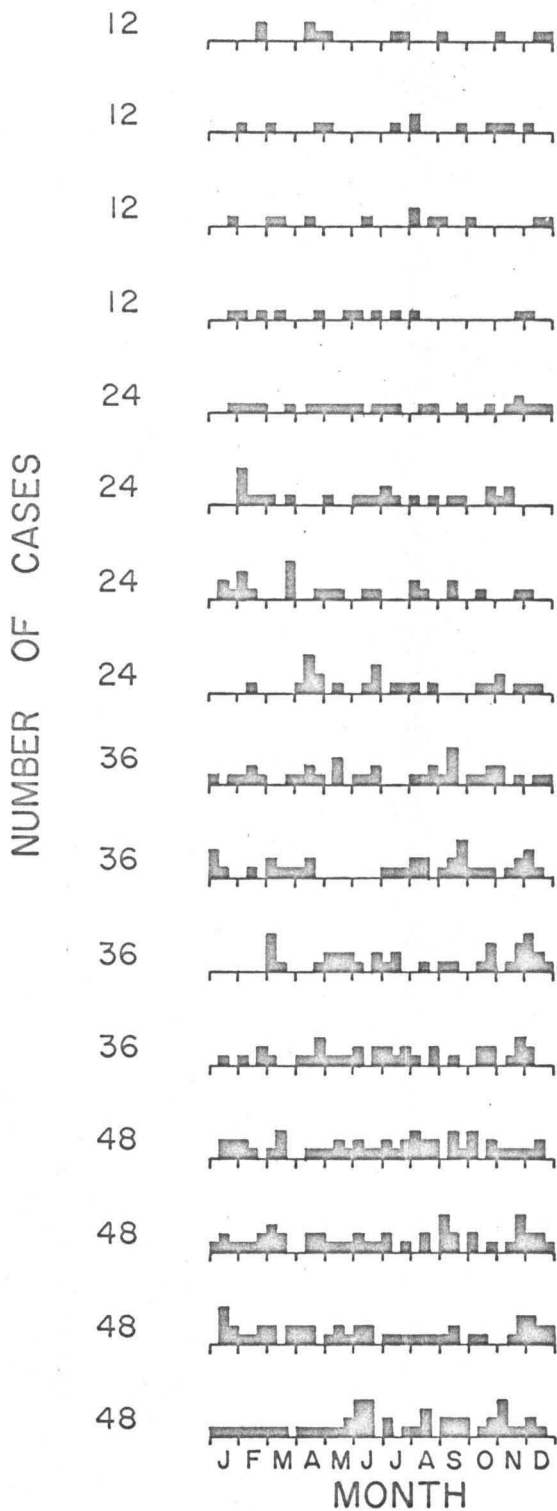


Figure 3-21. Synthetic monthly fall patterns derived from a random digit table.

- b) suggestion of 30-year periodicity, 1840-1870-1900-1930-1960(?), with falls grouped within  $\pm 10$  years around these years and absent from the middle decade between them (1850-1860, 1880-1890, 1910-1920, and 1940-1950).

Enstatite Chondrites:

- a) randomly distributed with month;
- b) no falls prior to 1860's;
- c) 1863-1875 group followed by 25-year gap;
- d) unusually high rate of fall during 1930;
- e) large fraction of nighttime falls (5 out of a total of 9).

Bronzite Chondrites:

- a) fell in all months with maximum in May;
- b) suggestion of 30-year periodicity with broad maxima around 1870 and 1930 separated by broad minima around 1900 and 1960;
- c) high rate of fall during May, 1855-1895 (only falls which occur in May).

Veined-Hypersthene Chondrites:

- a) fell in all months except March with apparent groupings in Feb., Apr.-May, and June;
- b) distributed very evenly with year but only one fall after 1940.

Veined-White Hypersthene Chondrites:

- a) display definite preference for certain 10-day intervals;

- b) rather unevenly distributed with year except for gaps from 1910-1930 and 1940-1960.

Carbonaceous Chondrites:

- a) randomly distributed with month;
- b) randomly distributed with year.

Achondrites:

- a) apparent groupings in monthly distribution-  
Mar. 20-May 10, June 10-Aug. 10, Aug. 20-  
Oct. 10, Nov. 20-Dec. 30;
- b) concentration of nighttime falls during early 1930's.

Howarditic Achondrites:

- a) Aug. 1-10 group;
- b) distributed evenly with year.

Since no clearcut monthly fall patterns emerged from these graphs, the chi-squared test for randomness (14) was applied to monthly intervals in order to find which distributions were least likely to be random. The results, shown in Table 3-2, must be interpreted with caution because of the poor statistics. In order to see exactly how much caution is required, the test was also applied to the synthetic monthly distributions in Figure 3-21. These were purposely generated for 12, 24, 36, and 48 cases to allow comparison to distributions involving similar numbers of meteorites. It is apparent that this test may yield low probabilities for randomness for distributions which are generated from

TABLE 3-2. Summary of the Results of the  
Chi-Squared Test for Randomness.

	<u>No. of Meteorites</u>	<u>Chi- Squared</u>	<u>Probability of Randomness*</u>
Observed distributions:			
Irons	27	9.9	0.5
Octahedrite irons	15	16.2	0.1
Stoney-irons	11	5.4	0.9
Enstatite chondrites	12	6.0	0.9
Bronzite chondrites	53	13.4	0.2
Veined-hypersthene chondrites	42	28.9	0.002
Veined-white hypersthene chondrites	18	23.3	0.02
Carbonaceous chondrites	18	10.0	0.53
Achondrites	50	17.7	0.1
Howarditic achondrites	14	18.6	0.08

<u>No. of Cases</u>	<u>Chi-Squared</u>				<u>Average Chi- Squared</u>	<u>Probability of Randomness*</u>
12	12.0	4.0	10.0	4.0	7.5	0.8
24	4.0	16.0	9.0	30.0	14.8	0.2
36	8.0	11.0	19.3	8.0	11.6	0.4
48	4.0	3.5	5.0	8.5	5.2	0.9

\*Probability that a random sample will give no better fit to a uniform distribution.

random digits if the number of cases is small. Thus, the only conclusion which may be drawn from the test is that the patterns which are least likely to be random are those for the veined-hypersthene chondrites, the veined-white hypersthene chondrites, the achondrites, and the howarditic achondrites.

No monthly fall patterns match the fall patterns calculated from the model but poor statistics preclude making the statement that these do not exist. Two observed distributions which come closest to matching are those for the bronzites, Mar. 10-June 10, and for the achondrites, June 10-Aug. 10.

#### Mass Composition of the Flux

Several investigators in recent years (15,16,17) have noted that the meteorites and asteroids have similar mass distributions. Kuiper (18) found that the absolute magnitudes of the asteroids obeyed the incremental law

$$dN = ar^{M_0} dM_0 \quad (3-10)$$

where  $dN$  is the number of asteroids with magnitudes between  $M_0$  and  $M_0 + dM_0$ ,  $a$  is a constant, and  $r$  is the ratio of increase for an increment of one magnitude.  $\log_{10} r$  was found to vary from 0.35 to 0.73 for different asteroidal zones with an average value of 0.56. The corresponding incremental law for mass is

$$dN = (N_0 c) m^{-(c+1)} dm \quad (3-11)$$

The statistics are improved by expressing the distribution in terms of the number of bodies having mass equal to or greater than a mass  $m$ . The mathematical expression for this "cumulative" law is obtained by integrating equation 3-11 from  $m$  to infinity and is

$$N = N_0 m^{-c} \quad (3-12a)$$

$$\text{or } \log N = \log N_0 - c \log m \quad (3-12b)$$

where  $N$  is the number of asteroids with mass equal to or greater than  $m$ .  $c$  is referred to as the "population index."

The authors mentioned above have used a variety of expressions and symbols to represent these incremental and cumulative laws. Hawkins (15) used

$$\log N = N_0 - 1.67 \log r \log m$$

for his cumulative mass law. Obviously his  $N_0$  is the  $\log N_0$  in equation 3-12b and his  $1.67 \log r$  is  $c$ . He also uses

$$\log N = N_0 + 0.667 M \log r$$

for the cumulative magnitude law, where  $M$  is the visual magnitude for a particle ablated in the earth's atmosphere. Now since  $M = \text{constant} - 2.5 \log m$ , his  $0.667 \log r$  in this expression corresponds to  $0.4c$ . Opik (16) uses the expressions

$$dN = Cx^{-p} dx \quad (\text{incremental law})$$

$$\text{and } N = N_0 x^{-s} \quad (\text{cumulative law})$$

where  $x$  is the diameter of a solar system body or of a crater on the moon. Hawkins gives for the cumulative radius law

$$\log N = N_0 - 2.5 \log r \log \rho^2$$

where  $\rho$  is the radius. Changing this expression to the exponential law, substituting the diameter,  $d$ , for the radius, and translating to the notation used in equation 3-12a yields

$$N = 4N_0 d^{-3.0c} . .$$

Thus Opik's  $N_0$  is 4 times my  $N_0$  and his  $s$  is  $3.0c$ . Brown (17) plots the log of the number of meteorites for the various increments of  $\log m$  as shown in Figures 3-22, 3-23, and 3-24. This is an incremental curve from which he finds the slope,  $d \log N / d \log m$ , of the straight line. In essence he is plotting  $\log(dN/d \log m)$  or  $\log(m dN/dm)$  vs.  $\log m$  and the equation of the straight line is

$$\log(m dN/dm) = \log(N_0 c) - c \log m .$$

From this expression it follows that

$$m dN/dm = (N_0 c) m^{-c} \quad (\text{cumulative law})$$

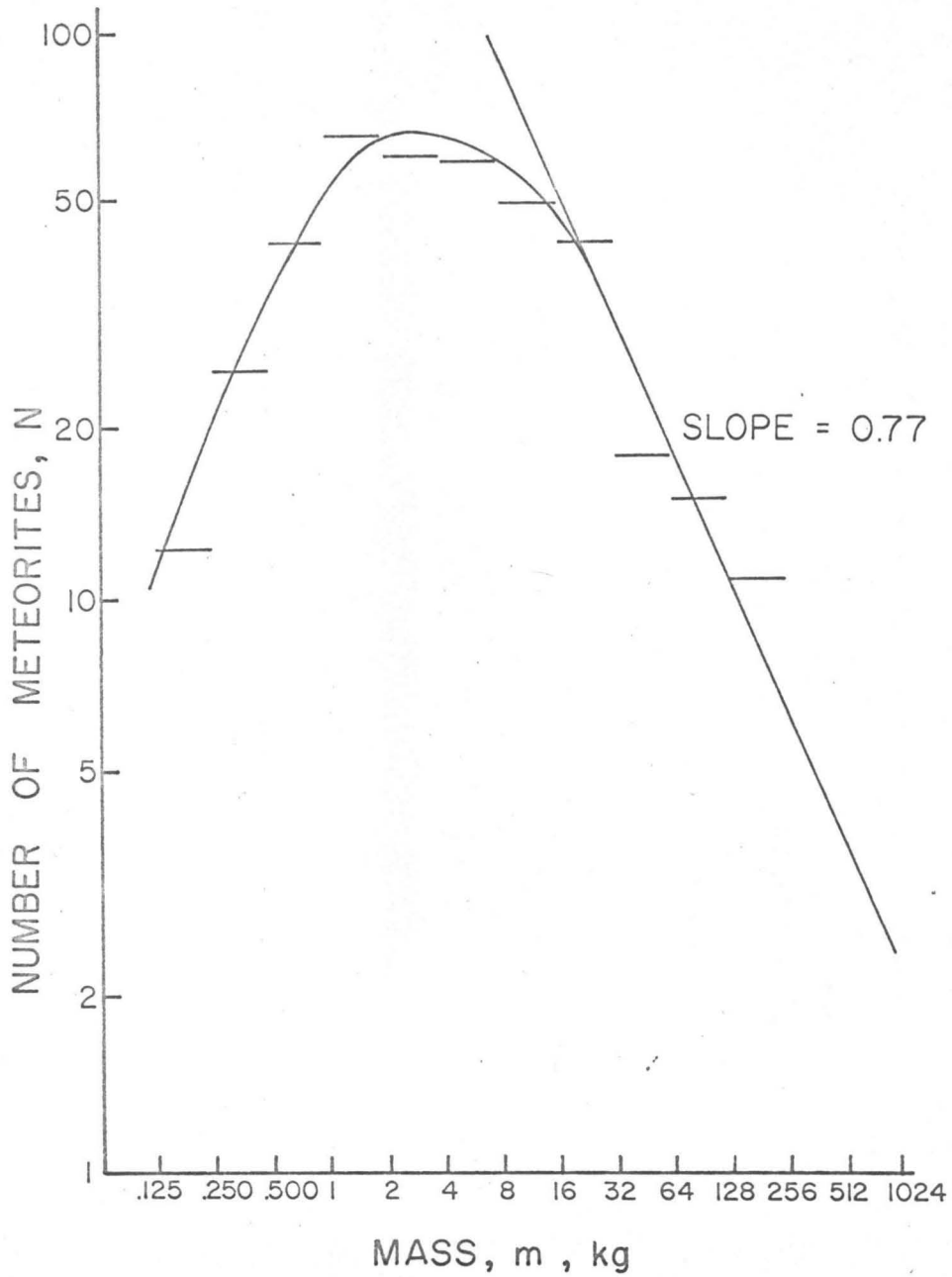


Figure 3-22. Mass distribution for 416 stone falls (17).

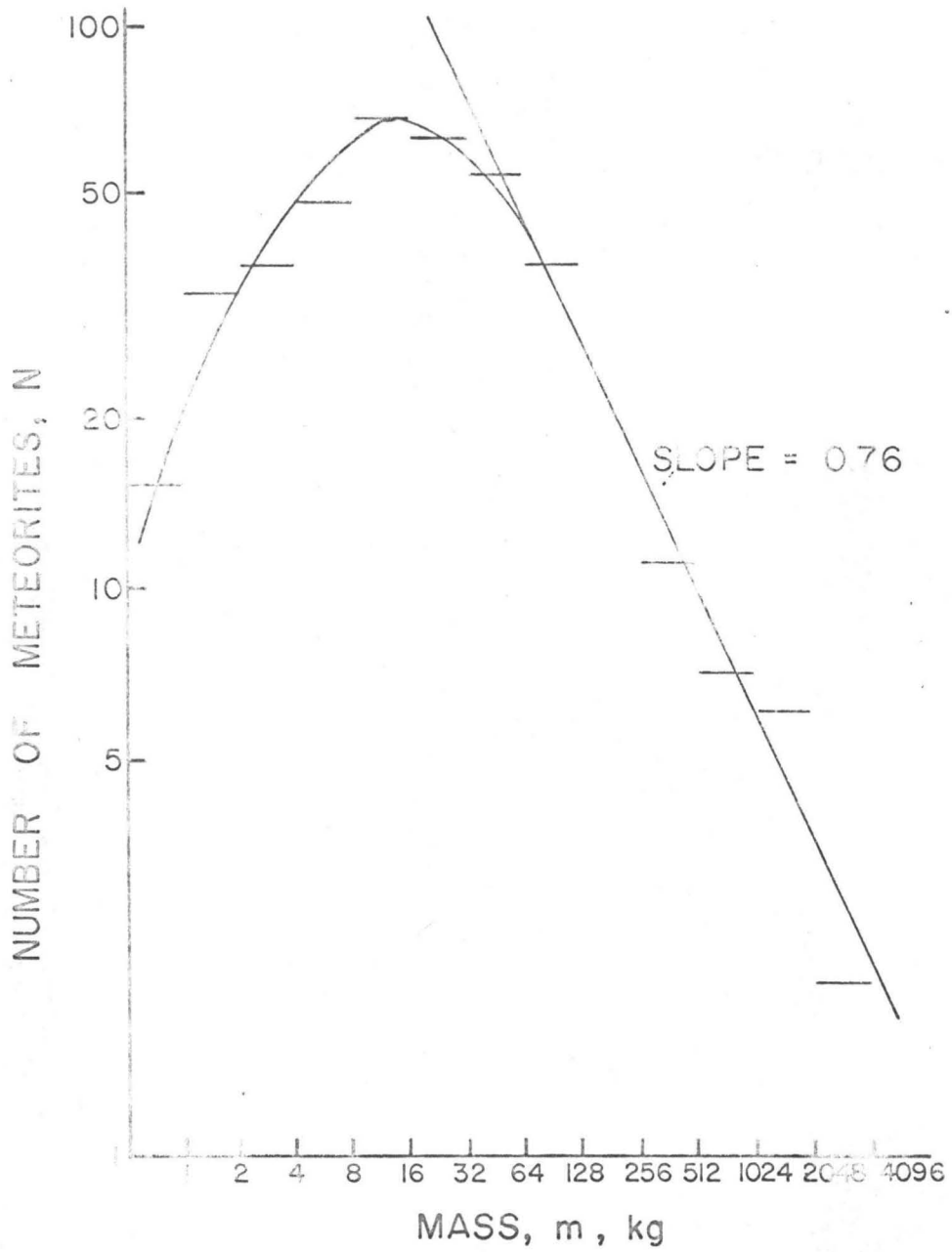


Figure 3-23. Mass distribution for 399 iron falls and finds (17).

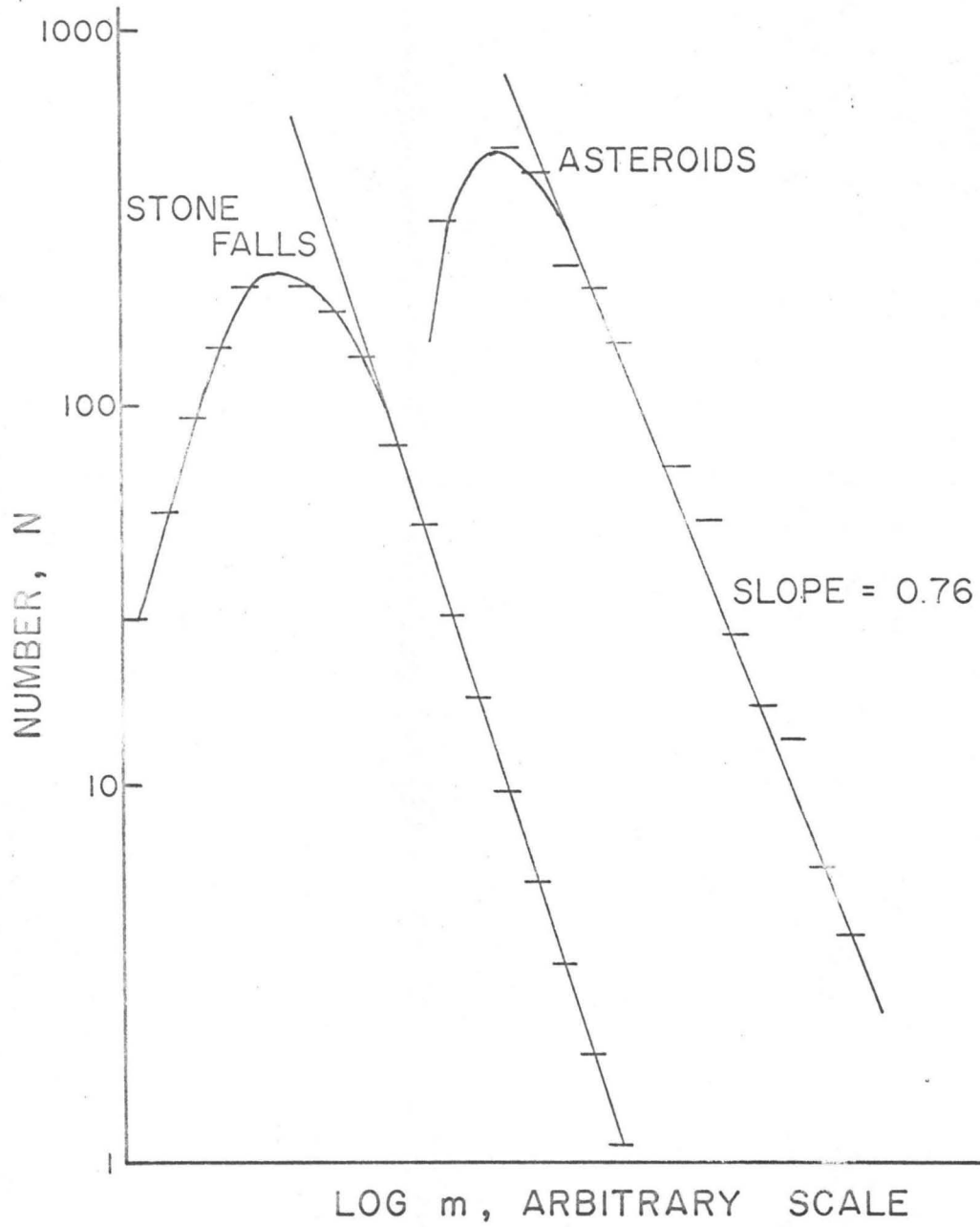


Figure 3-24. Mass distribution for stoney meteorites and asteroids (17).

or to put it in my incremental form,

$$dN = (N_0 c) m^{-(c+1)} dm \quad (\text{incremental law}).$$

These equations serve to show that the slope which he measures is the  $c$  in equation 3-12b.

With this glossary to the various notations it is possible to translate the findings of these three authors to a common notation for purposes of comparison. The results are shown in Table 3-3. Opik points out that the population index reflects the history of the population. That is, fragmentation yields a large value for  $c$  (e.g., the meteorites) while accretion yields small values (e.g., the planets). The agreement between the various authors is good and the the sequence: asteroids, meteorites, bright meteors, faint meteors appears clearcut with the increasing value of  $c$  representing greater and greater fragmentation. A word of caution is in order. Brown's data on meteoritic masses, as well as those of Hawkins, were taken from the Catalogue of Meteorites (1). Thus their distributions may reflect the results of atmospheric breakup and the statistics of recovery rather than the true distribution arriving at the atmosphere.

TABLE 3-3. Summary of Values of the Population Index,  $c$ , as  
Calculated from the Data of Other Authors.

	Radius (16)	c		
		Hawkins (15)	Opik (16)	Brown (17)
micrometeors	$10^{-4}$ - $10^{-2}$ cm.		0.53-0.60	
faint meteors	} $10^{-1}$ -1 cm.	1.34	} 1.1-1.4	
bright meteors		1.0		
meteorites	50- $10^4$ cm.	approaches 1	1.1	0.77
Apollo group asteroids	0.4-2.8 km.	} 0.58-1.22 Ave. = 0.93	0.9	} 0.76
asteroids:	2-90 km.		0.53	
	90-360 km.		0.83	
solar system planets and satellites	200-4,000 km.		0.17	
	4,000-64,000 km.		0.17	

Direction of the Flux

An attempt was made to study the direction of the meteoritic flux at the earth's orbit by observing the pattern of fall on the earth as a function of latitude and hour. A need for the transformation of the coordinates of fall of a meteorite arises from the fact that the earth's axis of rotation changes its orientation with respect to the sun as the earth traverses its orbit. As a result of this change, positions of fall for meteorites at one time of year cannot be correlated with those at other times of year. Any attempt to average over this effect reduces the resolution of the distribution. The coordinate system used to measure position on the surface of the earth is based on a spherical polar coordinate system having its polar axis perpendicular to the plane of the equator, with the azimuthal angle measured from midnight and the polar angle from the plane of the equator. The transformation must be made to another spherical polar coordinate system having its polar axis perpendicular to the plane of the ecliptic. Obviously, the angle between the polar axis of the two systems is 23.5 degrees.

Figure 3-25 defines the symbols used in the transformation equations. The axis pointing to the first point of Aries,  $\Upsilon$ , lies along the intersection between the ecliptic and equatorial planes and is used as the reference

AXIS THROUGH  
THE CENTER OF  
THE EARTH AND  
PERPENDICULAR  
TO THE PLANE  
OF THE ECLIPTIC

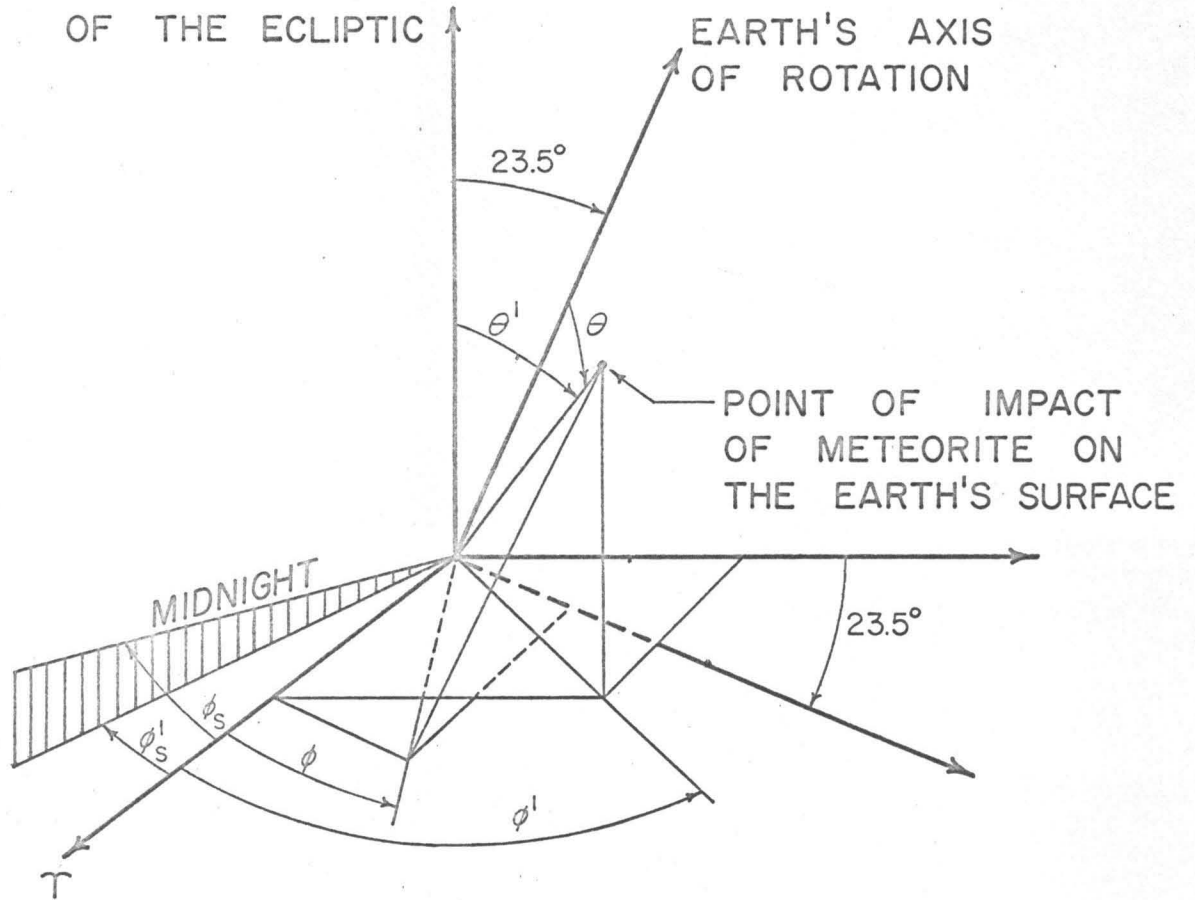


Figure 3-25. Quantities used in the equations for the transformation of the coordinates of fall of a meteorite.

from which azimuthal angles are measured.  $\phi_s$  is the hour angle (in degrees) and may be found in the Nautical Almanac for any day of the year. The angles  $\theta$  and  $\phi$  are found from the latitude and hour of fall by the equations

$$\theta \text{ (in degrees)} = \text{latitude} \mp 90^\circ \quad (3-13)$$

with - for latitude North and + for latitude South, and

$$\phi \text{ (in degrees)} = \phi_s + \text{hour of fall (in degrees)} \quad (3-14)$$

The transformation equations are

$$\theta' = \cos^{-1} (0.917 \cos \theta - 0.399 \sin \theta \sin \phi), \quad (3-15)$$

$$\phi' = \tan^{-1} (0.917 \tan \phi + 0.399 \cot \theta / \cos \phi), \text{ and} \quad (3-16)$$

$$\phi'_s = \tan^{-1} (0.917 \tan \phi_s) . \quad (3-17)$$

The transformed longitude is then calculated by the equation

$$\text{transformed longitude} = \phi - \phi'_s . \quad (3-18)$$

A computer was programmed to perform these calculations and the transformed coordinates of fall found for all meteorites for which the latitude and time of fall are known.

The distributions of falls with untransformed and with transformed latitude are shown in Figures 3-26 and 3-27. The first fact to be noted is that very few falls have occurred in the southern hemisphere which makes comparison with the northern hemisphere very difficult. The distributions are obviously biased in favor of those latitude having

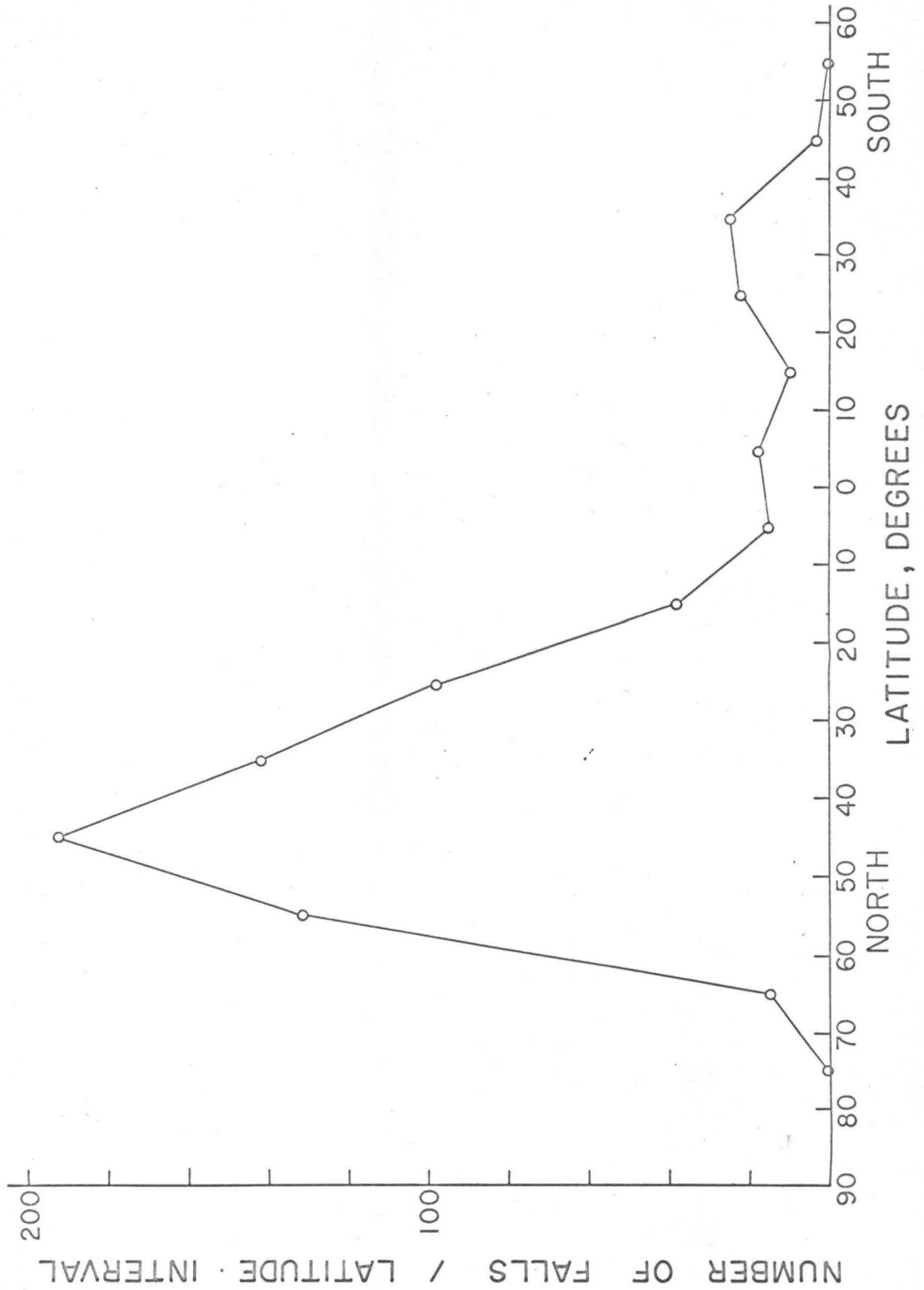


Figure 3-26. Distribution of falls with latitude.

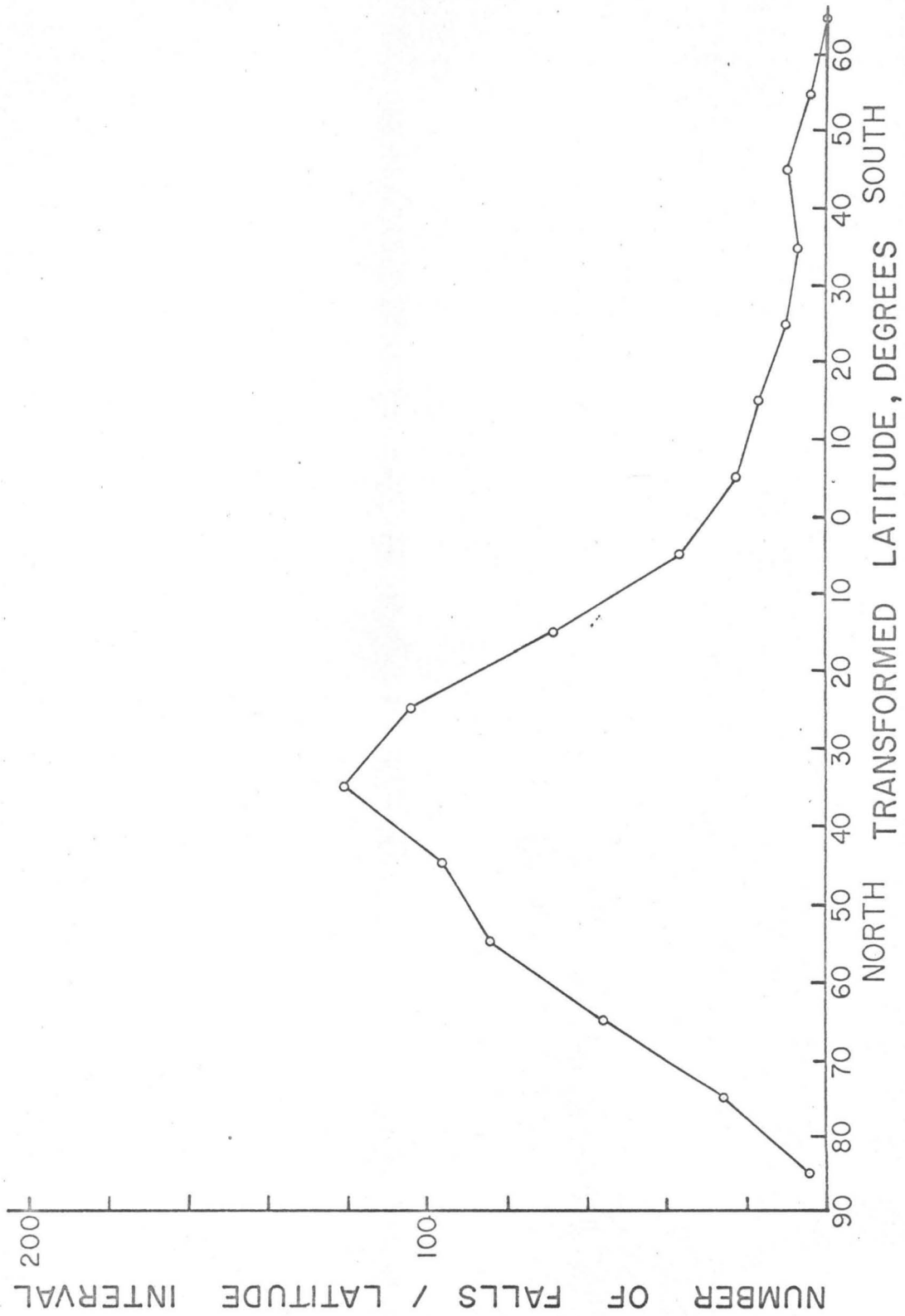


Figure 3-27. Distribution of falls with transformed latitude.

larger populations. A rough attempt at normalization to the population in each latitude was made by dividing the number of falls in each untransformed latitude interval by the estimated 1940 population in that interval (China was excluded). The results are shown in Figure 3-28. The northern and southern hemispheric distributions are more nearly equal than in the unnormalized graphs. At first glance it would appear that, on the average, there are two fluxes--one directed toward  $40^{\circ}$  North and the other toward  $40^{\circ}$  South, i.e., the orbits of the meteorites might not be distributed about the ecliptic or equatorial planes. This conclusion would be in opposition to the situation for sporadic meteors (19). However, the fact that a large fraction of the equatorial region is covered by jungle and does not have an efficient distribution of population for recovering meteorite falls must be taken into account. The latitude ranges for several regions, which are efficient meteorite collecting areas, are shown on the graph and these tend to support this conclusion.

The explosion model for the injection of asteroidal fragments into orbits intersecting that of the earth was used to calculate the expected hourly patterns of fall shown in Figures 3-29 and 3-30. These distributions were found by adding up the contributions to each hourly interval from the various fluxes. The fraction of a flux falling in one-hour time zones follows a cosine law as shown in Table 3-4.

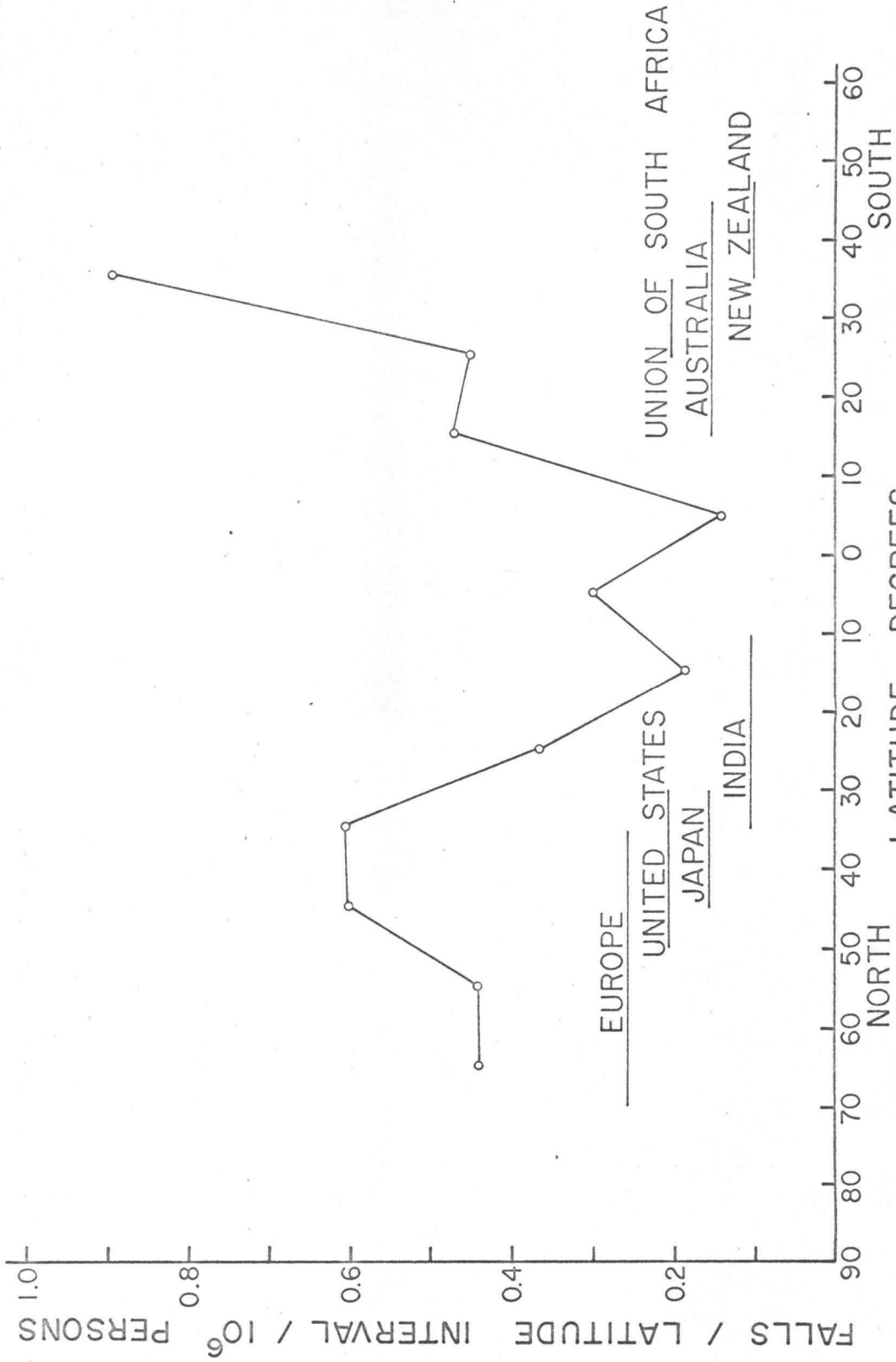


Figure 3-28. Latitude distribution normalized to the population in each latitude interval.

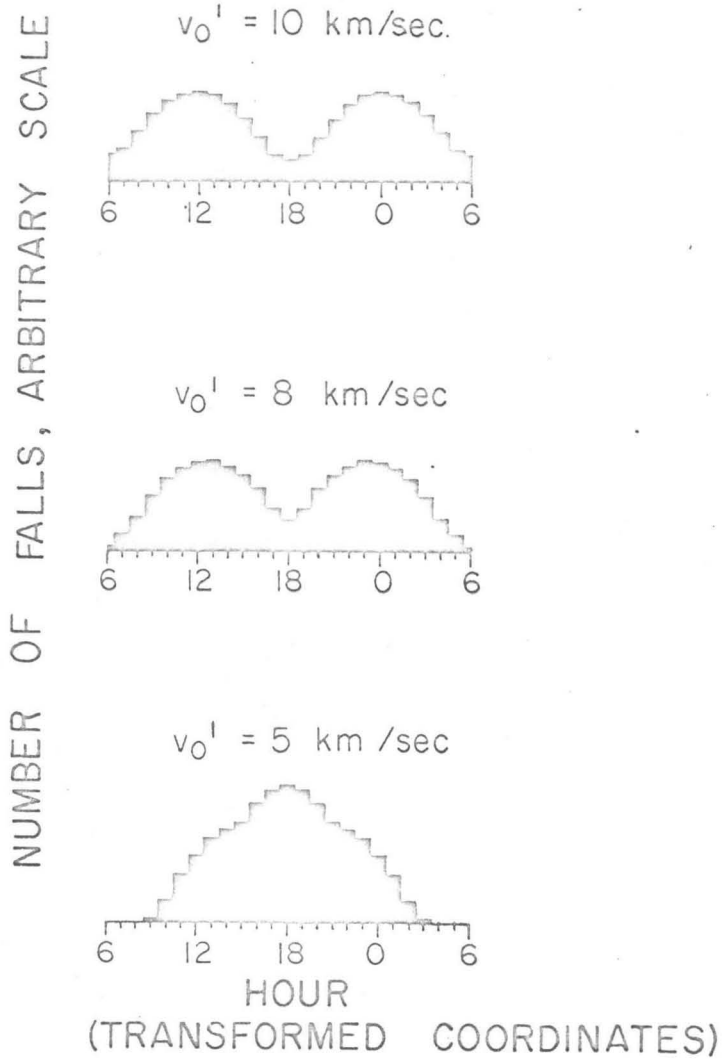


Figure 3-29. Hourly pattern of fall at the earth's orbit following isotropic breakup of asteroid. Initial orbit of asteroid: circular with  $r_a = 2.8 \text{ a.u.}$

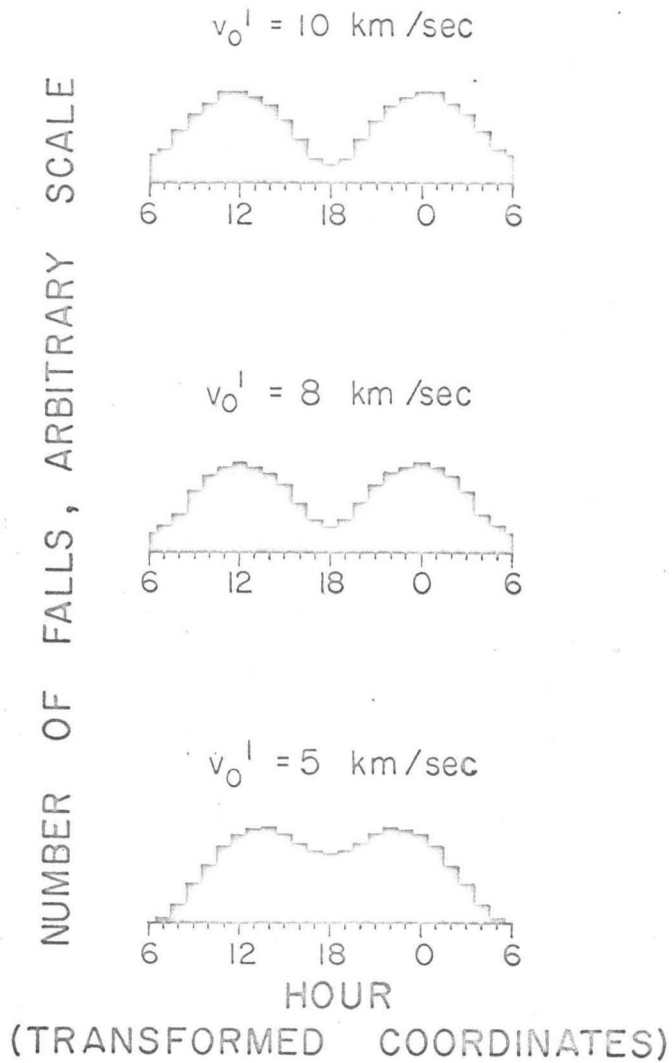


Figure 3-30. Hourly pattern of fall at the earth's orbit following isotropic breakup of asteroid. Initial orbit of asteroid:  $e = 0.5$ ,  $a = 3.3 \text{ a.u.}$ ,  $p = 2.4 \text{ a.u.}$ , with breakup occurring at  $\theta = 256^\circ$ ,  $r_a = 2.8 \text{ a.u.}$

TABLE 3-4. Fraction of a Single Meteorite Flux Falling on One-Hour Time Zones. Zero time zone corresponds to the direction from which the flux is arriving. The effect of terrestrial gravity has been ignored.

<u>Time Zone</u> (hour)	<u>Fraction</u>
-6	0.004
-5	0.033
-4	0.065
-3	0.092
-2	0.113
-1	0.126
0	0.130
+1	0.126
+2	0.113
+3	0.092
+4	0.065
+5	0.033
+6	0.004

Unlike the monthly fall pattern, the hourly pattern averages over all orbits which result from collisions in the asteroid belt and is symmetrical about the 18:00-6:00 axis. The calculated patterns are independent of  $v'_0$  and the choice of asteroid orbit prior to breakup until the lower limit of  $v'_0$  is approached. At this point the 18:00 component predominates at the expense of the 6:00 component and the bimodal distribution disappears.

The hourly pattern of fall actually observed is shown in Figure 3-31 as a function of the season, in Figure 3-32 as a function of the type of meteorite, and in Figure 3-33 as a function of the subclass of chondritic meteorite. All of these distributions are heavily biased toward the daylight hours (6:00 to 18:00) and the symmetry displayed in the calculated patterns cannot be expected in these actual situations. One trend, which is predicted by the calculated patterns and found in the histogram for "Entire Year," is the continuous rise from 6:00 to a maximum around 16:00. Another trend which stands out is the continuous shift of the area containing the maximum from 16:00 in the January-March distribution to about 12:00 in the July-September distribution. In the October-December pattern the 6:00 to 18:00 distribution becomes bimodal with maxima at 8:00 and 17:00 in preparation for the return to the January-March distribution. A possible explanation for this cyclic shift of the maximum lies in the fact that the hour at which the

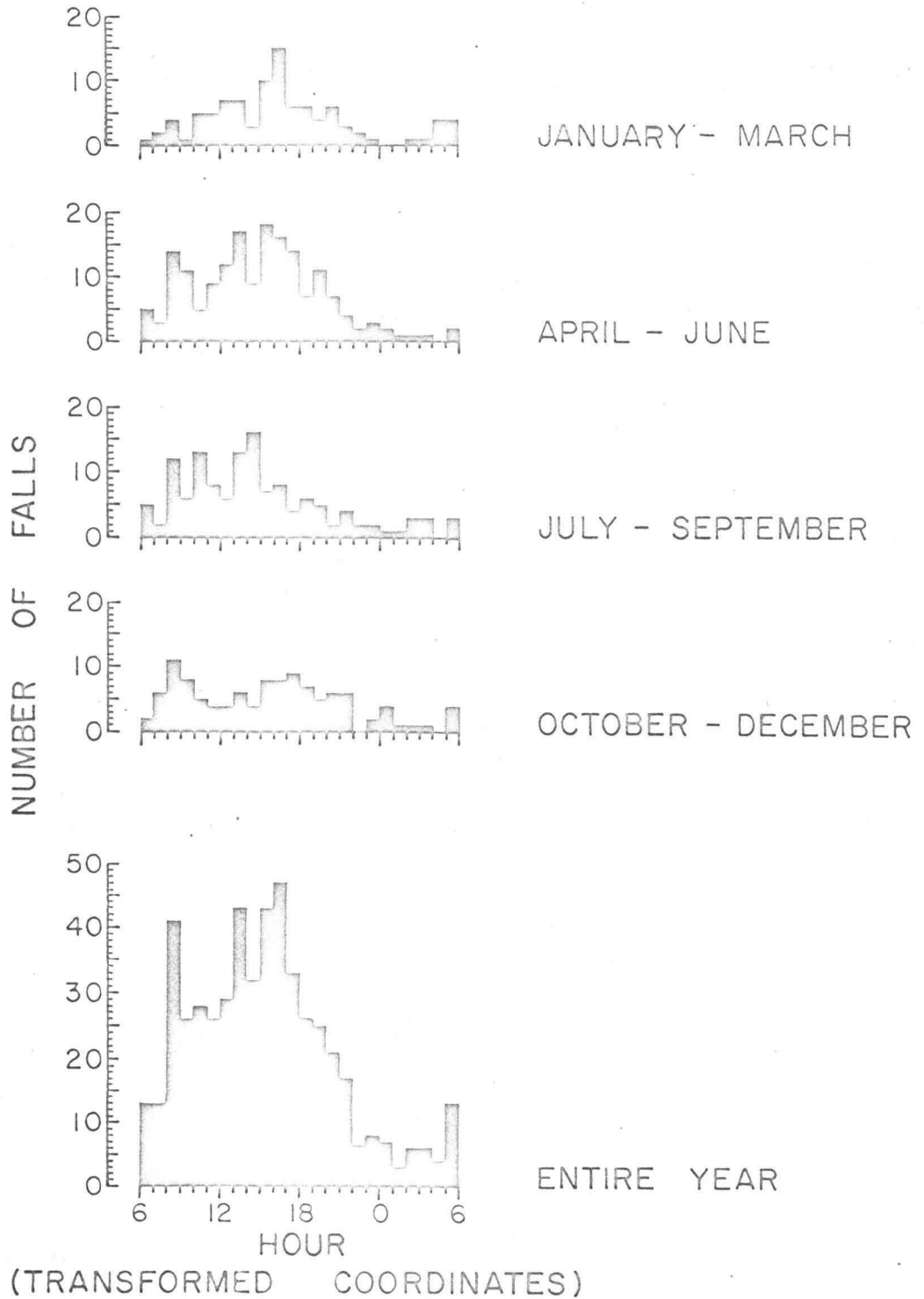


Figure 3-31. The hourly pattern of fall as a function of season.

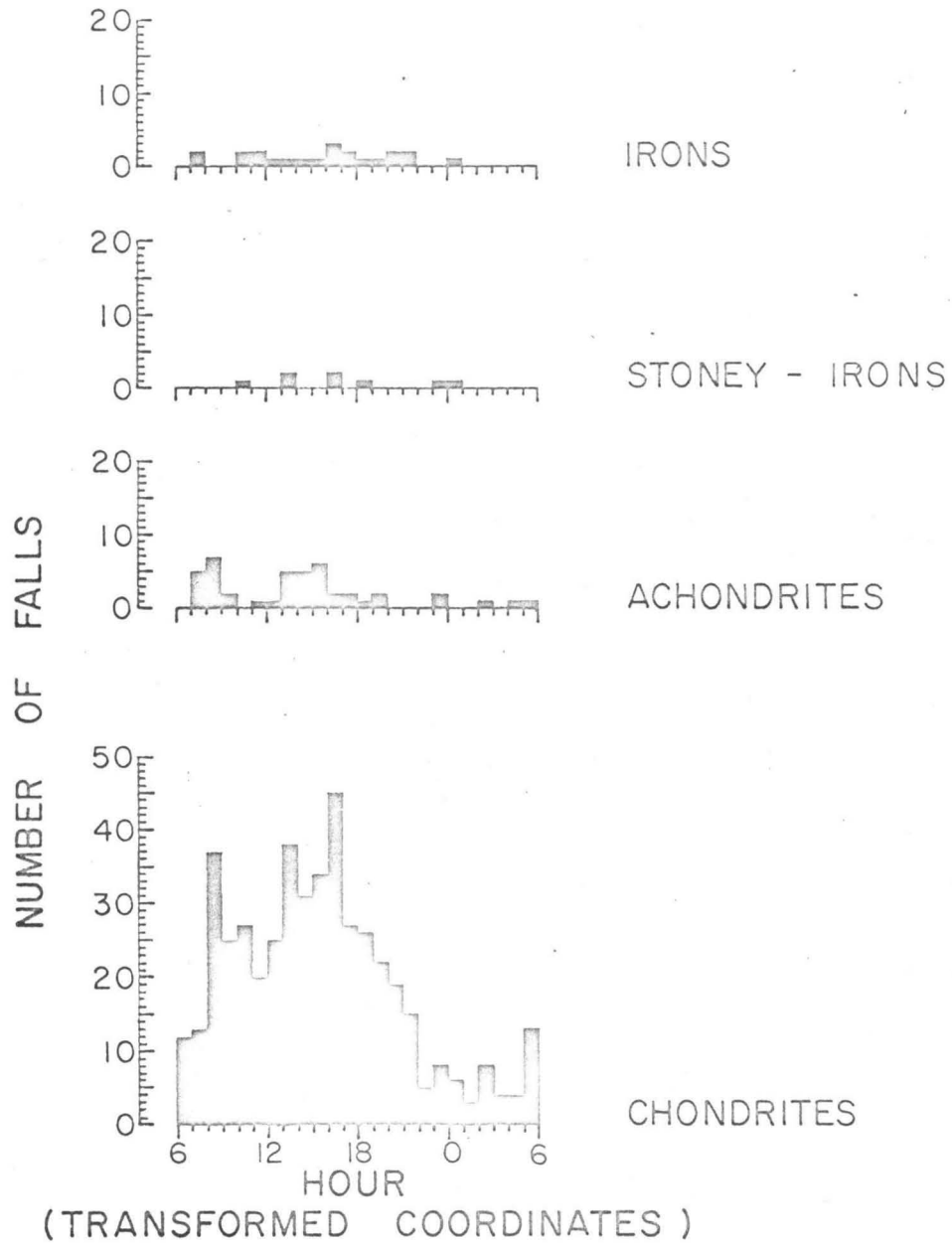


Figure 3-32. The hourly pattern of fall as a function of the type of meteorite.

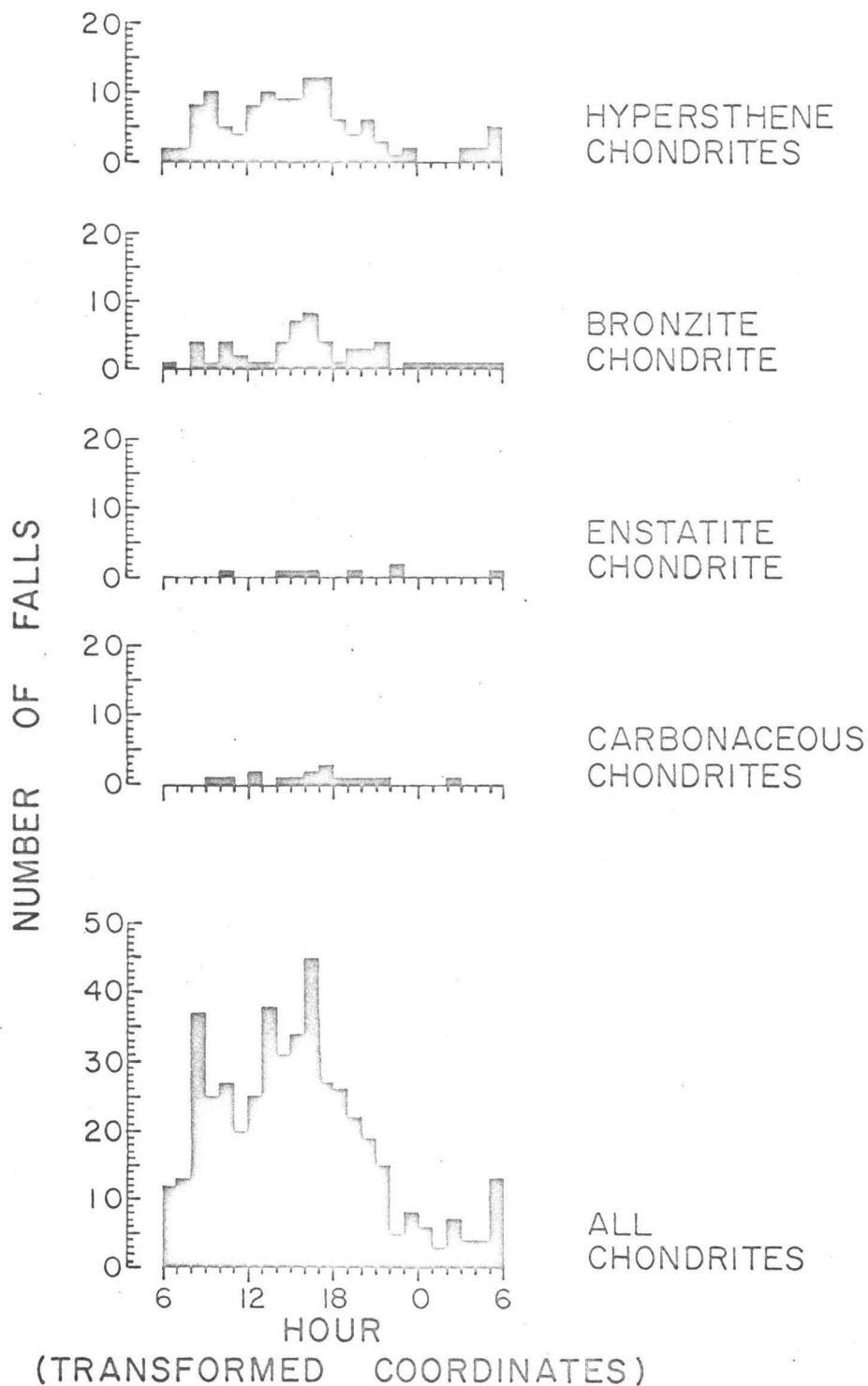


Figure 3-33. The hourly pattern of fall as a function of the type of chondritic meteorite.

northern temperate zones, which collect meteorites with the greatest efficiency, dip closest to the ecliptic plane varies with season. Thus, the 6:00 component should be at its maximum in January and the 18:00 component at its maximum in June. The high 16:00 component in January-March cannot be explained by this reasoning and may represent a flux of meteorites travelling in orbits of high inclination to the ecliptic.

The calculated patterns demonstrate that one-hour peaks should not be resolvable. Nevertheless, statistically significant peaks are present at 8:00 and 5:00 in the pattern for the entire year and in all of the seasonal patterns. It is difficult to find physical or sociological reasons for their presence.

The hourly patterns for the various types of meteorites differ markedly. The poor statistics for the irons and stoney-irons make interpretation of their patterns impossible. The achondrites display an interesting bimodal 6:00-18:00 distribution but no preference for one or the other of these peaks on the basis of type of achondrite, month of fall, or year of fall could be found. The hypersthene chondrites have a large 5:00 contribution which none of the other chondritic types possess.

None of these patterns show the 6:00 maximum displayed by the sporadic meteors (19). This maximum results from the high eccentricity of the meteor orbits confirming the fact that the meteorites travel in orbits of lower eccentricity.

#### 4. MAGNITUDE OF THE FLUX

In recent years, a great deal of effort has been expended in order to obtain a value for the magnitude of the meteoritic flux at the earth's orbit. The reasons for this, beyond wanting to know the rate of influx of meteorites on the earth, include a desire to date the lunar maria (16, 20, 21), to estimate the frequency of moonquakes caused by meteorite impacts (22), or even to estimate the danger to spacecraft from these projectiles. As we have seen, the meteorites display a definite frequency vs. mass relationship in which the frequency of occurrence increases rapidly with decreasing mass. This necessitates defining what is meant by "meteorite flux." This term will be used to denote the number rate of arrival per unit area of earth's surface of meteorites, the pieces of which after ablation in the earth's atmosphere are still large enough to be noticed, picked up and related to an observed fall. Although very minute fragments of meteoritic matter have been recovered as the result of special efforts, these cannot ordinarily be assigned with certainty to a definite fall. When several meteorites appear to have arrived in a group or cluster at the earth's atmosphere these are usually classified as a single fall. The units which will be used for the meteorite flux are: number/ $10^6$  sq./Km.-year.

Figure 4-1 shows the number of falls recovered in each decade since 1680. The recovery rate remained fairly constant until 1790 when it rose in a nearly linear fashion until 1940. This rapid rise is presumed to be due to growing populations as shown by Figure 4-2 (23) where the rate of recovery is normalized to the world population. Maxima appear in both graphs during the decades of 1810-20, 1860-70, and 1930-40 which can only be interpreted as periods of increased rate of influx. The precipitous decline after 1940 is probably real. There is often a time lag between the time of fall of a meteorite and the time at which it is brought to the attention of the scientific community. However, it seems unreasonable to assume that only half of the meteorites recovered during 1940-50 have found their way into the catalogs. If this lowering of the recovery rate is real, then the rate of influx of meteorites is returning to a level which existed around 1800 after maintaining a much higher rate from 1820 to 1940. This trend would pose a problem for the present-day theories on the origins of meteorites which assume that random events in the asteroid belt continuously inject meteorites into earth colliding orbits. The periods of these orbits should be of the order of 5 years and many revolutions should take place before the body is captured. One-hundred year cycles in the rate of influx are unlikely according to such a theory.

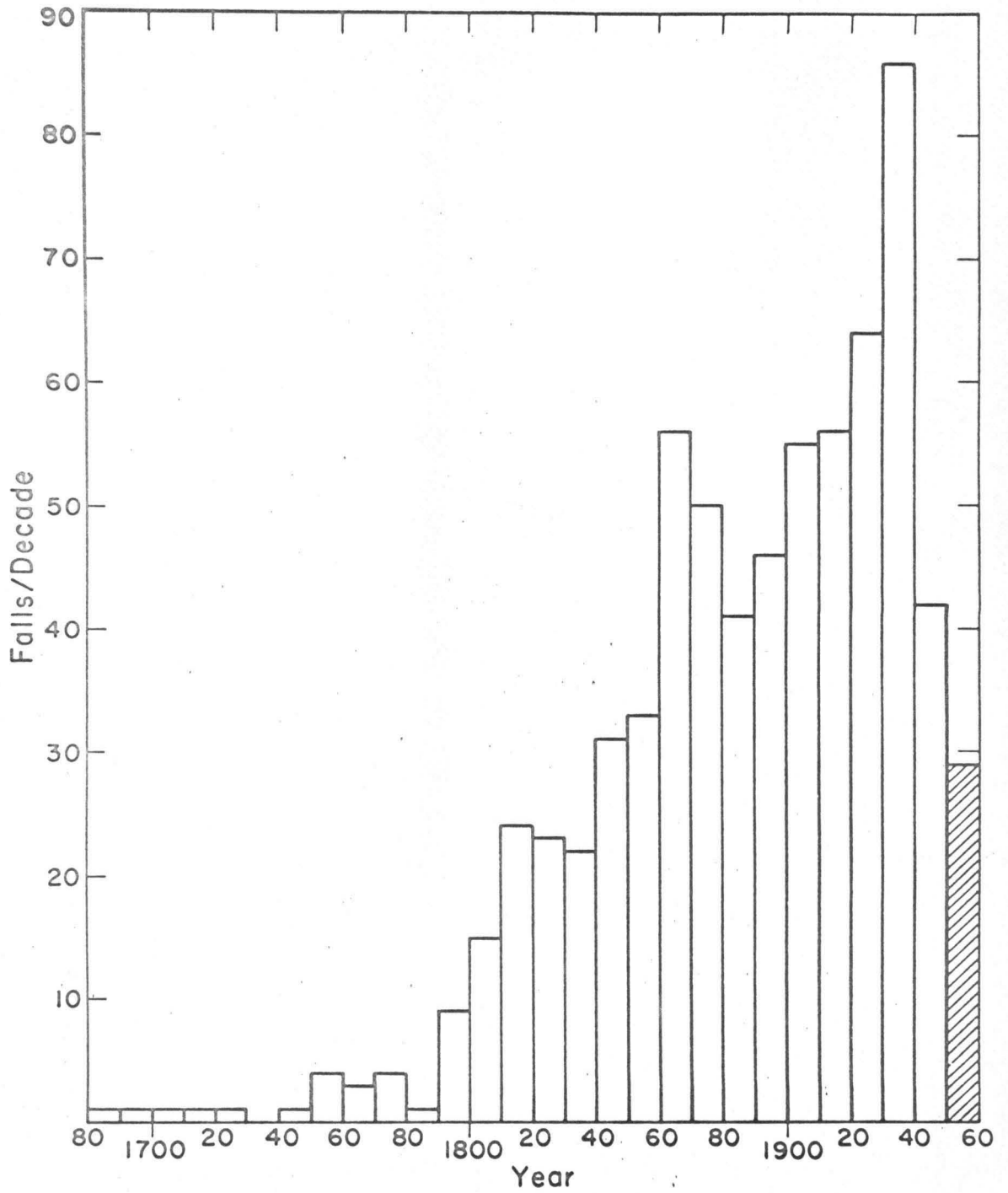


Figure 4-1. The rate of fall as a function of decade (23).

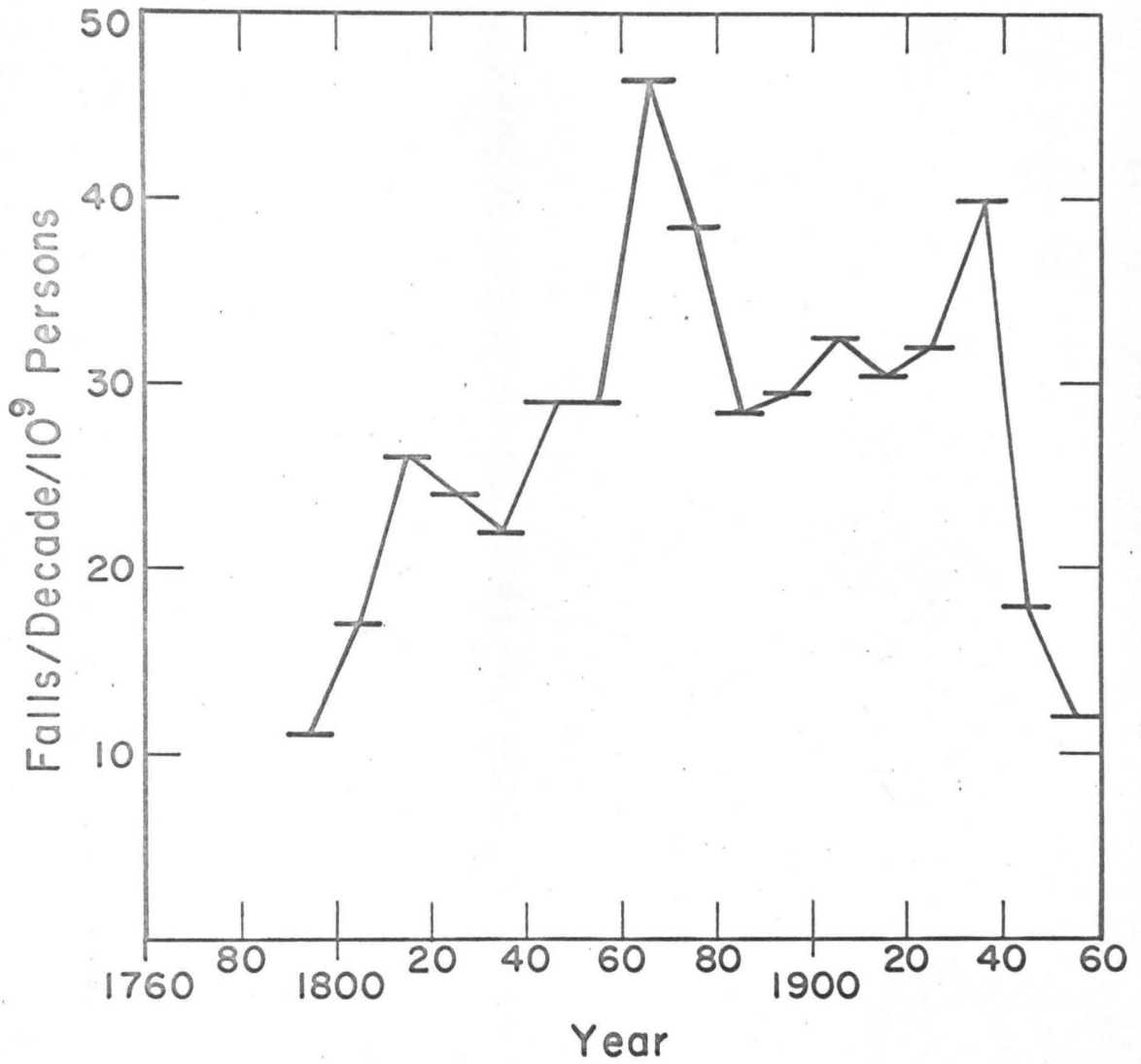


Figure 4-2. The rate of fall normalized to the world population (23).

From a purely logical point of view, it would be expected that the rate of recovery of fallen meteorites in a particular region is related to the population of that region. This relationship is demonstrated for the world as a whole by Figure 4-2 (23). Many previous attempts to determine the rate of arrival of meteorites at the earth's surface have used regions of the earth in which high population densities have been maintained for the period of time sampled. Silberrad (24) chose the United Provinces of India for this and other reasons. He noted that the number of falls recorded for the half-century, 1831 to 1880, was the same as the number for 1881 to 1930 and thus assumed that there existed an "intrinsic probability of regular recording." He also attempted to apply corrections for sparsely populated regions and for the decreased probability of recovery during nighttime. Table 4-1 shows the flux which he and other authors have calculated. Most of these values have been recalculated to give the units in "meteorites/ $10^6$  sq.km.-year" in order to establish a basis for comparison. Ninninger (25) arrived at his value by using an arbitrary factor of 10 to increase the number of recovered falls in Austria, Czechoslovakia, England, France, Germany, Hungary, Italy, Ireland, India, Japan, European Russia, and the United States. Hawkins (26) based his estimate upon the frequency vs. mass curve for meteorites and the frequency vs. estimated mass curve for bright meteors. His value shows the number of meteorites

TABLE 4-1. Estimated Values for the Meteorite Flux Arriving at the Earth's Surface.

	$R_o$ <hr/> (meteorite falls/ $10^6$ sq.km.-year)
Silberrad (24)	1.45
Ninninger (25)	1.25
Hawkins (26)	2.4*
Brown (17)	.32 to 1.0 (1.1 to 3.4)

\* flux entering atmosphere with mass  $\geq$  40 kg. and arriving at the surface of the earth with 10 kg. after ablation.

entering the atmosphere having mass greater than or equal to 40 kg. By the time it reaches the earth's surface, such a meteorite is reduced to about 10 kg. by ablation. Brown's (17) minimum value is taken from the data for falls in Japan, India, and Western Europe. His upper value results from applying corrections to the minimum value for the hourly and seasonal variations in the meteorite collection efficiency. He later applied a correction factor of 3.4 to these data on the basis of falls in limited, high population density regions in India and Japan (27), thus arriving at the values shown in parenthesis. All of these methods which are based upon the analysis of high population density regions suffer from a lack of knowledge of the relationship between population density and the probability of recovering a fallen meteorite. Only the method used by Hawkins circumvents this difficulty. However, he had to estimate the area of the sky seen by an observer in order to arrive at a figure for the influx of bright meteors.

The present discussion will attempt to find the relationship between the probability of recovering a fallen meteorite and the population density. A detailed study of the meteorite recovery efficiency of a particular region should take into account:

1. the number of people available to recover meteorites (which is determined by the total population, their occupations, the time of day, and the season of the year);

2. the average distance between a person performing the recovery and the point of impact of the meteorite (which is determined by the terrain, the time of day, and the season); and

3. the scientific cultural level of the people, i.e., will a meteorite, if picked up, be recorded and brought to the attention of the scientific community? This, in fact, is the definition of a "recovered fall."

With these points in mind, a model for meteorite recovery was formulated to which population statistics could be applied. It was assumed that there exists a certain fraction of a particular area,  $f$ , in which a meteorite will be recovered if it falls. This leads directly to the equation,

$$R = R_0 f ,$$

where  $R_0$  is the total meteoritic flux and  $R$  is the number rate of recovery per unit area. For the present discussion, it was assumed that the directions of the fluxes striking are distributed isotropically in the geocentric coordinate system. For cities, towns, and villages,  $f$  was assumed to be 1. For rural areas, the existence of rural population points (i.e., individual people or farms) was postulated. These rural population points were further assumed to be scattered at random and surrounded by circles of recovery, which have a certain average radius. This radius should depend on the terrain, the time of day, and the season and

could be made to depend upon the scientific cultural level of the people. However, due to the difficulty of measuring the latter quantity, the scientific cultural level was assumed to be high and invariant with time in all areas treated.

The functional relationship between the fraction of rural area covered,  $f_p$ , and the rural population point density,  $\rho$ , and the radius of recovery,  $r$ , is developed in Appendix A where it is shown to be:

$$f = \text{erf}(2.11 r^{1.6} \rho^{0.8}) .$$

The regions chosen for study (the United States, Europe, India, and Japan) were those which came closest to satisfying the following requirements over the period of time, 1810 to 1950:

1. adequate population figures,
2. large area, and
3. uniform population distribution.

Table 4-2 shows the number of falls recovered per  $10^6$  sq. km. per year for each country over the period 1810 to 1950. The  $\pm$  value is the standard deviation and assumes random arrival of the meteorites. The values in this table can be used as rough indices of the relative meteorite collecting efficiencies of the various regions. The United States (eastern half) comes closer to fulfilling the three requirements listed above than any of the other regions. If the rural

TABLE 4-2. Total Rates of Recovery  
for Falls (1810 to 1950).

<u>Region</u>	$\frac{R}{10^6 \text{ sq.km.-year}}$
United States (eastern half)	0.18 $\pm$ 0.02
Europe (excluding Norway, Sweden, Finland, and the U.S.S.R.)	0.30 $\pm$ 0.02
Northern India (Gangetic Plain and Punjab)	0.49 $\pm$ 0.06
Southern India (excluding states with very low population densities)	0.16 $\pm$ 0.03
Japan (excluding Hokkaido)	0.66 $\pm$ 0.14

population were much denser, this area could probably supply the desired meteorite flux value by itself. However, since the rural population density is relatively low, it gives a point in the lower region of the  $f_p$  vs.  $\rho$  curve. Europe has a higher meteorite recovery rate in keeping with its higher population density. The population figures for Europe as a whole are not as good as those for the United States but otherwise it fulfills the requirements fairly well. The division of India into "Northern" and "Southern" was done on the basis of meteorite recovery efficiencies and parallels the differences in population densities. Discussions of the population of India have filled many books and although the figures are not as good as those for Europe and the United States, they must be considered adequate. The high rural population density of the Gangetic Plain is reflected in the high rate of recovery of meteorites for Northern India. Japan has the finest population figures of any Asian country and a high rural population density. However, its small area has produced a low total number of meteorites recovered as shown by the rather large standard deviation for the rate of recovery.

Table 4-3 shows the total number of falls by region and then breaks these figures down according to the time of fall. The unclassified falls were distributed among the various categories by multiplying the total number of falls by the fraction of classified falls in a particular category. "Daytime" and "nighttime" refer to the periods

TABLE 4-3. Period of Fall.  
(for meteorites between 1810 and 1950)

Region	Total Number of Falls	Daytime		Nighttime		Summer		Winter	
		No.	Total	No.	Total	No.	Total	No.	Total
United States	89	55	65	19	23	51	52	36	37
Europe	156	99	119	31	37	101	102	53	54
N. India	58	33	45	10	13	33	35	22	23
S. India	32	20	26	5	6	12	12	19	20
Japan	23	9	19	2	4	15	15	8	8

	ds		ns		dw		nw	
	No.	Total	No.	Total	No.	Total	No.	Total
United States	37	44	8	10	18	22	11	13
Europe	64	77	17	20	35	42	14	17
N. India	18	24	7	9	15	20	3	4
S. India	10	13	1	1	10	13	4	5
Japan	6	13	1	2	3	6	1	2

between sunrise and sunset and vice versa and were determined for any particular time of year by referring to a Sunrise-Sunset Table (28). This method of categorizing the time of day of fall has greater meaning for the model under consideration than the method of dividing the day into equal parts from 6 to 18 o'clock and 18 to 6 o'clock.

The sight and sound phenomena attending the fall of a meteorite, in addition to the fact that very often more than one piece of meteorite is recovered from a fall (these pieces sometimes fit together), leads to the assumption that almost every fall is accompanied by the rupture of the meteorite during its passage through the atmosphere (9,29,30). This is probably more true of stones than of irons. For showers, where a large number of stones are recovered, the pattern of fall is usually found to be elliptical with the stones sorted by mass in such a way that the heavier stones travel farther than the lighter stones. One piece of evidence suggests that all falls (at least stone falls) are showers and that the number of pieces recovered depends upon where the inhabitants are situated in the ellipse. This evidence stems from the fact that when a careful and thorough investigation is made of an area where several stones are reported to have fallen, many more stones are discovered (29). These facts indicate that, in terms of the proposed model, the number

of pieces rather than the number of meteorites is the quantity having the greater significance. This is particularly true if a meaningful value for  $r$  is to be determined. With this in mind, the average number of pieces recovered per fall was determined for each country and the results shown in Table 4-4. Falls from which more than 10 pieces were recovered were classified as showers and were not included. The term "piece" is used here to denote a product of atmospheric rupture and not the fragments which result from striking the ground. The numbers in parenthesis indicate the number of falls used to calculate the average number of pieces. The figures in this table should be indicative of the relative recovery efficiency as a function of the region, the season of the year, or the time of day. In those cases where enough meteorites are included to give good statistics, the efficiency appears to increase with population density (e.g., N. India or Europe vs. the United States) and with improved weather (e.g., ds vs. dw for the United States).

A surprising result of the compilation in Table 4-4 is the fact that the average number of pieces recovered from nighttime falls is the same as that recovered from daytime falls. This fact requires a more detailed examination of the actual process of recovery. During both daytime and nighttime, the attention of the population is first attracted to the meteorite by the startling sight and sound

TABLE 4-4. Average Number of Pieces Recovered Per Meteorite Fall.

<u>Region</u>	<u>All Falls</u>	<u>Daytime</u>	<u>Nighttime</u>	<u>Summer</u>	<u>Winter</u>
United States	1.5 (77)	1.7 (49)	1.4 (14)	1.8 (44)	1.3 (31)
Europe	1.9 (131)	1.9 (86)	2.2 (25)	1.9 (83)	2.0 (46)
N. India	2.0 (52)	2.4 (31)	1.5 (8)	2.0 (29)	2.2 (20)
S. India	1.8 (28)	1.7 (16)	2.8 (5)	2.1 (11)	1.7 (16)
Japan	1.3 (15)	1.4 (7)	1.5 (2)	1.2 (11)	1.5 (4)
All Regions	1.8 (303)	1.9 (189)	1.9 (54)	1.8 (178)	1.75(117)
irons	1.3 (18)				
stones	1.8 (270)				

	<u>ds</u>	<u>ns</u>	<u>dw</u>	<u>nw</u>
United States	1.9 (32)	1.3 (6)	1.2 (17)	1.4 (8)
Europe	1.9 (54)	2.1 (15)	1.8 (32)	2.2 (10)
N. India	2.6 (18)	1.0 (5)	2.2 (13)	2.3 (3)
S. India	1.8 (9)		1.6 (7)	2.0 (4)
Japan	1.2 (5)		2.0 (2)	
All Regions	2.0 (118)	1.9 (28)	1.7 (71)	1.9 (26)

The numbers in parenthesis give the number of falls considered.  
No showers are included.

ds = day-summer  
ns = night-summer  
dw = day-winter  
nw = night-winter

phenomena attending its fall. In daylight the recovered pieces are usually seen to fall near the persons who pick them up. At nighttime this is not possible and the question remains as to how recovery is made. After reading a large number of descriptions of recoveries, it became evident that the recovery need not be made immediately after fall. Very often a hole is found in a freshly plowed field or damage to a building is discovered the next day, or even later, and recovery made at that time. Thus, the model under discussion is not valid when applied to nighttime falls because these pieces are not recovered during the time that the nighttime population distribution prevails. In addition, it appears that those pieces recovered in daytime in plowed agricultural areas would probably also have been recovered if they had fallen during nighttime because the hole (if the piece penetrates the soil) or the piece itself is very noticeable. There has been no evidence to indicate that the average rate of influx during the day is different from that at night and so the higher rate of recovery of falls during the daytime with no increase in the efficiency of recovery of pieces must be explained. It may be true that the excess number of daytime falls fell in areas where, if they had fallen at night, no pieces would have been recovered (e.g., heavily wooded regions). The data in Table 4-4 was combined with that in 4-3 to give Table 4-5 which shows the flux of pieces for the various regions.

TABLE 4-5. Flux of Meteoritic Pieces (1810 to 1950).

(pieces/10<sup>6</sup> sq. km.-year)

Region	Total for				
	All Falls	Daytime (12 hours)	Nighttime (12 hours)	Summer (6 mo.)	Winter (6 mo.)
United States	.27 ± .03	.22 ± .03	.07 ± .01	.18 ± .01	.12 ± .02
Europe	.57 ± .04	.42 ± .04	.15 ± .02	.38 ± .04	.20 ± .02
N. India	.98 ± .12	.91 ± .17	.17 ± .06	.60 ± .10	.42 ± .09
S. India	.29 ± .05	.22 ± .05	.08 ± .03	.13 ± .04	.17 ± .03
Japan	.86 ± .18	.77 ± .25	.18 ± .12	.52 ± .13	.35 ± .12

Region	<u>ds</u> (12 hours, 6 mo.)		<u>ns</u> (12 hours, 6 mo.)		<u>dw</u> (12 hours, 6 mo.)		<u>nw</u> (12 hours, 6 mo.)	
	United States	.15 ± .02	.04 ± .01	.06 ± .01	.04 ± .01	.06 ± .01	.04 ± .01	.04 ± .01
Europe	.23 ± .04	.10 ± .02	.18 ± .02	.07 ± .02	.18 ± .02	.07 ± .02	.07 ± .02	.07 ± .02
N. India	.47 ± .13	.08 ± .03	.40 ± .09	.07 ± .05	.40 ± .09	.07 ± .05	.07 ± .05	.07 ± .05
S. India	.11 ± .04		.10 ± .03	.06 ± .02	.10 ± .03	.06 ± .02	.06 ± .02	.06 ± .02
Japan	.40 ± .14		.38 ± .22		.38 ± .22			

ds = day-summer  
 ns = night-summer  
 dw = day-winter  
 nw = night-winter

The derivation of the population figures to be applied to the model is explained in Appendix B. It should be emphasized that high accuracy in compiling these figures was not required because they were averaged over a long period of time (1810 to 1950) and because of the relatively poor statistics for the meteorites themselves. Table 4-6 shows the results of the population survey in terms of rural population point densities for summer and winter daytime ( $\rho_{ds}$  and  $\rho_{dw}$ ) and gives the estimated fractions of area covered by cities and towns (FCT) or by cities, towns, and villages (FCTV). A key to the symbols and definitions used may be found in Appendix B. In addition, the table presents the flux data for meteoritic pieces in three separate columns for each season. The figures in the second of these columns have been corrected for FCT or FCTV so they represent only those meteoritic pieces falling in rural areas. This correction is quite small and is less than the standard deviation. The third of these three columns will be discussed later.

A graph of  $R_{\rho_{ds}}$  vs.  $\rho_{ds}$  is shown in Figure 4-3. The curve represents a least squares fit to the data. Southern India was not included when making this fit because of its anomalously low values. The fact that the European point is below the curve (farther than its standard deviation warrants) leads to an attempt to modify the flux from one which is isotropic relative to a stationary earth to one

TABLE 4-6. Population and the Flux of Meteorite Pieces.

Region	FCT or FCTV	$\frac{\rho_{ds}}{\text{people/sq.km.}}$	$R_{ds}$	$R_{\rho_{ds}}$	$R_{\rho_{ds}}$
				(corrected for FCT or FCTV)	(corrected for latitude effect)
United States	.01	7.4	.15 ± .02	.15 ± .02	.18 ± .02
Europe	.07	21	.23 ± .04	.21 ± .04	.29 ± .06
N. India	.03	39	.47 ± .13	.46 ± .13	.46 ± .13
S. India	.02	14	.11 ± .04	.11 ± .04	.11 ± .04
Japan	.05	40	.40 ± .14	.38 ± .13	.46 ± .16
		$\frac{\rho_{dw}}{\text{people/sq.km.}}$	$R_{dw}$	$R_{\rho_{dw}}$	$R_{\rho_{dw}}$
				(corrected for FCT or FCTV)	(corrected for latitude effect)
United States		3.8	.06 ± .01	.06 ± .01	.07 ± .01
Europe		17	.18 ± .02	.17 ± .02	.24 ± .03
N. India		49	.40 ± .09	.39 ± .09	.39 ± .09
S. India		18	.10 ± .03	.10 ± .03	.10 ± .03
Japan		28	.38 ± .22	.36 ± .21	.43 ± .25

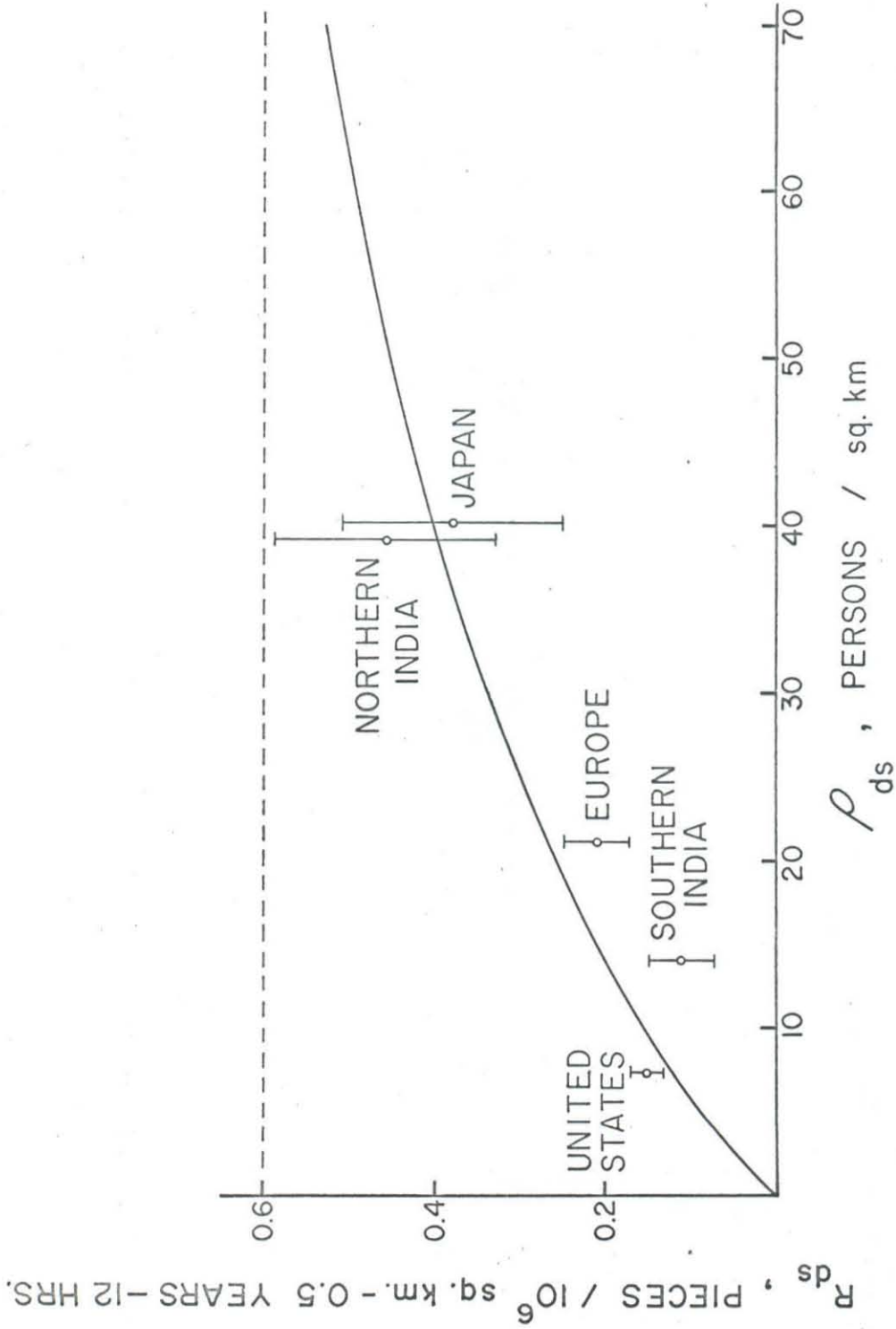


Figure 4-3. Flux of pieces vs. the rural population density, no latitude correction.

whose average direction is parallel to the plane of the ecliptic. This new, more realistic flux will vary with latitude on the earth (polar angle) but it is still assumed to be isotropic with respect to longitude (azimuthal angle). The corrections which this modification introduces into  $R_{\rho_{ds}}$  and  $R_{\rho_{dw}}$  are shown in the third of the three R columns in Table 4-6. These new points are plotted and the new least squares curve drawn in Figure 4-4. The improvement in the position of the European point relative to the curve is apparent. The values of  $r$  and  $R_0$  derived from the least squares fit to the ds and dw data are shown in Table 4-7. Combining the  $R_0$  values with the average number of pieces recovered per fall yields the  $R_0$  values for the meteorite flux which is also shown in the table. The last column in this table is calculated by assuming that  $R_0$  is independent of the season or time of day. The agreement between the two values for  $R_0$  is a fortunate result and lends credence to the fundamental approach. However, it should be emphasized that this value for  $R_0$  is an average for the period 1810 to 1950 and that the flux, as indicated by Figure 4-1, fluctuates rather widely. In addition, it has been assumed that the scientific cultural level in the regions studied has remained constant over the period 1810 to 1950. This is certainly not true and a somewhat higher value for  $R_0$  would probably be obtained if some method were found to take this fact into account. A valuable addition

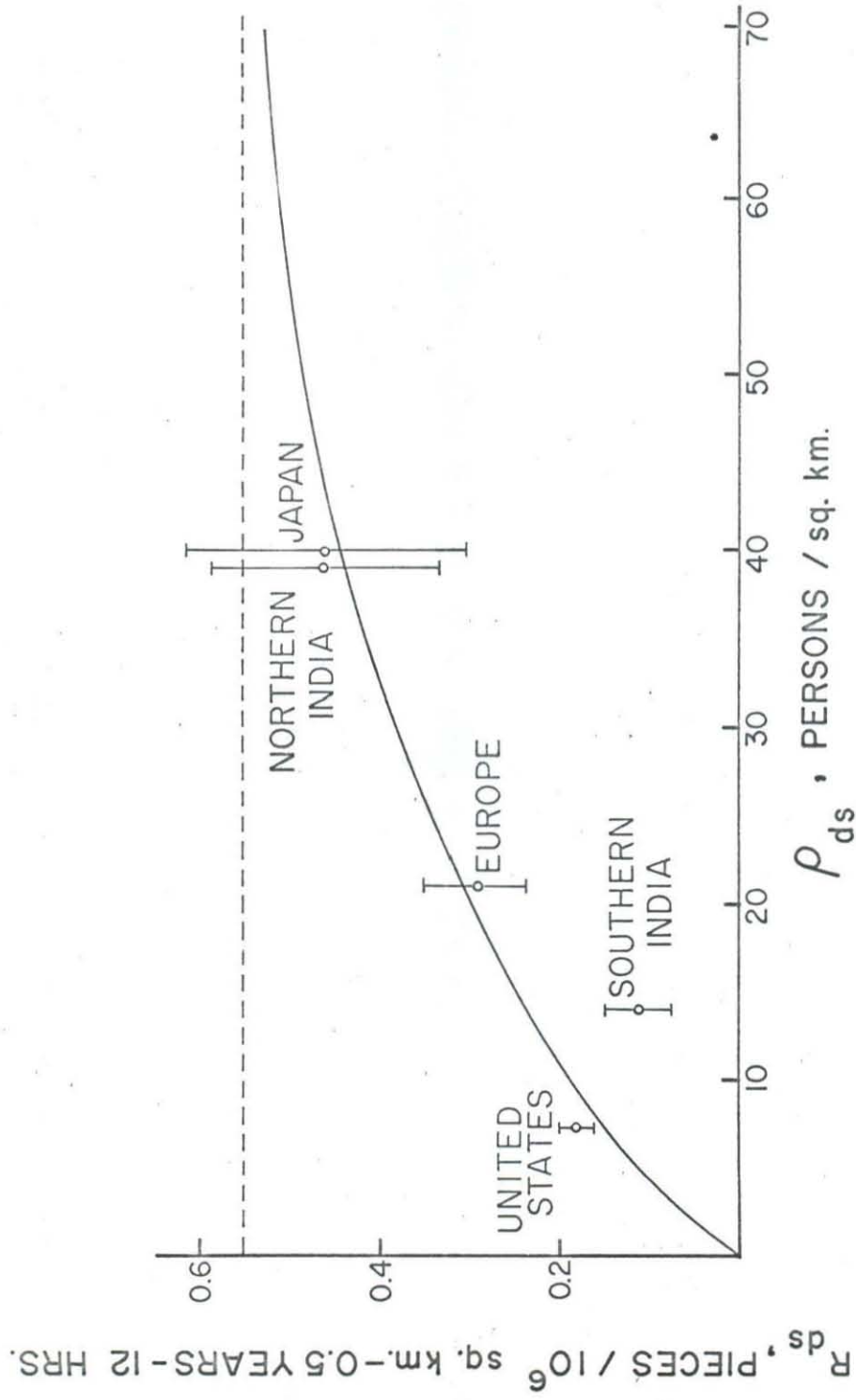


Figure 4-4. Flux of pieces vs. the rural population density, latitude correction applied.

TABLE 4-7. Least Squares Fit Data for  
Day-Summer and Day-Winter Falls.

	Least Squares Data		Average Number of Pieces Recovered Per Fall	$R_0$ (meteorites/ $10^6$ sq.km. -0.5 year-12 hour)	$R_0$ (meteorites/ $10^6$ sq.km.-year)
	$r$ (km.)	$R_0$ (pieces/ $10^6$ sq.km. -0.5 year-12 hour)			
ds	0.118	0.55	2.0	0.27	1.1
dw	0.14	0.42	1.7	0.25	1.0

to this survey would be the inclusion of the Soviet Union where about 70 meteorites falls have been recovered. However, reliable population statistics must be found. In any case, the value obtained for  $R_0$  by this survey is in good agreement with those of the other authors listed in Table 4-1.

In order to check the value found for  $r$ , a literature survey of 14 daytime falls was conducted to find the distance between the points of impact of the meteoritic pieces and the people who subsequently recovered them. Most of the falls included took place in the United States but one fall occurred in each of the following countries: the Phillipines, India, England, Algeria, and Canada. The distances found ranged from 3 to 2100 feet but the average was 350 feet or 0.11 km. which is in excellent agreement with the calculated values for  $r$  shown in Table 4-7.

## 5. SUMMARY

A survey of meteorite data was conducted in order to better characterize the meteoritic flux encountered by the earth and to search for correlations in fall pattern among the various types of meteorites. One result of this study has been an improved organization of the existing meteorite data in the form of a punch card catalog which is available for future surveys. Many sortings of these cards according to various categories were made and permanent printouts of the results obtained. In addition, the coordinates of fall for all falls were transformed to a more meaningful coordinate system which eliminates the seasonal variation found in the system ordinarily used to measure position on the surface of the earth.

It developed that the statistics for meteorite falls are too poor to reveal clearcut correlations among or between the various types of meteorites. The most that can be expected from such a survey are suggestions of these correlations and these were found among the monthly fall patterns where the veined-hypersthene chondrites, the veined-white hypersthene chondrites, the achondrites and the howarditic achondrites exhibited the greatest departures from randomness. Future chemical and mineralogical investigations should be conducted with these possible correlations in mind. The yearly fall patterns show variations which are important to the theories on the origins of these

bodies. Broad maxima and minima appear for various types and for a few types, concentrations of falls occur during periods of several years. These groupings suggest non-random arrival of these bodies. If, in the future, periodicity in the yearly fall patterns can be demonstrated then some mechanism for the injection of groups of these bodies into orbits having a small range of periods must be found. The observed hourly patterns of fall show a rise from 6:00 to a maximum around 16:00. It is impossible to tell whether the true maximum occurs at 16:00 or later (e.g., 18:00) because of the worsening chances for the recovery of meteorite falls due to the decreasing amount of daylight.

The magnitude of the flux varies with time and estimates of the magnitude based upon data covering short periods of time must necessarily be biased. One fluctuation which is of importance is the sharp decline after 1940. An attempt was made to estimate an average value for the magnitude of the flux from 1810 to 1950 by considering the relationship between the rate of recovery of falls and the prevailing rural population density. This attempt yielded concordant values for  $R_0$ , the rate of influx per unit area of the earth's surface, for day-summer and day-winter falls.

The extrapolation of the findings of this survey to the flux outside the earth's atmosphere will not be possible until more complete data on the selective sorting effects of atmospheric ablation are obtained or until material from the surface of the moon is available for analysis.

APPENDIX A

The "Fraction of Area Covered" vs.  
The "Point Density" Relationship

In order to apply the meteorite recovery model described in the text, it was necessary to determine the functional relationship between the fraction,  $f_p$ , of area covered by target circles drawn about randomly distributed points as a function of the point density,  $\rho$ , and the radius of the target circle,  $r$ . The point density and target circle correspond respectively to the population point density and the circle of recovery for meteorites in the model.

An empirical approach was employed to find this relationship. By using a table of random digits (13) as a source of coordinates, two sets of 100 random points were generated and plotted on a two dimensional coordinate system (Keuffel and Esser graph paper with 1 unit of length equal to 0.5 inches). With about 100 points per 416 square units, the point density for both distributions was about 0.24 points/sq. unit. Copies of these distributions were made and on each copy circles of a given radius ( $r = 0.25, 0.50, 1.0, 1.5, 2.0, 3.0, \text{ or } 4.0$  units) were drawn around the random points. The fraction of the area covered by these target circles was found for each  $r$  and plotted vs.  $r/A^{\frac{1}{2}}$  as shown in Figure A-1. ( $A^{\frac{1}{2}}$  was used in order to make

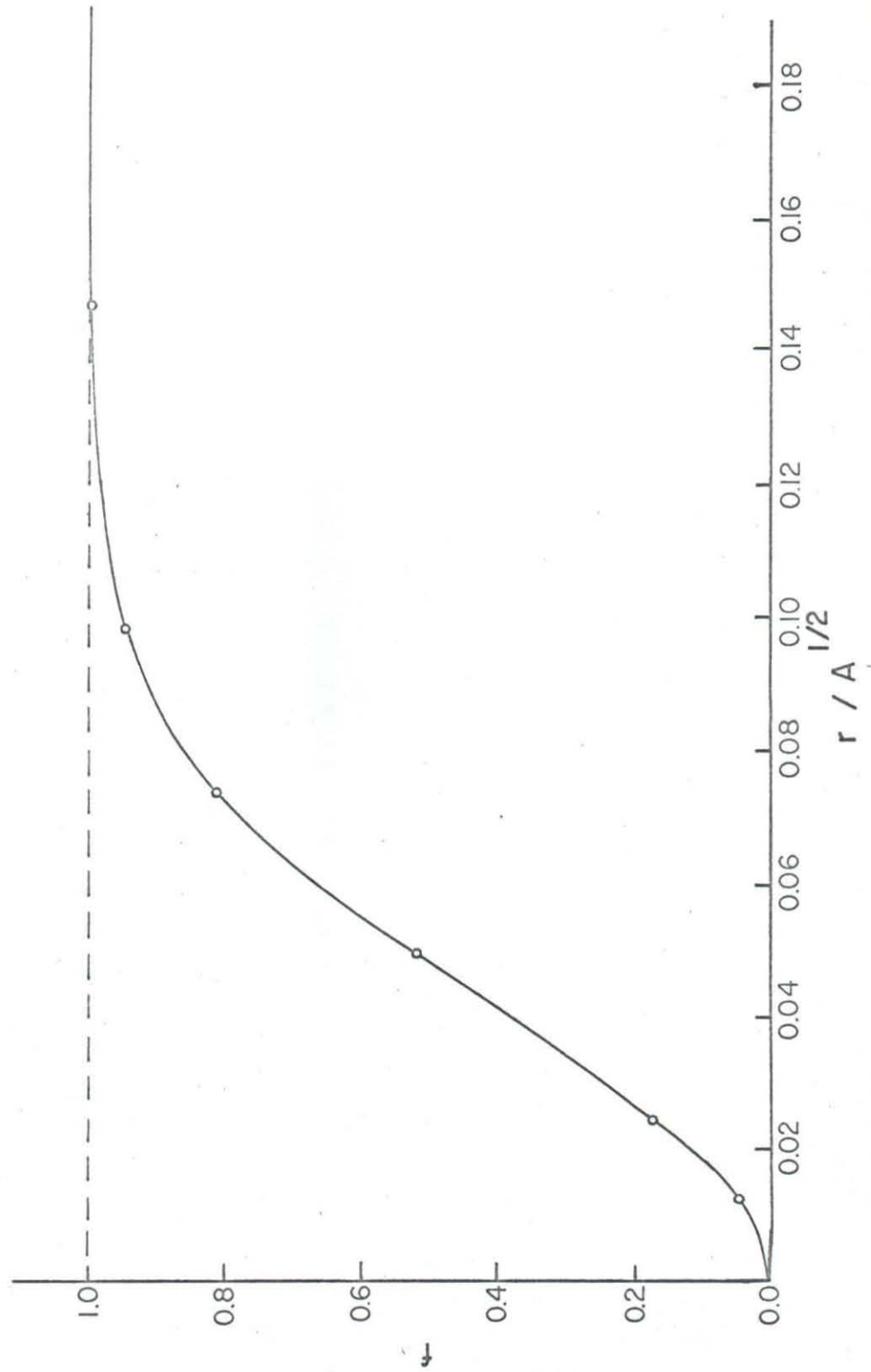


Figure A-1. Fraction of area covered by one-hundred random points.

the ratio dimensionless.) By assigning a value to  $r$  (in km.) it was possible to compute the  $A$  (in sq. km.) which corresponded to this  $r$  by the equation,

$$A = \left[ \frac{r}{(r/A^{\frac{1}{2}})} \right]^2 .$$

Knowing that there were 100 points within this  $A$ , the  $\rho$  could be computed thus giving the empirical relationship between  $f_{\rho}$  and  $\rho$ .

The functional relationship which matched the empirical relationship was found by trial and error. The first equation tried was:

$$1 - f_{\rho} = e^{-k\rho}$$

and the results are shown in Figure A-2. A good fit resulted for all but the lower values of  $1 - f_{\rho}$ . However, there was no simple relationship between  $k$  and  $r$  and a different  $k$  was required for each  $r$ .

The next equation tried was:

$$f_{\rho} = \text{erf}(ar^b \rho^c) .$$

This relationship provided a satisfactory fit to the empirical data as shown in Figure A-3 where  $a = 2.11$ ,  $b = 1.6$  and  $c = 0.8$  for every  $r$ . Thus,

$$f = \text{erf}(2.11 r^{1.6} \rho^{0.8})$$

was assumed to be the desired functional relationship.

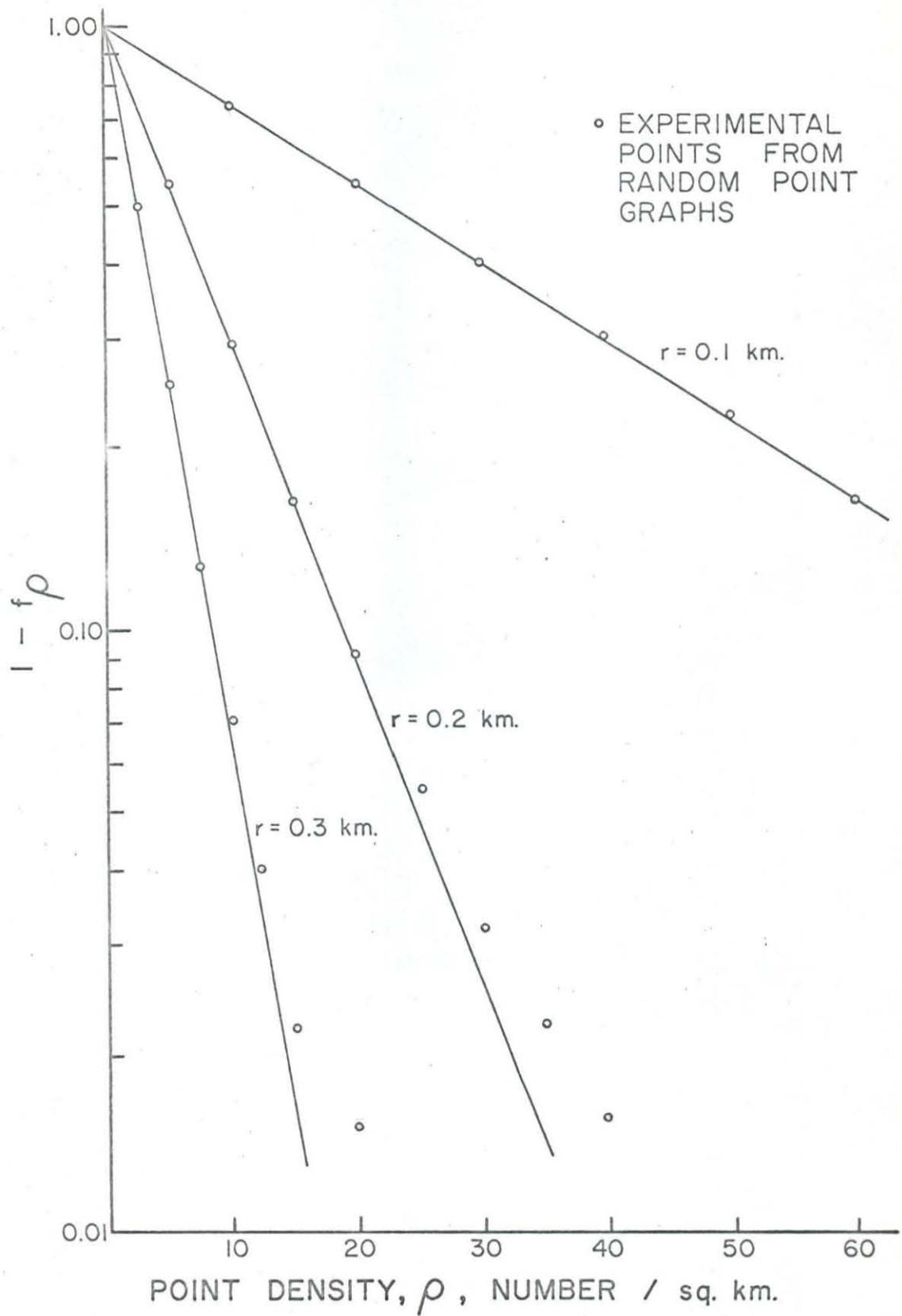


Figure A-2. Exponential function approximation to the experimental data.

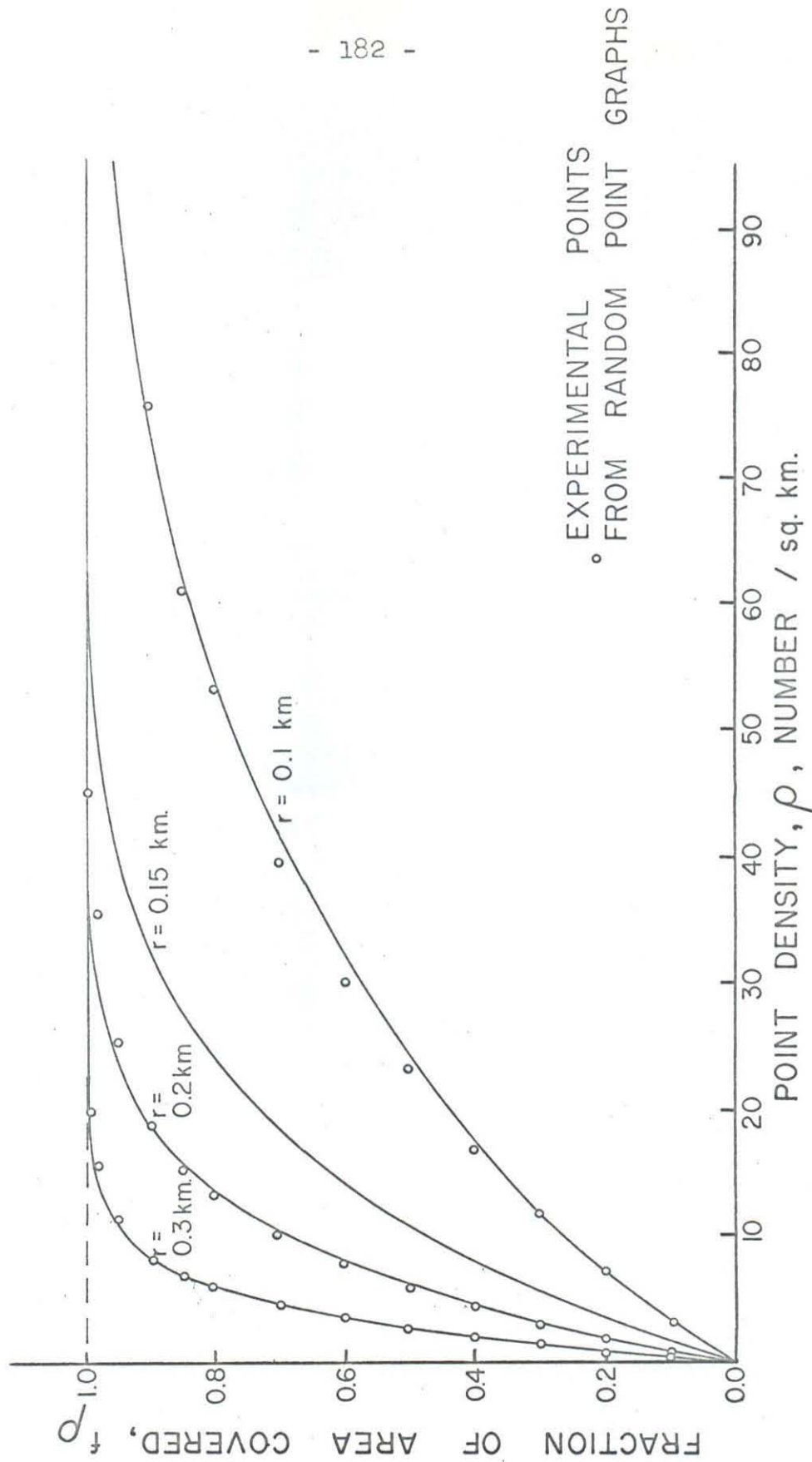


Figure A-3. Error function approximation to the experimental data.

APPENDIX B

Population Data and Calculations

The objective of this population survey was to obtain values for: a) the total population, b) the rural population, c) the urban population, and d) the number of agricultural workers in certain selected countries between 1820 and 1940. These figures were then used to estimate: 1) the rural population point densities for various seasons and 2) the fraction of the total area covered by communities larger than 10 people.

In order to present this information in a concise form it was necessary to adopt a convention of symbols and definitions which, it is hoped, will aid rather than hinder the understanding of the material. These symbols and definitions are summarized in the following list. The meaning of some of the terms will be made clearer in the subsequent discussion.

Symbol

A	total area under consideration
RA	rural area = $A(1 - FCT) \sim A$
TP	total population
CRP	census rural population--rural population reported in census data (involves a definition of "rural population")
CUP	census urban population--urban population reported in census data
CUPD	census urban population density = $CUP/A$

(For the purposes of the present discussion, the following arbitrary definitions were made:

city--community having population  $> n$

town--community having population = 10 to  $n$

where  $n$  is given by the rural population definition for any country. For example, in the United States, where the rural population is defined as "persons living in places having fewer than 2500 inhabitants,"  $n$  would be 2500.

village--places of residence of agricultural workers in a village-rural area)

$(\text{Pop.})_{\text{town}}$  population living in towns

$(\text{UPD})_{\text{town}}$  urban population density for towns =  
 $(\text{Pop.})_{\text{town}}/A$

$D_m$  density of population within a city, town, or village having  $m$  inhabitants

TRP true rural population = CRP -  $(\text{Pop.})_{\text{town}}$

TUP true urban population = CUP +  $(\text{Pop.})_{\text{town}}$

ACRP age-corrected rural population = TRP--  
(children 4 years of age or younger)

ACFRP age-corrected farm-rural population

FRP farm-rural population--people residing on farms in a farm-rural area

VRP village-rural population--people dependent on agriculture who reside in villages in a village-rural area

AW agricultural workers

SF average size of family

FCT	fraction of area covered by cities and towns
FV	fraction of area covered by villages
FCTV	fraction of area covered by cities, towns and villages
	rural population point--an individual person or farm surrounded by a circle of recovery
$\rho$	rural population point density = (number or rural population points)/RA; subscripts: d = daytime n = nighttime s = summer (April through September) w = winter (October through March)
r	radius of circle of recovery
f	fraction of area which can recover meteorites

The extreme variation in the quality and availability of population statistics required the limitation of the population survey to the United States, Europe, India, and Japan. To quote from the article on population in the Encyclopedia Britannica:

In a United Nations publication issued in 1947 in which an attempt was made to estimate the population of the world it was stated that 40% of the estimated population lived in regions with "poor" figures; i.e., "where the basis of the estimate was weak." A further 37% lived in areas for which the data was "fair"; i.e., "where the estimates were subject to substantial errors." Only the United States, Canada, Japan, north, west, central and southern Europe and Oceania were considered to provide "good" population figures. (11)

In order to make the present survey, it was necessary to estimate many of the earlier population figures. Wherever

possible, this was done by estimating early ratios (of the desired value to some known value, such as the total population) from more recent ratios since these ratios change much less rapidly than the values themselves.

The application of these population figures to the meteorite recovery model described in the main text required a detailed analysis of the distribution of the rural population. For this purpose, two types of distributions were recognized: a) farm rural, where the rural population resides on farms (e.g., the United States) and b) village-rural, where the rural population resides in villages (e.g., India). The fact that these definitions of rural population differ from the census definitions requires that corrections be applied to the census data.

Farm-rural. The following assumptions were made:

1. the CUPD is an index of the rural vs. urban character of an area, and
2. for a given CUPD, the size vs. frequency relationship for cities and towns is fixed.

Thus, by making a detailed study of the size vs. frequency relationship, it is possible to calculate and plot graphs for:

- (a) the  $(UPD)_{\text{town}}$  vs. the CUPD, from which the  $(Pop.)_{\text{town}}$  can be calculated, and
- (b) FCT vs. CUPD (knowing  $D_m$  as a function of  $m$ ).

Using the first graph to find  $(\text{Pop.})_{\text{town}}$  allows the calculation of the true rural and urban populations from the census values according to the equations,

$$\text{TRP} = \text{CRP} - (\text{Pop.})_{\text{town}}$$

$$\text{TUP} = \text{CRP} + (\text{Pop.})_{\text{town}} .$$

An age correction is then applied in order to subtract children too young to contribute to the meteorite collecting population,

$$\text{ACRP} = \text{TRP} - (\text{children 4 years of age or younger}) .$$

These figures are then used to calculate the  $\rho$ 's by using the following equations:

$$\rho_{\text{ds}} = \text{ACRP}/\text{RA} \quad (\text{population points} = \text{rural inhabitants who are assumed to be scattered at random during a summer day}), \text{ and}$$
$$\rho_{\text{dw}} = a\rho_{\text{ds}} \quad (\text{arbitrary fraction, } a, \text{ of rural inhabitants scattered at random during a winter day.})$$

Village-rural. The CUPD is retained as an index of the rural vs. urban character of the region. The size-frequency relationship for communities is assumed to be composed of two parts:

- (a) the size-frequency relationship for cities and towns (same as for farm-rural), and

(b) the villages, which are assumed to have an average population density,  $D_{\text{village}}$ .

Thus,  $FCTV = FCT + FV$

where  $FV = TRP/D_{\text{village}}^A$ .

the  $\rho$ 's are found by:

$\rho_{ds} = AW/RA$  (population points = agricultural workers who are assumed to be scattered at random during a summer day), and

$\rho_{dw} = b\rho_{ds}$  (arbitrary fraction,  $b$ , of agricultural workers scattered at random during a winter day.)

United States. Due to the fact that the United States was expanding westward into almost uninhabited territory during the period, 1820 to 1940, the population density displays extreme variation with space and time. For this reason, only those states in and east of the tier of states from North Dakota to Texas were included in this survey. In addition, a state was excluded until its population density had reached 1 person/sq. km. In support of this latter requirement, it should be noted that no meteorite falls were recorded in a state whose population density was less than 1 person/sq. km., while 4 falls occurred in states having population densities of 1 to 2 persons/sq. km.

The results of the population survey are shown in Table B-1. The following sources of data and assumptions were used in constructing this table.

1. The United States was assumed to be farm-rural.
2. A and TP were found by summing the areas and total populations of the individual states (31) which fulfilled the previously stated requirements for a given year.

3. The CRP for each state was:

- (a) taken directly from the Encyclopedia Britannica (11),
- (b) estimated by interpolation between known values, or
- (c) calculated from the total population and reasonable "per cent rural" values,

and these figures summed to give the CRP shown in the table.

4. The CUP was obtained by subtraction (TP minus CRP).

5. The areas of cities and towns of various sizes were obtained (11,32,33) and used to calculate  $D_m$ .  $D_m$  was then plotted as a function of  $m$  in Figures B-1 and B-2 for the United States and the rest of the world respectively. A good deal of scatter is evident but averages of  $\log D_m$  for intervals of  $\log m$  fall approximately on a straight line. A detailed study of the size vs. frequency relationship for cities and towns in 10 states of the United States was made for the census year, 1940. Combining these data

TABLE B-1. Population Survey for the United States.

Year	A ( $10^6$ sq.km.)	TP (millions)	CUP (millions)	CUPD (no./sq.km.)	FCT	(Pop.) town (millions)	CRP (millions)	TRP (millions)	ACRP (millions)
1820	1.424	9.138	2.0	1.4	.01	0.8	7.1	6.3	5.1
1840	2.285	16.837	3.8	1.7	.01	1.0	13.0	12.0	10.0
1860	2.713	29.768	7.8	2.9	.01	1.3	22.0	20.7	23.6
1880	4.189	48.253	14.0	3.3	.01	1.4	34.3	32.9	28.3
1900	4.841	71.903	28.6	5.9	.01	2.0	43.3	41.3	36.3
1920	4.841	96.807	50.4	10.4	.02	2.7	46.4	43.7	38.9
1940	4.841	117.785	66.3	17.6	.02	3.6	51.5	47.9	44.1

Ave. = 3.59

Ave. = .01

Ave. = 27.8 Ave. = 26.7

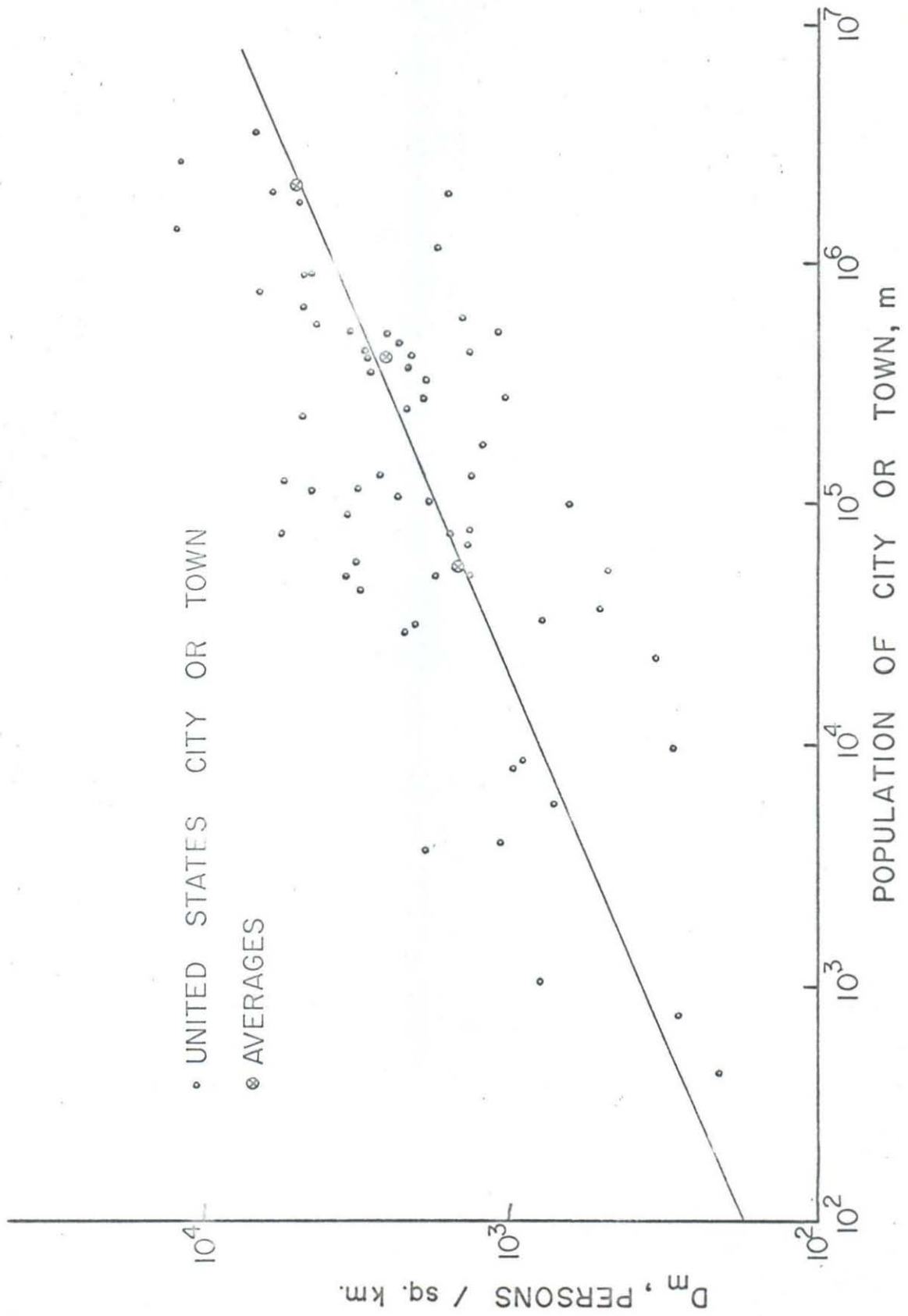


Figure B-1.  $D_m$  for United States cities and towns.



with the  $D_m$  data in Figure B-1 gave the FCT vs. CUPD relationship shown in Figure B-3. This curve was then used to obtain the FCT and  $(Pop.)_{town}$  in Table B-1.

6. The TRP was obtained by subtracting  $(Pop.)_{town}$  from the CRP.

7. The ACRP was calculated using the data in Table B-2.

Europe. Due to the extremely low population densities found in far northern Europe; Finland, Sweden, and Norway were excluded from the population survey. The U.S.S.R. was also excluded but European Turkey was included. Post-World War II boundaries were used. The literature sources and assumptions used in constructing Table B-3 are listed below.

1. Europe was arbitrarily assumed to be 10% farm-rural and 90% village-rural. Thus,  $FRP = (.10)(TRP)$  and  $VRP = (.90)(TRP)$ .

2. The figures for the TP came from Figure B-4 which in turn was drawn from the data in Table B-4. The data in column 2 of this table were taken from several sources (35,36,37,38,39,40). The values for 1800 and 1850 are estimates (e = estimated) based upon the quotation, "Since 1850 the population has doubled and since 1800 it has almost tripled. . . .," referring to the year 1939 (41). Column 3 of Table B-4 gives the TP for Belgium, France, Germany, Italy, the Netherlands, Spain, Switzerland, and the United Kingdom which are referred to as "reference countries" since data for them is more readily available.

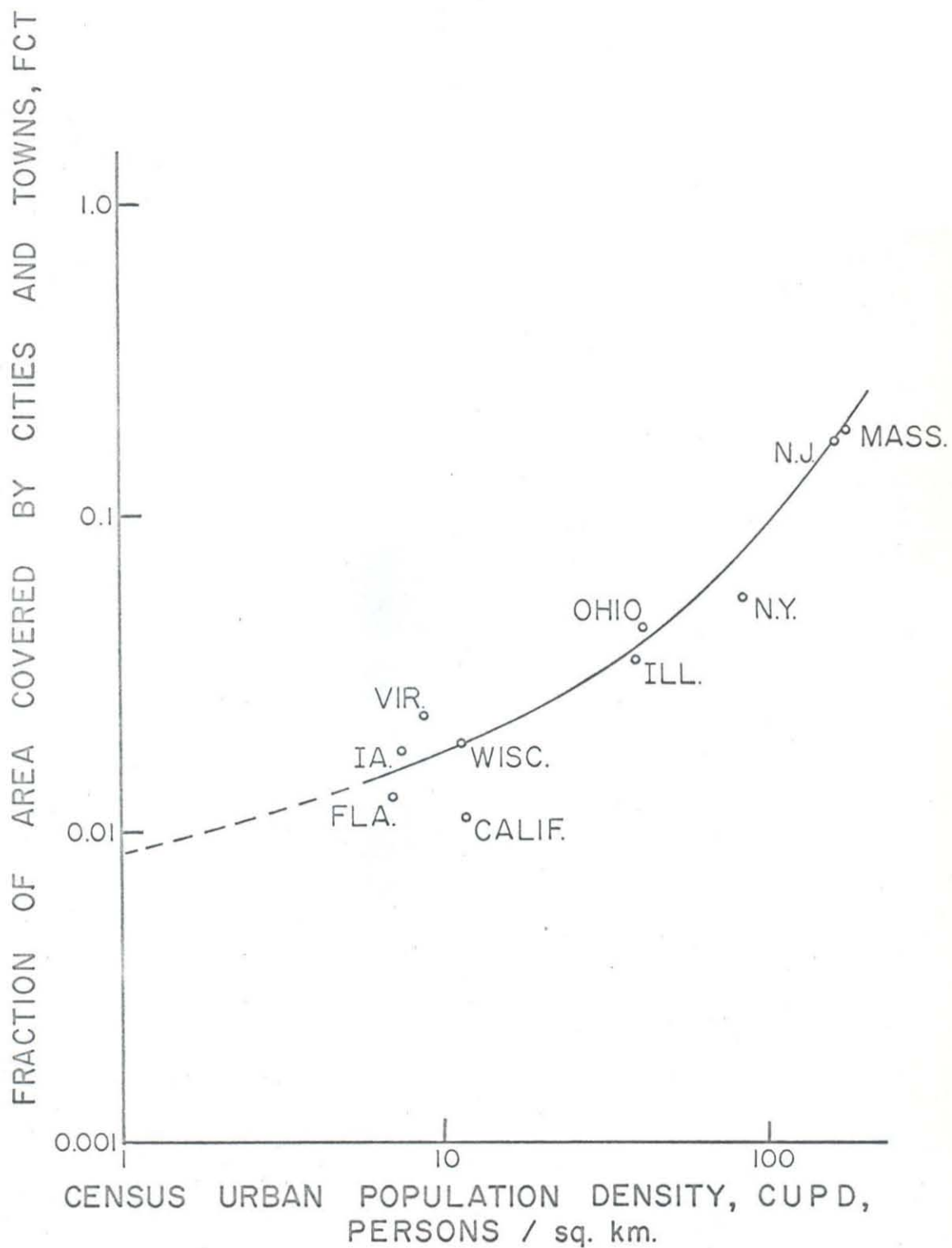


Figure B-3. Fraction of area covered by cities and towns.

TABLE B-2. Fraction of People  
in 0 to 4 Year Age Group (34).

<u>Year</u>	<u>Fraction of People in 0 to 4 Year Age Group</u>
1820	.19
1840	.17
1860	.15
1880	.14
1900	.12
1920	.11
1940	.08

TABLE B-3. Population Survey for Europe.

Area =  $3.68 \cdot 10^6$  sq. km.

<u>Year</u>	<u>TP</u> (millions)	<u>CUP</u> (millions)	<u>CUPD</u> (no./sq. km.)	<u>FCT</u>	<u>FCTV</u>
1820	150	30	8	.02	.05
1840	175	45	12	.02	.05
1860	200	50	14	.02	.06
1880	240	80	22	.03	.07
1900	280	120	33	.03	.07
1920	320	150	41	.04	.08
1940	379	190	52	.04	.08
				Ave. =	.07

<u>Year</u>	<u>(Pop.) town</u> (millions)	<u>CRP</u> (millions)	<u>TRP</u> (millions)	<u>VRP</u> (millions)	<u>FRP</u> (millions)	<u>ACFRP</u> (millions)	<u>AM</u> (millions)	<u>Total ACRP</u> (millions)
1820	6	120	114	100	11	9	54	63
1840	7	130	123	110	12	10	59	69
1860	8	150	142	130	14	12	62	74
1880	11	160	149	130	15	13	70	83
1900	14	160	146	130	15	13	76	89
1920	15	170	155	140	16	14	67	81
1940	18	186	168	150	17	15	80	95
				Ave. = 130	Ave. = 14		Ave. = 67	Ave. = 79

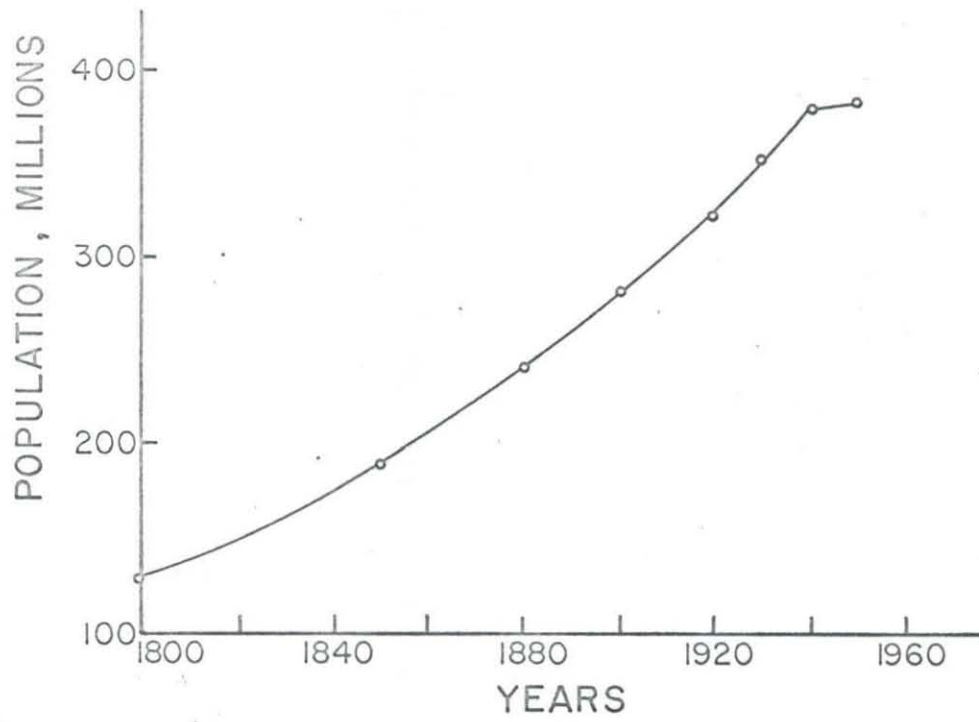


Figure B-4. European total population.

European TP found

in column 3 which

of values for 1850 and 1900. (The error

TABLE B-4. European Total Population.

<u>Year</u>	<u>TP</u> <u>(millions)</u>	<u>Population</u> <u>of</u> <u>Reference</u> <u>Countries</u> <u>(millions)</u>	<u>% of TP</u>	<u>Calculated</u> <u>TP</u> <u>(millions)</u>
1800	130 e	104	80	
1850	190 e	149	78	
1880		175	74 e	240
1900		201	71 e	280
1920	320	221	69	
1930	351	237	67.5	
1940	379	260	68.5	
1950	380	260	68.4	

The per cent of the European TP found in these reference countries is shown in column 4 which allows the estimation of values for 1880 and 1900. (The error of the estimation is small because a large percentage of the European TP resides in these reference countries.) This estimation in turn yields the calculated TP in column 5.

3. Any estimation of the CRP or AW is made difficult by the lack of data for the whole of Europe prior to 1910. Recourse is again made to reference countries and the resulting trends applied to the whole of Europe. The data in Table B-5 were taken from several sources (11,35,38,39) and the liberty of applying the data to the nearest decade year was exercised. One country was taken from each of the 1930 per cent rural population groups thus ensuring adequate representation of all degrees of rurality. Each group was then weighted on the basis of the 1930 TP for that group. The rural population definitions differ from country to country in Europe (e.g., n=2000 and 5000 in Czechoslovakia and Yugoslavia respectively) but the average was arbitrarily assumed to be 2500.

4. The FCT vs. CUPD and  $(\text{Pop.})_{\text{town}}$  vs. CUPD relationships established for the United States were applied without modification to obtain the European FCT and  $(\text{Pop.})_{\text{town}}$ .

5. The ACFRP was obtained from the FRP by using Table B-6.

TABLE B-5. Agricultural Workers and Rural Population in Europe.

Year	Great Britain	Germany	France	Italy	Poland	Bulgaria	Yugoslavia	Europe
number of agricultural workers (percentage of total population):								
1800	10 e	30 e	35 e	45 e	50 e	50 e	50 e	38 e
1820								36 e
1840								34 e
1860	6 e	20 e	26 e	40 e	45 e	50 e	45 e	31 e
1870	5 e		25 e					
1880								29 e
1900	5 e	16 e	23 e	30 e	40 e	45 e	40 e	27 e
1910	5	15	22	26				
1920	5	17	23	27	34 e	42	33	21
1930			18		31 e	46		
1940	2 e	15 e	18	20	30 e	40 e	30 e	21 e
1950	2		16	16				
census rural population (percentage of total population):								
1800	60 e	80 e	80 e	85 e	90 e	95 e	99 e	82 e
1820								79 e
1840								76 e
1850			75					
1860	35 e	70 e	72 e	75 e	85 e	90 e	97 e	73 e
1870		64						
1880		59						65 e
1890		53						
1900	25 e	46	50	60 e	75 e	80 e	95 e	57 e
1910		40						
1920	23 e	38 e	50 e	58 e.	73 e	78 e	90	54 e
1930					72		88	
1940	21	30	47	55	65 e	75	86 e	49
1950	15 e	31		50	64	75 e	84	
1930 percent rural population group:								
20-30	30-40	40-50	50-60	60-70	70-80	80-90		
other countries in population group:								
	Austria	Neth.	Czech.	Greece	Romania	Albania		
	Belgium			Hungary	Spain			
	Denmark			Ireland	Turkey			
				Portugal				
				Switzerland				
weighting factor (based on 1930 total population):								
50	83	50	56	60	49	15	363	

TABLE B-6. Fraction of People  
in 0 to 4 Year Age Group (41).

<u>Year</u>	<u>England</u>	<u>Germany</u>	<u>Southern and Eastern Europe</u>	<u>Europe</u>
1840	.13			
1910		.09		
1930	.08	.06		
1940		.04	.10	.09
1820-1860				.16 e
1880-1900				.13 e
1920-1940				.10 e

6. The FCTV was calculated by arbitrarily assuming  
 $D_{\text{village}} = 1000 \text{ people/sq. km.}$

7. The Total ACRP was calculated by using the equation,

$$\text{Total ACRP} = \text{ACFRP} + (.90)AW .$$

Northern India. In order to obtain an idea of the relative meteorite collecting capabilities of the various Indian states, Table B-7 was constructed. A wide range of recovery rates is evident from this table and for this reason, India was divided into "Northern" (high rate of recovery) and "Southern" (lower rate of recovery) parts. Included in Northern India were the Gangetic Plain states of Uttar Pradesh, Bihar and West Bengal plus Punjab and the Pakistani state of East Pakistan. These states also lie in the high population density area of India. The results of the population survey for Northern India are shown in Table B-8 and the literature sources and assumptions employed in constructing the table are listed below.

1. India was assumed to be village-rural.

2. The TP for Northern India was taken from Table B-9 the data for which was drawn from several sources (11,42,43). "Old" India and "Modern" India refer to pre-partition and post-partition boundaries respectively. The twentieth century ratios of Modern/Old and Northern/Modern were computed from known figures and the earlier ratios estimated from them. These estimated ratios were then used to calculate the Modern India TP and Northern TP.

TABLE B-7. Rates of Recovery of Meteorite Falls  
for Indian States (1810 to 1950).

<u>State</u>	$\frac{R}{(\text{falls}/10^6 \text{ sq.km.}-\text{year})}$
Uttar Pradesh	0.81 $\pm$ 0.14
West Bengal	0.49 $\pm$ 0.19
Punjab	0.41 $\pm$ 0.15
East Pakistan	0.40 $\pm$ 0.14
Madras	0.28 $\pm$ 0.12
Himachal Pradesh	0.25 $\pm$ 0.25
Mysore	0.18 $\pm$ 0.08
Kerala	0.19 $\pm$ 0.19
Bihar	0.16 $\pm$ 0.08
Rajasthan	0.15 $\pm$ 0.05
Madhya Pradesh	0.15 $\pm$ 0.05
Andhra Pradesh	0.13 $\pm$ 0.06
Bombay	0.10 $\pm$ 0.04
Orissa	0.09 $\pm$ 0.06
Assam	0.00

TABLE B-8. Population Survey for Northern India.

Area =  $0.846 \cdot 10^6$  sq. km.

<u>Year</u>	<u>TP</u> (millions)	<u>CUP</u> ( <u>&gt; 5000</u> ) (millions)	<u>CUP</u> ( <u>&gt; 2500</u> ) (millions)	<u>CUPD</u> (no./sq. km.)	<u>FCT</u>	<u>FCTV</u>
1821	66	3	4	5	.01	.02
1841	66	5	6	7	.01	.02
1861	96	9	11	13	.02	.03
1881	126	12	14	17	.02	.03
1901	133	13	16	19	.02	.03
1921	134	16	19	22	.03	.04
1941	173	24	29	34	.03	.05

Ave. = .03

<u>Year</u>	<u>(Pop.)<sub>town</sub></u> (millions)	<u>CRP</u> ( <u>&lt; 5000</u> ) (millions)	<u>CRP</u> ( <u>&lt; 2500</u> ) (millions)	<u>TRP</u> (millions)	<u>AW</u> (millions)
1821	1	63	62	61	30 e
1841	1	61	60	59	30 e
1861	2	87	85	83	41 e
1881	2	114	112	110	50 e
1901	2	120	117	115	50 e
1921	2	118	115	113	44
1941	3	149	144	141	43 e

Ave. = 97

Ave. = 41

TABLE B-9. Total Population of Northern India.

<u>Year</u>	<u>Old India TP (millions)</u>	<u>Modern India TP (millions)</u>	<u>Ratio of Modern Old</u>	<u>Northern TP (millions)</u>	<u>Ratio of Northern Modern</u>
1821	130	110 e	.85 e	66 e	.60 e
1841	130	110 e	.85 e	66 e	.60 e
1861	190	160 e	.85 e	96 e	.60 e
1881	257	218 e	.85 e	126 e	.58 e
1901	285	235	.83	133	.57
1921	305	248	.81	134	.54
1941	389	314	.81	173	.55

urban definition = "communities larger than 5000"

3. The CRP figures were taken from Table B-10. The per cent rural values for all India in this table were either taken from the literature (42,43) or estimated and were applied without correction to both Northern and Southern India. India employs a rural population definition having  $n = 5000$ . An attempt was made in Table B-8 to change the data to apply to a definition having  $n = 2500$  by moving 20% of the CRP to CUP. Justification for this step may be found in the value for the ratio of  $(\text{Pop.})_{2500-5000} / (\text{Pop.})_{5000-10^7}$  for India, 1951 (0.2) and for Virginia, 1940 (0.19). Virginia comes the closest of the ten American states studied to the village-rural distribution.

4. The FCTV was calculated by letting  $D_{\text{village}} = 10^4$  people/sq. km. This value was taken from a survey of Indian village population densities (42) which showed a high of  $26 \cdot 10^3$  persons/sq. km. and a low of  $9 \cdot 10^3$  persons/sq. km. It was assumed that the low value was more typical thus arriving at an average of about  $10 \cdot 10^3$  persons/sq. km.

5. The 1921 value of AW was taken from Table B-11. Values for other years in Table B-8 were estimated.

Southern India. On the basis of Table B-7, Southern India was made to include the Indian states of Andhra Pradesh, Kerala, Madhya Pradesh, Madras, Mysore, and Rajasthan. Table B-12 showing the results of the population survey

TABLE B-10. Census Rural Population of India.

<u>Year</u>	<u>Percent Rural for all India</u>	<u>Northern CRP (millions)</u>	<u>Southern CRP (millions)</u>
1821	95 e	63	31
1841	93 e	61	32
1861	91 e	87	48
1881	90.7	114	69
1901	90.0	120	77
1921	88.6	118	83
1941	86.1	149	102

urban definition = "communities larger than 5000"

TABLE B-11. Percentage of Indian Population in Agriculture and Fishing (35, 36).

Year	Population (Millions)	Year	%	Average
1911	23	1911	36	.03
1921	36	1921	33	.01
1931	53	1931	28	.01
1941	78			.01
1950	150			.03
1961	230			.03
1971	360			.03
1981	530			.03
1991	780			.03
2001	1050			.03
2011	1350			.03
2021	1700			.03
2031	2100			.03
2041	2500			.03
2051	2900			.03
2061	3300			.03
2071	3700			.03
2081	4100			.03
2091	4500			.03
2101	4900			.03
2111	5300			.03
2121	5700			.03
2131	6100			.03
2141	6500			.03
2151	6900			.03
2161	7300			.03
2171	7700			.03
2181	8100			.03
2191	8500			.03
2201	8900			.03
2211	9300			.03
2221	9700			.03
2231	10100			.03
2241	10500			.03
2251	10900			.03
2261	11300			.03
2271	11700			.03
2281	12100			.03
2291	12500			.03
2301	12900			.03
2311	13300			.03
2321	13700			.03
2331	14100			.03
2341	14500			.03
2351	14900			.03
2361	15300			.03
2371	15700			.03
2381	16100			.03
2391	16500			.03
2401	16900			.03
2411	17300			.03
2421	17700			.03
2431	18100			.03
2441	18500			.03
2451	18900			.03
2461	19300			.03
2471	19700			.03
2481	20100			.03
2491	20500			.03
2501	20900			.03
2511	21300			.03
2521	21700			.03
2531	22100			.03
2541	22500			.03
2551	22900			.03
2561	23300			.03
2571	23700			.03
2581	24100			.03
2591	24500			.03
2601	24900			.03
2611	25300			.03
2621	25700			.03
2631	26100			.03
2641	26500			.03
2651	26900			.03
2661	27300			.03
2671	27700			.03
2681	28100			.03
2691	28500			.03
2701	28900			.03
2711	29300			.03
2721	29700			.03
2731	30100			.03
2741	30500			.03
2751	30900			.03
2761	31300			.03
2771	31700			.03
2781	32100			.03
2791	32500			.03
2801	32900			.03
2811	33300			.03
2821	33700			.03
2831	34100			.03
2841	34500			.03
2851	34900			.03
2861	35300			.03
2871	35700			.03
2881	36100			.03
2891	36500			.03
2901	36900			.03
2911	37300			.03
2921	37700			.03
2931	38100			.03
2941	38500			.03
2951	38900			.03
2961	39300			.03
2971	39700			.03
2981	40100			.03
2991	40500			.03
3001	40900			.03

TABLE B-12. Population Survey for Southern India.

Area =  $1.420 \cdot 10^6$  sq. km.

<u>Year</u>	<u>TP</u> (millions)	<u>CUP</u> ( <u>&gt; 5000</u> ) (millions)	<u>CUP</u> ( <u>&gt; 2500</u> ) (millions)	<u>CUPD</u> (no./sq. km.)	<u>FCT</u>	<u>FCTV</u>
1821	33	2	2	1	.01	.01
1841	34	2	2	1	.01	.01
1861	53	5	6	4	.01	.01
1881	76	7	8	6	.01	.01
1901	85.0	8	10	7	.02	.03
1921	93.7	11	13	9	.02	.03
1941	118.7	17	20	14	.02	.03

Ave. = .02

<u>Year</u>	<u>(Pop.)<sub>town</sub></u> (millions)	<u>CRP</u> ( <u>&lt; 5000</u> ) (millions)	<u>CRP</u> ( <u>&lt; 2500</u> ) (millions)	<u>TRP</u> (millions)	<u>AW</u> (millions)
1821	1	31	31	30	15 e
1841	1	32	32	31	15 e
1861	2	48	47	45	22 e
1881	2	69	68	66	30 e
1901	2	77	75	73	32 e
1921	2	83	81	79	31
1941	3	102	99	96	31 e

Ave. = 60

Ave. = 25

for Southern India was constructed by the same methods as Table B-8. The values for TP were taken from Table B-13 which is an extension of Table B-9.

Japan. The results of the population survey for Japan are shown in Table B-14. Assumptions and literature sources used in constructing this table are listed below.

1. Japan was assumed to be village-rural.
2. The figures for TP and CRP are taken from Table B-15 which in turn is composed of data from several sources (37, 44, 45). Since it has a very low population density, the island of Hokkaido was excluded from the survey by subtracting 2% of the Japanese TP for the years 1820 to 1880 and 5% for 1900 to 1940. The basis for these values is the fact that the ratio of the population on Hokkaido to that of all Japan in 1955 was 0.05 (11). The rural population definition for Japan cannot be translated directly into American terms because the political subdivisions do not correspond. However, for the purposes of this survey, the Japanese definition was arbitrarily assumed to be the same as that for the United States.
3. The  $D_{\text{village}}$  used in calculating FCTV was arbitrarily assumed to be slightly smaller than that for India and was assigned a value of  $8 \cdot 10^3$  persons/sq. km.
4. The AW was estimated by using Table B-16.

TABLE B-13. Total Population of Southern India.

<u>Year</u>	<u>Modern India TP (millions)</u>	<u>Southern India TP (millions)</u>	<u>Ratio of Southern Modern</u>
1821	110 e	33 e	.30 e
1841	110 e	34 e	.31 e
1861	160 e	53 e	.33 e
1881	218 e	76 e	.35 e
1901	235	85.0	.36
1921	248	93.7	.38
1941	314	118.7	.38

TABLE B-14. Population Survey for Japan.

Area =  $0.249 \cdot 10^6$  sq. km.

<u>Year</u>	<u>TP</u> (millions)	<u>CUP</u> (millions)	<u>CUPD</u> (no./sq. km.)	<u>FCT</u>	<u>FCTV</u>
1820	20	1	4	.01	.02
1840	25	2	8	.02	.03
1860	30	3	12	.02	.03
1880	36	5	20	.02	.04
1900	44	7	28	.03	.05
1920	53	10	40	.04	.06
1940	69	17	68	.06	.09

Ave. = .05

<u>Year</u>	<u>(Pop.) town</u> (millions)	<u>CRP</u> (millions)	<u>TRP</u> (millions)	<u>AW</u> (millions)
1820	0.3	19	19	10 e
1840	0.4	23	23	9 e
1860	0.5	27	27	9 e
1880	0.7	31	30	10 e
1900	0.8	37	36	11 e
1920	1.0	43	42	12 e
1940	1.4	52	51	13

Ave. = 33

Ave. = 10

TABLE B-15. Total Population and Census Rural Population of Japan.

<u>Year</u>	<u>TP</u> <u>(millions)</u>	<u>TP</u> <u>(no Hokkaido)</u> <u>(millions)</u>	<u>CRP</u> <u>(millions)</u>	<u>Percent</u> <u>Rural</u>	<u>CRP</u> <u>(no Hokkaido)</u> <u>(millions)</u>
1820		20 e		95 e	19 e
1840		25 e		93 e	23 e
1846	26.9				
1860		30 e		90 e	27 e
1872	33.1				
1880	37.0	36		87 e	31 e
1893	41.4				
1900	46.7	44		84 e	37 e
1920	56.0	53	45.9	82	43 e
1940	72.5	69		75 e	52 e
1947	78.6		52.2	66	

Agricultural Workers

The total population of Japan in 1955 was 83,000,000. The agricultural workers in Japan in 1955 were 16,500,000, or 19.8% of the total population. The agricultural workers in Japan in 1938 were 13,500,000, or 19% of the total population. The agricultural workers in Japan in 1950 were 16,700,000, or 20% of the total population.

The following table shows the number of agricultural workers in Japan in 1938, 1950, and 1955, and the percentage of the total population that they represent.

TABLE B-16. Agricultural Workers in Japan (46).

<u>Year</u>	<u>AW</u> <u>(millions)</u>	<u>Percent of TP</u>
1938	13.5	19
1950	16.7	20
1955	16.5	18

Rural Population Point Densities. The assumptions and data used to arrive at the rural population point densities are outlined in Table B-17. An attempt was made to compare climatic conditions of the various regions by listing the average temperature and precipitation for reference cities within the regions. These data (11) are shown at the top of the table. On the basis of these figures, somewhat arbitrary values were assigned to the coefficients "a" and "b" for each region (where a = the fraction of rural inhabitants scattered at random during a winter day in a farm-rural area and b = the fraction of agricultural workers so scattered in a village-rural area). Northern and Southern India were assumed to experience similar weather. Their summer weather during the months of June, July, and August is largely dominated by the Southwest Monsoons which should make the summer months less favorable for the recovery of meteorites. Japan, Europe, and the United States were assumed to have similar winter weather.

The densities of farms and of cities, towns, and villages were computed as indicated below:

United States - An average of 5 persons per farm household for the period 1820 to 1940 was estimated from Table B-18 (34). The calculated value is much greater than the density of cities and towns.

TABLE B-17. Climatic Conditions and Calculated Population Point Densities.

reference city	<u>United States</u>			<u>Europe</u>			<u>Northern and Southern India</u>		<u>Japan</u>
	Chicago	Charleston	Greenwich	Berlin	Rome	Calcutta	Calcutta	Tokyo	
ave. summer temp. (°F.)	63°	75°	56°	59°	68°	83°	83°	68°	
ave. summer ppt. (in.)	3.1	4.6	2.1	2.0	1.6	8.4	8.4	6.1	
ave. winter temp. (°F.)	26°	55°	42°	37°	58°	71°	71°	45°	
ave. winter ppt. (in.)	2.2	3.0	2.0	1.6	5.3	1.1	1.1	4.8	
"a" (farm-rural), summer	1.0			1.0					
"a" (farm-rural), winter	0.3			0.3					
"b" (village-rural), summer				1.0			0.8	1.0	
"b" (village-rural), winter				0.7			1.0	0.7	
density of farms (no./sq.km.)	1.5			0.8					
density of towns and villages (no./sq.km.)				0.1 (France)	0.4	0.15	0.02	0.5	
FCT or FCTV	0.01			0.07			0.03	0.05	
$\rho_{ds}$	7.4			21			39	40	
$\rho_{ns}$	1.5			0.8			0	0	
$\rho_{dw}$	3.8			17			49	28	
$\rho_{nw}$	1.5			0.8			0	0	

Northern Southern

1 216 1

TABLE B-18. Population Per Household (34).

<u>Year</u>	<u>All Types</u>	<u>Farm</u>
1890	5.0	5.3 e
1900	4.8	5.1 e
1910	4.5	
1920	4.3	4.7
1930	4.1	4.6
1940	3.8	4.3
1950	3.5	4.0

- Europe - The average number of people per farm household was arbitrarily assumed to be the same as the United States figure. It should be noted that this leads to a density of farms about one-half that of the United States which may be too high. France was chosen as a reference country for the calculation of the density of cities, towns and villages. In that country, in 1954, there were 37,000 communes (out of a total of 38,000) which had populations of fewer than 2000 people (11). Thus the village-rural character of this region is very apparent.
- N. India - According to the Indian Census, there were 558,000 villages (places having fewer than 5000 inhabitants) in 1951 (43). The fraction of these in Northern India was estimated by simply multiplying by the fraction of the Indian TP in Northern India in 1951.
- S. India - The same method as that used in Northern India was used here.
- Japan - The density of villages was estimated to be about 0.5 villages/sq. km. on the basis of a conversation with an inhabitant of

that country. This would give the average Japanese village about 250 inhabitants which is a reasonable figure.

The FCT or FCTV were taken directly from Tables B-1, B-3, B-8, B-12, and B-14. The ACRP, AW, and RA from these tables along with the values of "a" or "b" were then used to calculate the  $\rho$ 's according to the equations given near the beginning of this Appendix. It is evident that the densities of farms and of cities, towns, and villages are negligible compared to the daytime rural population densities.

A rough check on the values for  $\rho_{ds}$  and  $\rho_{ns}$  for the United States may be made by referring to Ninninger's values of 6.2 people/sq. km. and 3.1 families/sq. km. in a west-central Missouri area during August of 1932 (29).

With the calculation of these values for the  $\rho$ 's, the population survey was completed.

REFERENCES

1. Prior, G. T. and Hey, M. H., Catalogue of Meteorites, British Museum (London, 1953).
2. The Meteoritical Bulletin, The Permanent Commission on Meteorites of the International Geological Congress (Moscow).
3. Newton, H. A., Am. J. Sci. 36, 1-14 (1888).
4. Whipple, F. L. and Hughes, R. F., Meteors: Special Supplement (Vol. 2) to J. Atmosph. Terr. Phys., 149-56 (1955).
5. Porter, J. G., Comets and Meteor Streams, John Wiley and Sons, Inc. (New York, 1952).
6. Piotrowski, S. L., Astron. J. 57, 23-4 (1952).
7. Baldwin, R. B., The Face of the Moon, The University of Chicago Press (Chicago, 1949).
8. Shoemaker, E. M., Report of the International Geological Congress, XXI Session, Norden, 1960, part XVIII.
9. Krinov, E. L., Principles of Meteoritics, Pergamon Press (New York, 1960).
10. Noren, C. H., Quart. Colo. School Mines 51, 212-225 (1956).
11. Encyclopedia Britannica, Encyclopedia Britannica, Inc. (Chicago, London, Toronto, 1960).
12. Goldberg, E., Uchiyama, A., and Brown, H., Geochim. et Cosmochim. Acta 2 1-25 (1951).
13. The Rand Corporation, A Million Random Digits with 100,000 Normal Deviates, The Free Press (Glencoe, Illinois, 1955).
14. Dixon, W. J. and Massey, F. J., Jr., Introduction to Statistical Analysis, McGraw-Hill Book Co., Inc., (New York, 1957), p. 221.
15. Hawkins, G. S., Astron. J. 64, 450-4 (1959).
16. Opik, E. J., AFOSR Doc. No. TN., The Lunar Surface as an Impact Counter (1959).

17. Brown, H., J. Geophys. Res. 65, 1679-83 (1960).
18. Kuiper, G. P., Fujita, Y., Gehrels, T., Groeneveld, I., Kent, J., Van Biesbroeck, G., and Van Houten, C. J., Ap. J. Supplement 32 III, 289 (July, 1958).
19. Lovell, A. C. B., Meteor Astronomy, Oxford University Press (London, 1954).
20. Kreiter, T. J., Publications of the Astron. Soc. of the Pacific 72, 393-8 (1960).
21. Lyubarskiy, K. A., Missels and Rockets, No. 9, 30 (1960).
22. Press, F., Buwalda, P., and Neugebauer, M., J. Geophys. Res. 65, 3097-3105 (1960).
23. Brown, H. (private communication).
24. Silberrad, C. A., Mineral. Mag. 23, 290-304 (1932).
25. Ninninger, H. H., Our Stone-Pelted Planet, Houghton Mifflin Co. (Boston, New York, 1933), pp. 78-80.
26. Hawkins, G. S., Interim Report 42, Contract AF19 (122)-458 Sub Contract 57 (1959).
27. Brown, H., J. Geophys. Res. 66, 1316-17 (1960).
28. United States Nautical Almanac Office, The American Ephemeris and Nautical Almanac for the Year 1960, United States Government Printing Office (Washington, 1958), pp. 394-401.
29. Ninninger, H. H., Out of the Sky, Dover Publications, Inc. (New York, 1952).
30. Opik, E. J., Physics of Meteor Flight in the Atmosphere, Interscience Publishers, Inc. (New York, 1958), p. 26.
31. U. S. Bureau of the Census, Historical Statistics of the United States, Colonial Times to 1957 (Washington, 1960).
32. Robson, W. A. (editor), Great Cities of the World, The MacMillan Co. (New York, 1955), p. 26.
33. Personal survey conducted by mailing inquiries to towns chosen at random in the United States.

34. Bogue, D. J., The Population of the United States,  
The Free Press (Glencoe, Illinois, 1959).
35. Statistical Year-Book of the League of Nations 1931/32  
(Geneva, 1932).
36. Statistical Year-Book of the League of Nations 1934/35  
(Geneva, 1935).
37. Woytinsky, W. S. and Woytinsky, E. S., World Population  
and Production, The Twentieth Century Fund, Inc.  
(New York, 1953), pp. 44, 48.
38. U.S. Bureau of the Census, International Population  
Statistics Reports: No. 1, pp. 55, 63; No. 2,  
p. 15; No. 4, p. 123; No. 5, pp. 31, 115, 119.
39. Demographic Yearbook 1948, United Nations (New York,  
1957), p. 213.
40. Demographic Yearbook 1957, United Nations (New York,  
1957), p. 123.
41. Notestein, F. W. et al., The Future Population of  
Europe and the Soviet Union, League of Nations  
(Geneva, 1944), p. 44.
42. Davis, K., The Population of India and Pakistan,  
Princeton University Press (Princeton, N. J.,  
1951).
43. India, A Reference Annual, 1958, Government of India.
44. Encyclopedia Britannica, Encyclopedia Britannica, Inc.  
(Chicago, London, Toronto, 1929).
45. Population Census of Japan, October 1, 1947, Office  
of the Prime Minister, Bureau of Statistics  
(October, 1949), p. 50.
46. Dore, R. P., Land Reform in Japan, Oxford University  
Press (London, New York, Toronto, 1959), p. 263.

PROPOSITION 2

to be determined accordingly

**PROPOSITIONS**

PROPOSITION 1

In radiochemical procedures, where a carrier is employed and the yield of the radioactive component is found from the carrier yield (e.g., many neutron activation analytical procedures), electroplating offers a convenient method for separating elements and, at the same time, presents them in a form suitable for radioactive counting. Where several elements are to be determined simultaneously, controlled-potential electrolysis must be used. However, if more than several elements are to be separated by this method, the usual procedure of removing the cathode between platings is cumbersome and time consuming and a method providing for continuous plating and removal of the deposit from the solution would be very desirable.

A plating apparatus, built for this purpose, is shown in Figure 1. The cathode is a strip of gold foil (1.5 x 36 inches) which is moved continuously through the solution. The area exposed for plating is about 1.5 square inches. The potential of this cathode is monitored by a saturated calomel electrode and is advanced (to more negative values) at a uniform rate by means of a motor-driven potentiostat. The plated foil strip is dried with alcohol vapor as it emerges from the solution. Theoretically, the metals should begin to deposit when the cathode potential reaches their decomposition potentials and should continue to deposit until they are completely removed from the solution. Because the

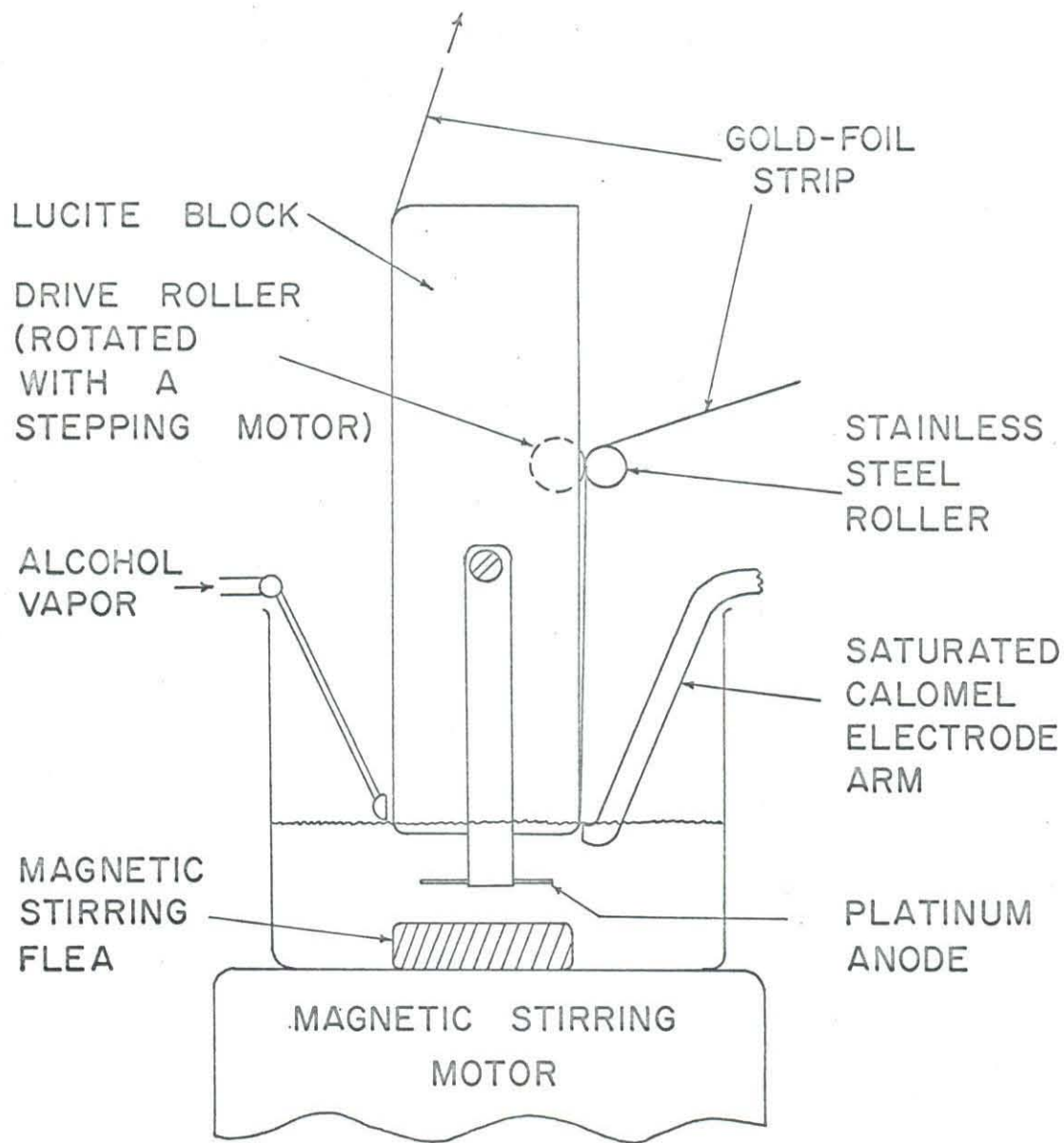


Figure 1. The continuous plating apparatus or "potentiograph."

potential plays a major role in any separations achieved by this apparatus, I have called it a "potentiograph" and the plated foil strip is then a "potentiogram." The potentiogram would be cut up and the sections placed in a counter (presumably a gamma-spectrometer) and the activity due to the various radionuclides determined. The amount of each carrier element on each section would then be found by some method, the carrier yields calculated, and thus the amount of each element in the original sample determined.

Two opposing factors help to determine the rate at which the foil strip and cathode potential are advanced. The fact that the activity to be measured may be decaying with a relatively short half-life leads to the desire to plate the metal in as short a time as possible. However, maximum resolution (i.e., ratio of the distance over which the metal is plated on the foil strip to the length of the strip) is achieved by advancing the foil strip and potential very slowly. A compromise rate must be found.

A trial experiment was performed using a 30-ml., 0.5F HCl solution containing 10 mg. each of mercury, nickel, cadmium, chromium, zinc, tin, germanium, copper, iron, molybdenum, cobalt, palladium, platinum, osmium, rhenium, and gold, 1 mg. of arsenic, and 2 mg. each of antimony and indium. The tape was advanced at about 2 inches per hour and the cathode potential at 0.15 volts per hour for 7 hours while covering the range +0.70 v. to -0.4 v. vs. S.C.E. At

this point, hydrogen evolution became excessive and 25 drops concentrated ammonium hydroxide were added changing the pH to 9.0. A brown precipitate formed and was later found to contain portions of the platinum, copper, iron, cobalt, nickel, cadmium, zinc, tin, germanium, molybdenum, and chromium. Electrolysis was continued for 1.5 hours while the cathode potential was advanced from -0.80 v. to -1.05 v. vs. S.C.E. The gold foil strip was then cut into 1-inch sections and examined by an x-ray fluorescence apparatus. Earlier platings of 0.3 mg./sq. cm. copper over gold had showed no reduction in the counting rate for the gold-L $\beta$  peak and thus this peak was used as a standard to which the intensities of all other peaks were referred. This method of analysis yielded a very rough indication of where the elements plated out and the results are shown in Figure 2. The conclusion must be drawn that some separations were achieved but the resolution would have to be better for practical applications.

Thus, it is proposed that the potentiograph be further investigated as an apparatus for obtaining separations of radioactive metals and that different supporting electrolytes be tried.

Convenient methods for determining the yield of carrier element on the strip (other than x-ray fluorescence which is not adequate for all elements) present themselves. After counting, the sections could be reirradiated with thermal

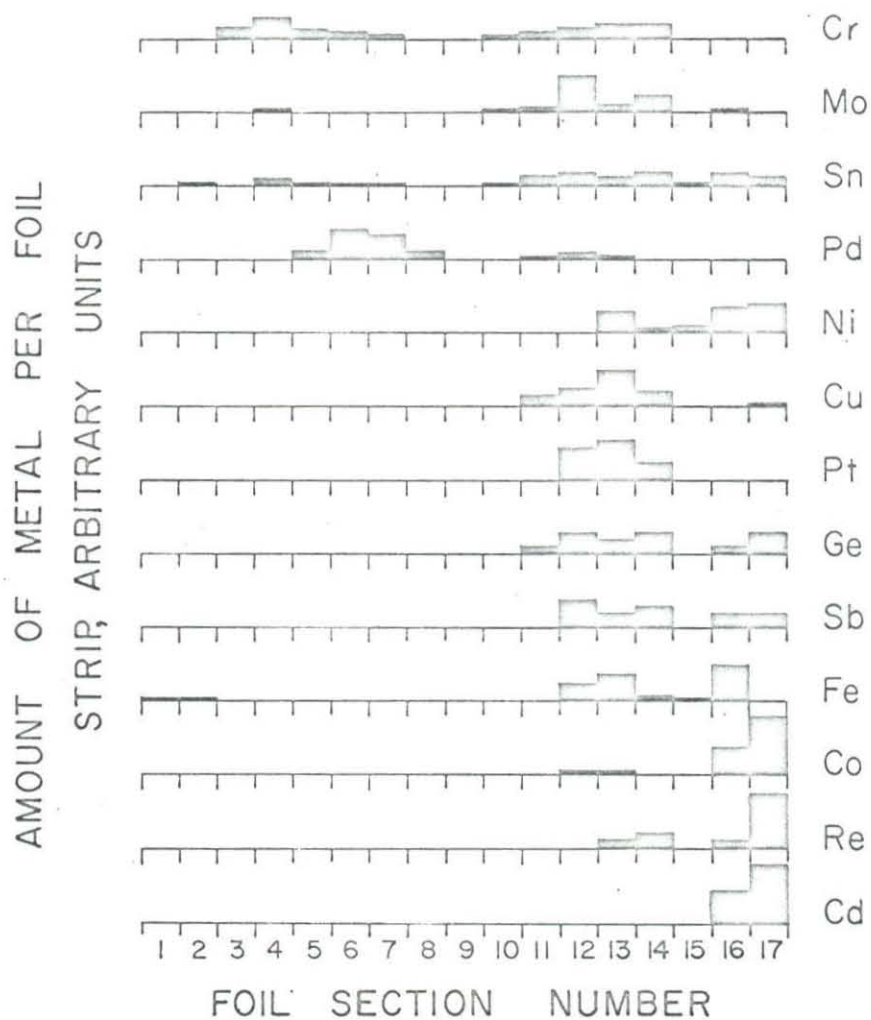


Figure 2. Positions on the gold foil strip at which the metals plated out.

neutrons for short periods of time, recounted, and the yield of carrier calculated from the new activity. Another approach might involve the dissolution of the plated metals and their analysis by polarographic methods.

Advancing the cathode potential with time is not the only way to achieve separations with this apparatus. Complexing agents, such as ethylenediamine tetraacetic acid (EDTA), could be used to prevent the deposition of certain metals by employing techniques similar to those used in controlled-potential coulometric analysis. Since the ratio of uncomplexed to complexed metal is pH dependent, titration of the initially complexed metals with acid should "free" these for deposition at the controlled cathode potential at different points in the titration. Preliminary calculations indicate that the ratio of complexed to uncomplexed metal is reduced to 10 over a range of several pH units for the metals cobalt, cadmium, zinc, nickel, copper, mercury, chromium, and iron. Another possibility is the separation of halide ions. A silver strip could be used as an anode and the anode potential advanced to more positive potentials with time.

PROPOSITION 2

As will be discussed in Proposition 3, a proposed method for finding the amount of manganese-53 in a sample involves neutron activation to manganese-54. However, the activation cross section for manganese-53 is unknown and must therefore be estimated. No methods could be found in the literature to perform this estimation. The relationship between cross section and level density in the resonance region is fairly well understood and smooth variations with mass number are known to exist. However, in the  $1/v$  region, the cross sections are strongly influenced by the proximity of the lowest lying resonance peaks and smooth variations with mass number are not found (1).

I decided to search for a correlation between the thermal neutron activation cross section and parameters which could be calculated from nuclide masses. The latter qualification was applied because the mass is one of the first quantities determined for a new nuclide and therefore is ordinarily available for use. The approach adopted was to assume that the absorption of a neutron by a nucleus leads to a change in the stability of that nucleus where stability,  $S$ , is related to the nuclide's position on its mass vs.  $Z$ . parabola by the equation

$$S(Z,A) = (M(Z_A, A) \pm \delta) - M(Z,A) . \quad (1)$$

The change in stability,  $\Delta S$ , which the nuclide undergoes in absorbing a neutron is given by the equation

$$\Delta S = S(Z, A+1) - S(Z, A) \quad (2)$$

and is the parameter which I tried to relate to the cross section. A computer program was written which took the tabulated nuclide masses and calculated:

1. the constants for the parabolas at each mass number (by making a least squares fit at mass numbers where enough nuclides existed or interpolating where there were not enough nuclides),
2.  $S$  for each nuclide, and
3.  $\Delta S$  for each nuclide (wherever  $S$  for the activation product was known).

The values for  $\Delta S$  were then plotted against the log of the cross section,  $\sigma$ , for the nuclides after dividing these into groups on the basis of even or odd  $Z$  and even or odd  $N$ . Only for the even  $N$ -odd  $Z$  nuclides, with  $N$  less than 33, did a clearcut correlation appear. Fortunately, manganese-53 belongs in this classification.  $\sigma$  for these nuclides is shown plotted against  $\Delta S$  in Figure 3. These points tend to group themselves according to three separate trends which approximate straight lines on this graph. The nuclides in each of these three groups are filling one of the three neutron shells:  $3d_{5/2}$ - $3d_{3/2}$ - $2s_{1/2}$ ,  $4f_{7/2}$ , and  $4f_{5/2}$ . Thus the correlation between  $\sigma$  and  $\Delta S$  cannot be made only on the basis of even  $N$ -odd  $Z$  but must also include the neutron shell being

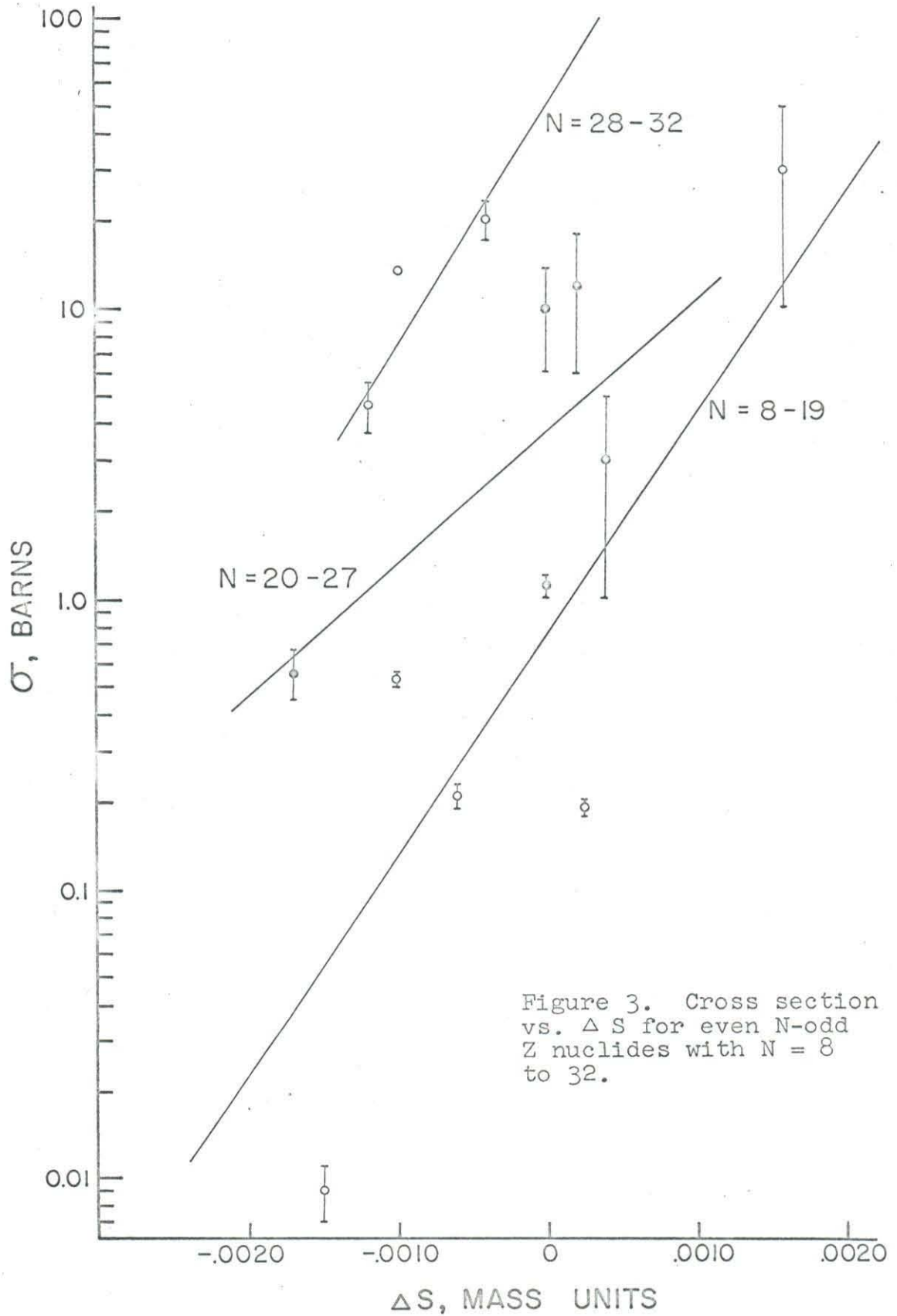


Figure 3. Cross section vs.  $\Delta S$  for even N-odd Z nuclides with N = 8 to 32.

filled. The straight lines in Figure 3 represent least square fits to those nuclides belonging to each of the three groups. The average value for the factors separating these points from their respective lines is 2.8 and the largest such factor is 7. These values provide some indication of the degree of correlation.

The value of plot such as that in Figure 3, lies in its ability to predict as yet unmeasured cross sections for other nuclides. Two nuclides to which this method might be applied are phosphorus-33 and the previously mentioned manganese-53. Phosphorus-33 is thought to be of importance as a radioactive tracer in biochemical experiments because its half-life (25 days) is longer than that of the commonly used, phosphorus-32 (14.3 days). Proposals for the production of phosphorus-33 are contained in the literature (2,3). The predictions for the thermal neutron activation cross sections found in Figure 3 for these two nuclides are 0.03 barns for phosphorus-33 ( $\Delta S = -0.0018$ ) and the rather large value of 200 barns for manganese-53 ( $\Delta S = 0.0008$ ).

In view of the facts described above, it is proposed that the correlation found between  $\sigma$  and  $\Delta S$  for even N-odd Z nuclides with  $N < 33$  be further verified by a determination of the thermal neutron activation cross sections for manganese-53 and phosphorus-33.

PROPOSITION 3

After the prediction of the presence of cosmic-ray produced manganese-53 in iron meteorites by Sheline and Hooper (4), Honda, Shedlovsky, and Arnold (5) separated this nuclide from the Grant, Williamstown, Odessa, and Canyon Diablo meteorites and measured its activity finding respectively 299, 285, 197, and 92 d.p.m./kg. of meteorite. However, the actual amount of manganese-53 could not be calculated because no accurate determination of its half-life has been made. Wilkenson and Sheline (6) tried to establish an approximate value of 140 years for the half-life on the basis of an estimated cross section for the nuclear reaction,  $\text{Cr}^{53}(\text{p},\text{n})\text{Mn}^{53}$ . This value corresponded to a ground state of  $f_{5/2}$  for the manganese-53 nucleus but Dobrowolski, et al. (7) found a ground state of  $f_{7/2}$  which would mean a much longer half-life. Huizenga and Wing (8) suggested a lower limit of  $1.3 \times 10^5$  years on the basis of proportional and scintillation spectrometer measurements. Sheline and Hooper (4), using calculated log ft values, set the range for the half-life at  $1 \times 10^6$  to  $2 \times 10^7$  years.

A precise measurement of the half-life of manganese-53 must be based upon a determination of the amount of this nuclide present according to the equation

$$t_{1/2} = 0.693 n/A , \quad (3)$$

where n is the number of atoms and A is the activity. Since

manganese-53 is found in such small quantities, it must be separated by using manganese carrier and thus the problem is reduced to measuring a very small amount of manganese-53 in the presence of a much larger amount of manganese-55. If a value for the half-life of  $1 \times 10^6$  years is assumed and 20 mg. carrier are used for 1 kg. of Canyon Diablo meteorite, the ratio of manganese-55 to manganese-53 should be  $3 \times 10^6$ . Two methods are proposed for making this measurement.

Mass spectrometer method.--The use of a mass spectrometer to determine the amount of manganese-53 has been proposed by Brown and Arnold (9). In order to measure 1 part manganese-53 in  $3 \times 10^6$  parts of manganese-55, an ion beam of high intensity is needed. This was achieved by Charles McKinney by employing a triple filament in the mass spectrometer source. However, measurements at the mass-53 peak location are complicated by the presence of a chromium-53 peak (the natural abundance of chromium-53 in chromium is 9.43%). Even though chromium may be present in the manganese to a very small extent, a sizeable mass-53 background results because chromium is ionized much more efficiently than manganese. One way to circumvent this difficulty, without taking elaborate precautions to remove chromium, would be to distill added portions of enriched chromium-53 (99.97% chromium-52 obtained from Oak Ridge) as chromyl chloride (10). The

isotopic composition of the chromium remaining with the manganese should approach closer to that of the enriched chromium-52 with each distillation and, if enough distillations are performed, the final isotopic composition of the chromium should be essentially the same. A separate measurement of the isotopic composition of the enriched chromium-52 would provide data for the subtraction of any residual chromium-53 peak.

Neutron activation measurement.--In Proposition 2 the thermal neutron activation cross section for manganese-53 was estimated to be about 200 barns. Using a more conservative value of 10 barns, the activity to be expected from manganese-54 after irradiation for 5 days in a flux of  $10^{14}$  followed by a decay time of 3 days is shown in Table 1. The activity from the reaction  $\text{Mn}^{55}(n,\gamma)\text{Mn}^{56}$  is also shown. Fortunately, the half-life of manganese-54 is much longer than that for manganese-56 and the latter will eventually decay to negligible levels. While the manganese-56 still has activity comparable to that of manganese-54, it can be used as a calibrating standard and thus the concentration of manganese-53 will be directly referred to that of manganese-55. A gamma-spectrometer may be used to single out the peak at about 0.84 Mev (common to both nuclides) in order to sharpen the comparison. The thermal neutron flux which is to be used must be well moderated to avoid the interfering reaction,  $\text{Mn}^{55}(n,2n)\text{Mn}^{54}$ .

TABLE 1. Activities Resulting from Thermal Neutron Activation.

Flux =  $1 \times 10^{14}$  neutrons/sq.cm.-sec.

Irradiation time = 5 days

Decay time = 3 days

<u>Activation Reaction</u>	<u>Half-Life of Daughter</u>	<u>Decay Mode of Daughter</u>	<u>Activity</u>
$\text{Mn}^{53}(n,\gamma)\text{Mn}^{54}$	300 days	E.C. (100%) 0.835 $\gamma$ (100%)	$5 \times 10^4$ d.p.m./kg. of original meteorite
$\text{Mn}^{55}(n,\gamma)\text{Mn}^{56}$	2.58 hours	$\beta^-$ (100%) 0.845 $\gamma$ (100%) 1.81 $\gamma$ ( 30%) 2.13 $\gamma$ ( 20%)	$20 \times 10^4$ d.p.m./20 mg.Mn
$\text{Fe}^{54}(n,\gamma)\text{Fe}^{55}$	2.94 years	E.C. (100%)	
$\text{Cr}^{50}(n,\gamma)\text{Cr}^{51}$	27.8 days	0.323 $\gamma$ ( 10%) E.C. (100%)	

The last two reactions in Table 1 may be used to provide standards to calibrate the initial counting of the soft x-rays from manganese-53.

It is proposed that the following procedure be employed to attempt to obtain two values for the half-life of manganese-53.

1. 650 grams of the Canyon Diablo iron have already been dissolved. 13 mg. manganese carrier will be added and this carrier separated according to the procedure used by Honda, Shedlovsky, and Arnold (5). Final purification will be attempted by the cyclic electrodeposition or precipitation of manganese dioxide.
2. The concentration of chromium-53 will be reduced by the repeated distillation, as chromyl chloride, of added portions of enriched chromium-53. The final yield of manganese carrier may be determined colorimetrically.
3. The soft x-ray activity from manganese-53 will be counted.
4. The manganese carrier (containing the manganese-52) will be exposed to a moderated thermal neutron flux of  $10^{14}$  neutrons/sq. cm.-sec. and the manganese-56 formed allowed to decay to levels anticipated for the manganese-54 formed from manganese-53. A search will be made for the manganese-54

gamma-radiation using the remaining manganese-56 radiation as a calibrating standard. The concentration of manganese-53 in the carrier will be calculated from these counting data.

5. The manganese will then be loaded onto a mass spectrometer filament by electrodeposition and an attempt made to detect the manganese-53 peak. If detected, its intensity may be referred to that of manganese-55 thus determining the amount of manganese-53 in the carrier.
6. The data for the amount of manganese-53 will be combined with the counting data for this nuclide and the half-life determined by equation 3.

PROPOSITION 4

Neutron activation as an analytical method has two major assets:

1. the analytical sensitivity for certain elements is greater than that which can be achieved by any other method, and
2. when used in conjunction with gamma-spectrometry, the degree of separation of the element of interest, which is needed before interferences are eliminated, may be reduced and, if carried to the ultimate extreme, non-destructive analysis becomes a possibility. The latter asset is of particular importance when materials, such as meteorites, are available only in limited quantities.

Any sample to be analyzed by this method may be considered to consist of: 1) a matrix containing 2) the element for which analysis is sought. A major problem to the analyst is the estimation of the degree to which the matrix must be simplified (through physical and chemical separations) before the gamma-spectrometric interferences from the matrix are reduced to negligible levels. The adjustment of the parameters: neutron flux, weight of sample, irradiation time, and decay time following irradiation provides added power for the analyst but multiplies the problems of engineering the analysis, particularly if many elements are to be analyzed in a complex matrix. In addition, the reduction

of the gamma-spectra to meaningful analytical values provides further data handling problems. Computers have been applied to the latter problem and a program developed by Kuykendall and coworkers at the Texas Engineering Experiment Station has been published (11). Savitsky (12) has presented a discussion of the use of computers in generating and analyzing infrared spectra which is also of interest in the present problem.

I believe that any solution to these problems should be:

1. comprehensive--every conceivable source of radioactivity should be considered, and
2. versatile--the ability to vary each of the significant parameters in the problem should be provided.

With these objectives in mind, I have written a series of computer programs which

- (a) synthesize the gamma-spectra to be expected following neutron irradiation, and
- (b) analyze these synthetic gamma-spectra and, it is hoped, the experimental gamma-spectra which will eventually be recorded.

Block diagrams showing the steps in these calculations are displayed in Figures 4 and 5. The symbols and abbreviations used in these diagrams are defined below.

FLUX	neutron flux
DSS(n)	time-independent coefficients in the Batemann equations for nuclear and radioactive transformations

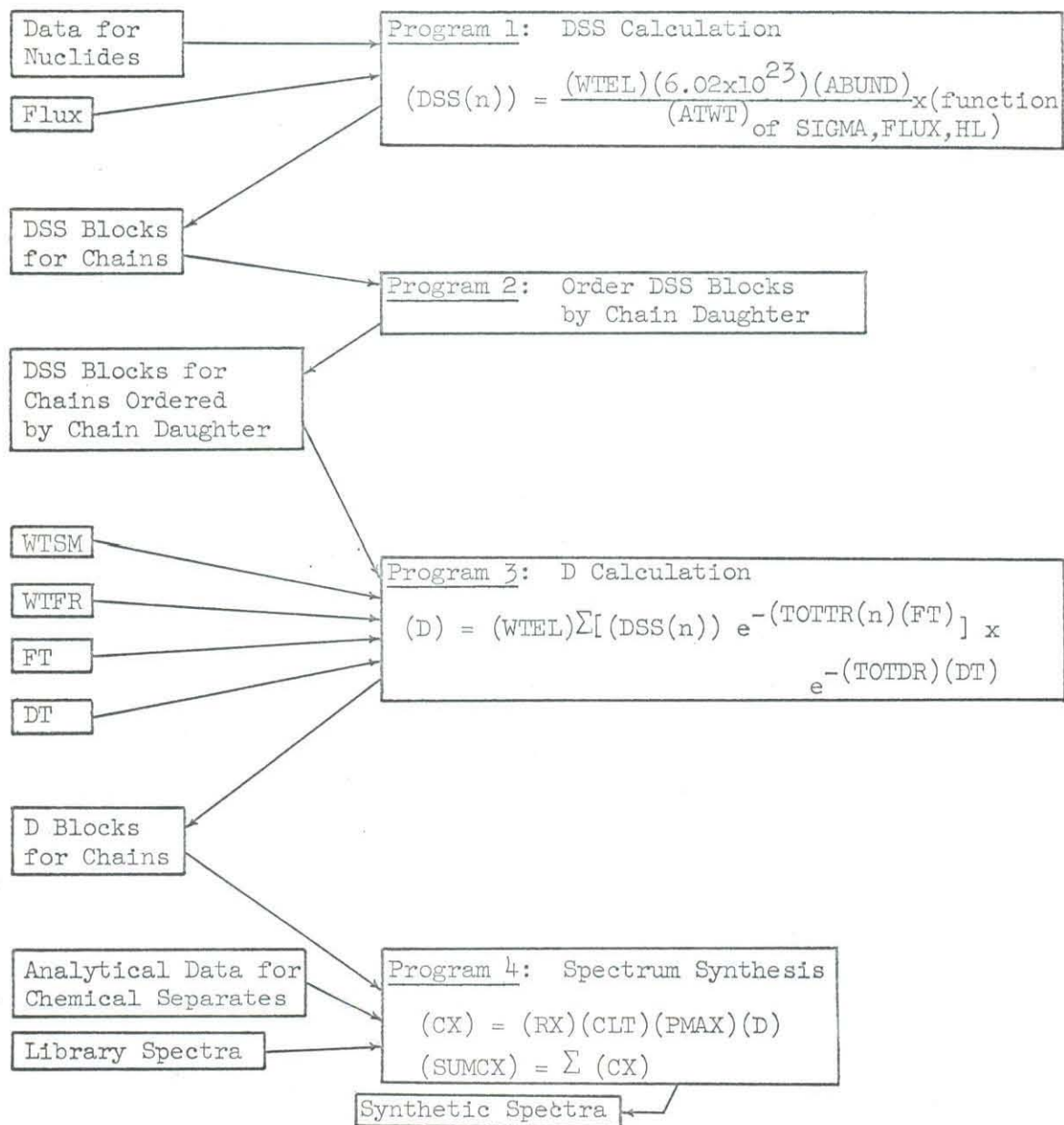


Figure 4. Block diagram showing the flow of data for the synthesis of gamma-spectra resulting from neutron activation.

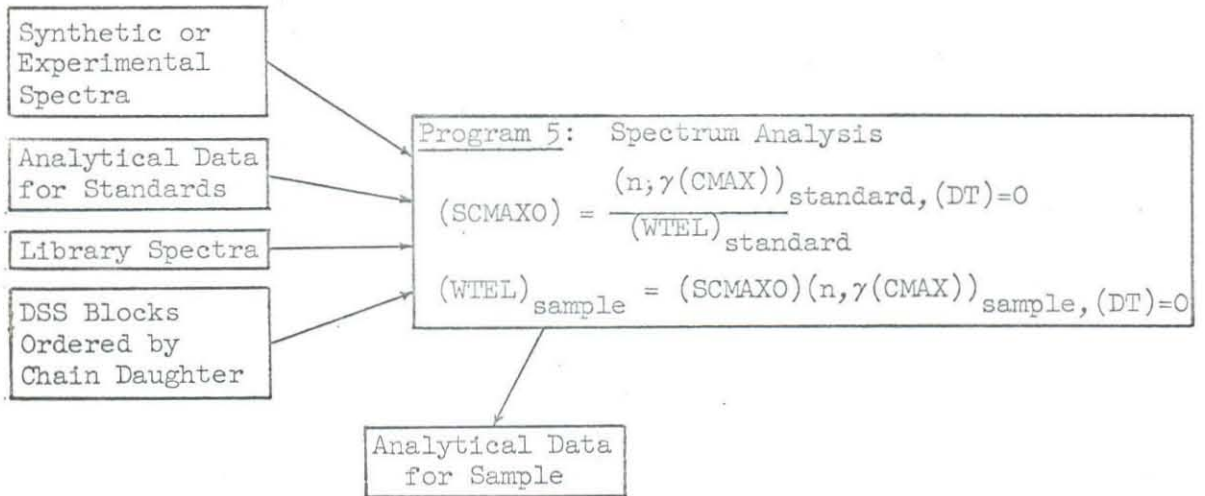


Figure 5. Block diagram showing the flow of data for the analysis of gamma-spectra resulting from neutron activation.

WTEL	weight of the chain parent element (1 gram is used)
ABUND	isotopic abundance of the chain parent
ATWT	atomic weight of the chain parent
SIGMA	neutron activation cross section for a chain member
HL	half-life of a chain member
WTSM	weight of the sample
WTFR	weight fraction of the chain parent element in the sample
FT	irradiation time
DT	decay time after removal from the neutron flux
D	disintegration rate for the chain daughter
TOTTR(n)	total transformation constant for a chain member
TOTDR	decay constant for the chain daughter
CX	counts in channel x of a spectrum
RX	ratio of counts in channel x to the counts contained under the maximum energy peak
CLT	live-counting time
PMAX	fraction of total disintegrations con- tained under the maximum energy peak
SUMCX	counts in channel x resulting from the summation of two or more spectra

SCMAXO . factor which converts the activity under  
the maximum energy peak to the weight of  
n, $\gamma$ -chain parent element  
n, $\gamma$ (CMAX) activity under the maximum energy peak  
due to the n, $\gamma$ -chain.

Program 1 takes the elementary nuclear data and a value for the neutron flux, synthesizes all possible nuclear transformation chains (these chains start with a stable nuclide, end with an unstable nuclide, contain 5 or fewer members, and must yield at least 1 d.p.m. after a 3-year irradiation) and computes the time-independent coefficients for the Batemann equations for these chains (see Friedlander and Kennedy (13)). Program 2 orders these chains according to the chain daughters for convenience in later calculations. Program 3 computes the disintegration rate for each chain daughter for a sample of a particular composition under specified irradiation conditions. Finally, program 4 takes the output from program 3 and library spectra (obtained from the Scintillation Spectrometry Gamma-Ray Spectrum Catalogue (14) or experimental spectra for pure elements) and computes the gamma-spectra to be expected. Provision is made in program 4 for entering the composition of separates resulting from anticipated physical or chemical separations and for calculating the spectra of these separates.

Program 5 is designed to take synthetic or experimental spectra and analyze these by finding the activity under the

maximum energy peak in each spectrum. A stripping procedure is then followed (using the library spectrum corresponding to the nuclide for the maximum energy peak) thus exposing the next maximum energy peak in the spectrum. By this method a value for the activity under the maximum energy peak is obtained for each nuclide. The analytical data for the standards, which are exposed to the same flux as the samples, are combined with the activities under the maximum energy peaks in the spectra for these standards to obtain conversion factors, SCMAXO, and these factors then used to find the analytical data for the samples. However, if all conceivable sources of the chain daughter nuclide are to be treated, then the contributions from chains other than the simple  $n, \gamma$ -chain must be considered. This is done by recycling all calculated analytical data for the samples and computing the contributions from the other chains using the DSS blocks (the computations in this step are essentially the same as those in programs 3 and 4). These other contributions are then subtracted from the total activity under the maximum energy peak thus yielding a new value for the activity from the  $n, \gamma$ -chain. Further recycling should provide the correct sample composition by iteration.

It is proposed that the programs described above be further tested and eventually applied to the prediction and analysis of gamma-spectra resulting from neutron activation.

PROPOSITION 5

Neutron activation may offer a method for analyzing for a number of elements in a chondritic meteorite without chemically destroying the material. The statement of the problem of neutron activation analysis in complex matrices given in Proposition 4 may be restated for the present situation in the following way: to what degree must the system be reduced (preferably by physical methods) before useful analytical data for the minor constituents are obtained? Ideally, the procedure for the reduction of the system should yield separates, a knowledge of whose composition will be of value in explaining the structure, origins, and history of the meteorites. Correlations between individual meteorites and divisions into families having similar composition might be a byproduct of any survey conducted on this basis. Physical separation of the mineral phases is the most direct method and should yield the most information. If activation is to be performed following separation, then this method would also introduce the least amount of contamination. A method, which was used during an investigation of the Bruderheim meteorite (15) is outlined in Figure 6. Five separates result from this procedure with varying degrees of cross contamination among them. However, with careful work this contamination could be reduced to nearly negligible levels. The separation of these phases would be conducted as

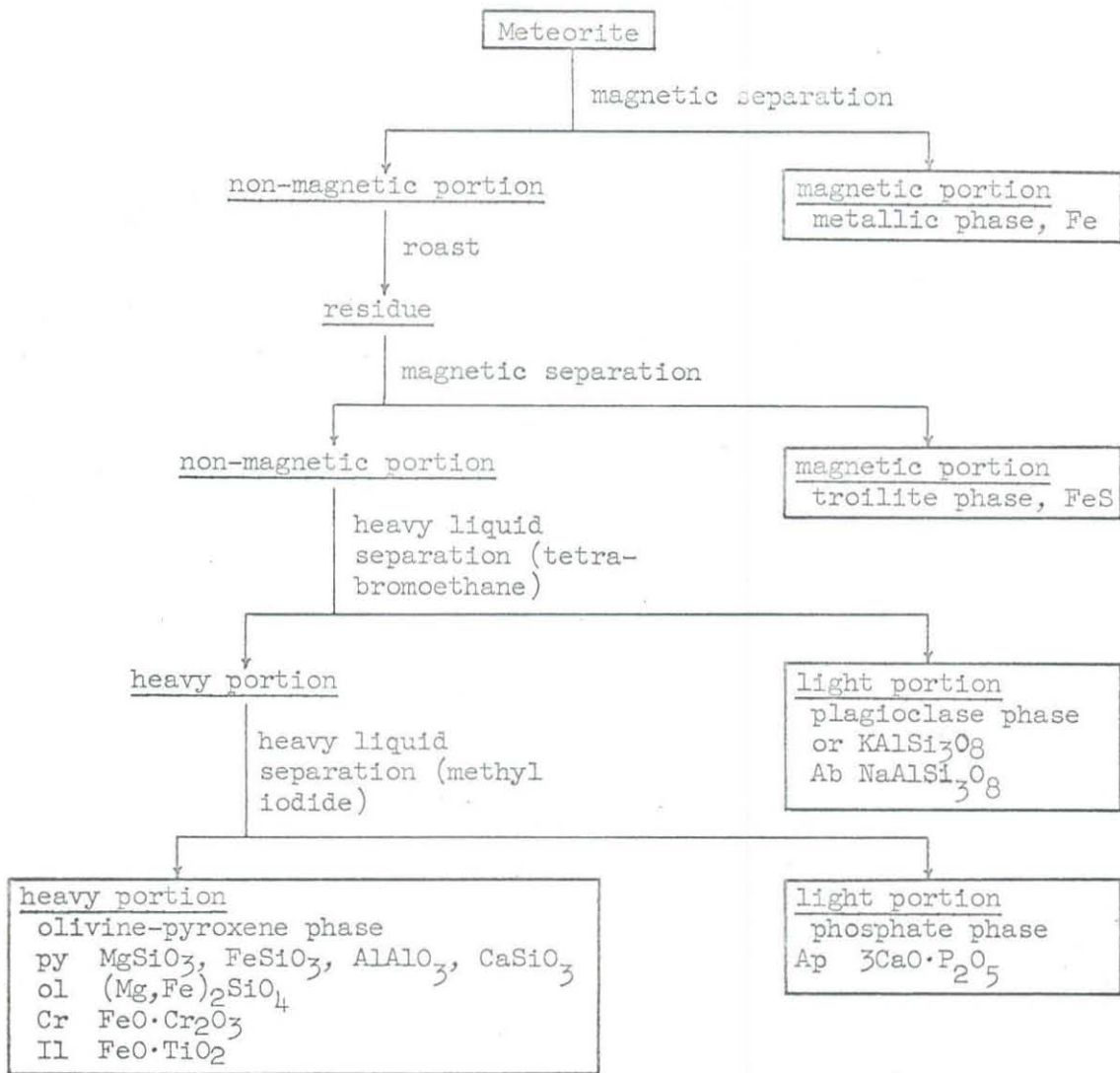


Figure 6. Scheme for the separation of chondritic meteorite phases (15).

part of a more general survey including mineralogical examination and chemical analysis for the major constituents. After these investigations have been completed, then neutron analysis would be attempted to find the concentrations of the minor constituents in these phases.

Table 2 shows estimated fractions of the elements to be expected in each of these separates. The values shown for the major elements at the top of the table were calculated from the data for the Bruderheim meteorite (15). The bracketed values, which include those for the minor constituents shown in the second half of the table, were calculated from data presented by Krinov (16). The major activities to be expected after the thermal neutron irradiation of an "average" chondrite in a flux of  $1 \times 10^{11}$  neutrons/sq.cm.-sec. for eight combinations of irradiation and decay times are shown in Table 3. These activities were calculated by programs 1 through 3 as described in Proposition 4. The detailed examination of the analytical possibilities must wait until programs 4 and 5 can be applied. However, a number of facts are revealed by an examination of Tables 2 and 3.

1. The activities listed under  $DT = 0$  are not of value unless special facilities exist for counting the samples immediately after removal from the flux.
2. The phosphorus and silicon activities consist entirely of beta-radiation and thus their only effect on the analysis will be the contribution of a bremsstrahlung background to the gamma-spectra.

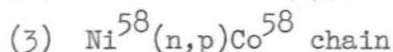
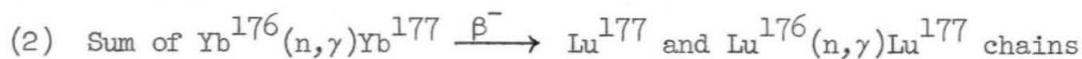
TABLE 2. Fractional Amount of Element Expected in Each Separate.

The bracketed values are estimated from (16).

Element	Total Amount (g./g. of meteorite)	Weight of Element in Separate				
		Metallic	Troilite	Plagioclase	Phosphate	Olivine -Pyroxene
O	0.372	0.06		0.11	0.01	0.82
Fe	0.224	0.35	0.20			0.45
Si	0.184	0.05		0.15		0.80
Mg	0.148	0.04				0.96
S	0.024	0.04	0.96			
Ni	0.013	0.99	0.01			
Ca	0.013	0.05			0.23	0.72
Al	0.012	0.06		0.75		0.19
Na	0.0069	(0.04)		(0.94)		
Cr	0.0037	0.06				0.94
K	0.0009	(0.04)		(0.94)		
Ti	0.0006	0.06				0.94
Mn	0.0024	(0.09)	(0.16)		(0.75)	
P	0.0015	(0.27)	(0.48)		(0.24)	
Co	0.0011	(0.98)	(0.02)			
Cl	0.00047				(1.00)	
Cu	0.00017	(0.50)	(0.50)			
Ge	53	p.p.m.	(0.83)	(0.12)	(0.05)	
V	50	p.p.m.	(0.04)	(0.30)	(0.66)	
Br	25	p.p.m.	(0.04)		(0.96)	
As	18	p.p.m.	(0.25)	(0.75)		
W	16	p.p.m.	(0.97)		(0.03)	
Dy	2.1	p.p.m.	(0.03)		(0.97)	
Ag	1.4	p.p.m.	(0.13)	(0.87)		
Sm	1.1	p.p.m.	(0.02)		(0.98)	
Ho	0.60	p.p.m.			(1.00)	
Lu	0.54	p.p.m.			(1.00)	
Ir	0.38	p.p.m.	(0.91)	(0.09)	(1.00)	
Eu	0.27	p.p.m.			(1.00)	

TABLE 3. Major Activities Expected After Thermal Neutron Irradiation of an "Average" Chondrite. Flux =  $1 \times 10^{11}$  neutrons/sq.cm.-sec.

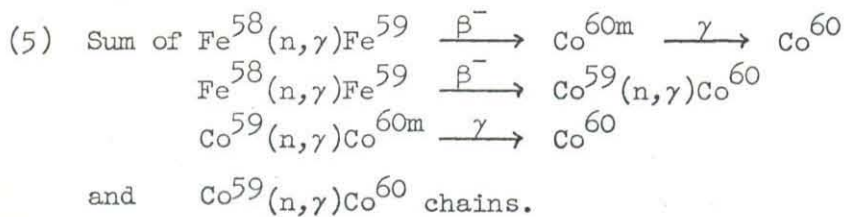
Chain Parent Element	Daughter Half Life	Decay Mode	Activity ( $10^6$ d.p.m.)			
			FT = 1 h.			
			DT=0	3.5 h.	22 h.	7 d.
Dy	1.2m	$\gamma$	6.6			
Ag	2.3m	$\beta, \gamma$	1.0			
Al	2.3m	$\beta, \gamma$	400			
Cr	3.5m	$\beta$	1.7			
V	3.7m	$\beta, \gamma$	16			
Cu	5.1m	$\beta, \gamma$	5.3			
Ca	8.8m	$\beta, \gamma$	2.2			
Mg	9.5m	$\beta, \gamma$	57			
Co	10.5m	$\gamma$	1060			
Br	17.5m	$\beta, \gamma$	4.7			
Cl	37.3m	$\beta, \gamma$	4.3	0.09		
Ca(1)	57.1m	$\beta, \gamma$	0.94	0.07		
Dy	2.3h	$\beta, \gamma$	8.8	3.1	0.012	
Si	2.6h	$\beta$	17	6.7	0.050	
Mn	2.6h	$\beta, \gamma$	490	193	1.3	
Ni	2.6h	$\beta, \gamma$	3.6	1.4	0.010	
Eu	9.2h	$\beta, \gamma$	0.32	0.25	0.062	
K	12.5h	$\beta, \gamma$	0.33	0.27	0.099	
Cu	12.8h	$\beta^+, \beta^-$	1.6	1.3	0.048	
Na	15.0h	$\beta, \gamma$	29	24	11	0.012
Ir	19.0h	$\beta, \gamma$		0.02	0.009	
W	1.0d	$\beta, \gamma$		0.078	0.045	
As	1.1d	$\beta, \gamma$	0.12	0.11	0.069	0.003
Ho	1.1d	$\beta, \gamma$		0.018	0.011	
Br	1.5d	$\beta, \gamma$		0.030	0.021	0.001
Sm	1.9d	$\beta, \gamma$		0.014	0.010	0.001
Yb, Lu(2)	6.8d	$\beta, \gamma$			0.005	0.003
Ge	11.3d	E.C.			0.005	0.004
P	14.0d	$\beta$		0.067	0.064	0.048
Cr	27.7d	$\gamma$	0.12	0.12	0.11	0.099
Fe	45.0d	$\beta, \gamma$		0.030	0.030	0.027
Ni(3)	71.2d	$\beta^+, \gamma$			0.008	0.007
S, Cl(4)	86.6d	$\beta$		0.010	0.010	0.009
Fe	2.6y	E.C.		0.071	0.071	0.071
Co, Fe(5)	5.2y	$\beta, \gamma$		0.061	0.061	0.061
Total Activity			2140	232	13	0.37



Activity ( $10^6$  d.p.m.)

FT = 24 h.

DT=0	3.5 h.	22 h.	7 d.
6.6			
1.0			
400			
1.7			
16			
5.3			
2.2			
57			
1080			
6.6			
6.4	0.13		
2.2	0.17		
34	12	0.047	
72	29	0.22	
2090	818	5.6	
15	5.9	0.040	
3.6	2.8	0.69	
4.4	3.6	1.3	
21	17	6.4	
418	356	151	0.18
0.33	0.29	0.15	
1.5	1.3	0.79	0.012
2.2	2.0	1.2	0.026
0.36	0.33	0.20	0.005
0.63	0.59	0.41	0.025
0.29	0.27	0.21	0.024
0.11	0.11	0.10	0.056
0.13	0.13	0.12	0.087
1.6	1.6	1.5	1.1
2.8	2.8	2.7	2.4
0.72	0.72	0.71	0.65
0.19	0.19	0.19	0.18
0.24	0.24	0.24	0.23
1.7	1.7	1.7	1.7
0.90	0.90	0.90	0.90
4290	1260	180	8.0



3. The troilite phase offers interesting possibilities for the analysis of minor constituents since the major elements, iron and sulfur, do not contribute a great deal to the overall activity.
4. The metallic phase also contains few major contributors to the total activity and thus also might yield valuable information.
5. The silicate phases are less clearcut since the distribution of the minor elements among these phases is not known. However, this method of analysis might be expected to provide just such information.

It is proposed that the data in Table 2 be applied by the computer programs 4 and 5 to evaluate the possibility of using neutron activation to analyze for the minor constituents in the phase separates of chondritic meteorites.

REFERENCES FOR THE PROPOSITIONS

1. Mayer, M. G. and Jensen, J. H. D., Elementary Theory of Nuclear Shell Structure, John Wiley and Sons, Inc. (New York, 1955), p. 35.
2. Fogelstrom-Fineman, I. G. A. and Westermark, T., Nucleonics 14, No. 2, 62-5 (1956).
3. Westermark, E. G. T., Fogelstrom-Fineman, I. G. A., and Forberg, S. R., Radioisotopes in Scientific Research, Proc. Intern. Conf. Paris 1957 1, 19-34 (1958).
4. Sheline, R. K. and Hooper, J. E., Nature 179, 85 (1957).
5. Honda, M., Shedlovsky, J. P., and Arnold, J. R., Geochim. et Cosmochim. Acta 22, 133-54 (1961).
6. Wilkinson, J. R. and Sheline, R. K., Phys. Rev. 99, 752 (1955).
7. Dobrowolski, W., Jones, R. V., and Jeffries, C. D., Phys. Rev. 104, 1378 (1956).
8. Huizenga, J. R. and Wing, J., U.S. Atomic Energy Comm. ANL-5738 (1957) 6 pp.; Chem. Abstr. 51, 17497f (1957).
9. Brown, H. S. and Arnold, J. R. (personal communication).
10. Pijck, J., The Radiochemistry of Chromium, NAS-NS 3007, 23-6 (1960).
11. Kuykendall, W. E., et al., Computer Techniques for Radioactivation Analysis, AEC Report No. AT-(40-1)-2565 (1960).
12. Savitsky, A., Anal. Chem. 13, 35A-40A (December, 1961).
13. Friedlander, G. and Kennedy, J. W., Nuclear and Radiochemistry, John Wiley and Sons, Inc. (New York, 1955), p. 136.
14. Heath, R. L., Scintillation Spectrometry Gamma-Ray Spectrum Catalogue, AEC Research and Development Report IDO-16408 (1957).

15. Duke, M., Maynes, D., and Brown, H., J. Geophys. Res.  
66, 3557-63 (1961).
16. Krinov, E. L., Principles of Meteorites, Pergamon  
Press (New York, 1960), p. 304.